2017

UNDERSTANDING AND IMPROVING MANUFACTURING PROCESSES FOR MAKING LITHIUM-ION BATTERY ELECTRODES

Mohanad N. AL-Shroofy
University of Kentucky, mohanad.al-shroofy@uky.edu
Digital Object Identifier: https://doi.org/10.13023/ETD.2017.296

STUDENT AGREEMENT:

I represent that my thesis or dissertation and abstract are my original work. Proper attribution has been given to all outside sources. I understand that I am solely responsible for obtaining any needed copyright permissions. I have obtained needed written permission statement(s) from the owner(s) of each third-party copyrighted matter to be included in my work, allowing electronic distribution (if such use is not permitted by the fair use doctrine) which will be submitted to UKnowledge as Additional File.

I hereby grant to The University of Kentucky and its agents the irrevocable, non-exclusive, and royalty-free license to archive and make accessible my work in whole or in part in all forms of media, now or hereafter known. I agree that the document mentioned above may be made available immediately for worldwide access unless an embargo applies.

I retain all other ownership rights to the copyright of my work. I also retain the right to use in future works (such as articles or books) all or part of my work. I understand that I am free to register the copyright to my work.

REVIEW, APPROVAL AND ACCEPTANCE

The document mentioned above has been reviewed and accepted by the student's advisor, on behalf of the advisory committee, and by the Director of Graduate Studies (DGS), on behalf of the program; we verify that this is the final, approved version of the student's thesis including all changes required by the advisory committee. The undersigned agree to abide by the statements above.

Mohanad N. AL-Shroofy, Student

Dr. Yang-Tse Cheng, Major Professor

Dr. Thomas Dziubla, Director of Graduate Studies

UNDERSTANDING AND IMPROVING MANUFACTURING PROCESSES FOR MAKING LITHIUM-ION BATTERY ELECTRODES

DISSERTATION

A dissertation submitted in partial
fulfillment of the requirements for
the degree of Doctor of Philosophy
in the College of Engineering at the
University of Kentucky

By
Mohanad AL-Shroofy
Lexington, Kentucky

Director: Dr. Yang-Tse Cheng, Professor of Chemical and Materials
Engineering
Lexington, Kentucky

2017

ABSTRACT OF DISSERTATION

UNDERSTANDING AND IMPROVING MANUFACTURING PROCESSES FOR MAKING LITHIUM-ION BATTERY ELECTRODES

Lithium-ion batteries (LIBs) have been widely used as the most popular rechargeable energy storage and power sources in today's portable electronics, electric vehicles, and plug-in hybrid electric vehicles. LIBs have gained much interest worldwide in the last three decades because of their high energy density, voltage, rate of charge and discharge, reliability, and design flexibility. I am exploring the possibility of developing battery manufacturing technologies that would lower the cost, reduce the environmental impact, and increase cell performance and durability.

This dissertation is focused firstly on understanding the effect of mixing sequence (the order of introducing materials) and optimizing the electrode fabrication for the best electrochemical performance, durability, lower cost, and improve the existing manufacturing processes. The electrode system consists of active material, polymer binder, conductive agent, and solvent. I have investigated four different mixing sequences to prepare the slurries for making the positive electrode. The key sequence-related factor appears to be whether the active material and conductive agent are mixed in the presence of or prior to the introduction of the binder solution. The mixing sequences 1, 2, 3, and 4 were optimized, and the rheological behavior of the slurries, morphology, conductivity, and mechanical and electrochemical properties of electrodes were investigated. Slurries from sequences 1 and 4 show different rheological properties from 2 and 3. The amount of NMP required to achieve a comparable final slurry viscosity differed significantly for the sequences under study. The sequence 1 shows better long-term cycling behavior than sequences 2, 3 and 4. This study quantifies the link between electrode slurry mix parameters and electrode quality.

Secondly, a new method of making lithium-ion battery electrodes by adapting an immersion precipitation (IP) technology commonly used in membrane manufacturing was developed and demonstrated. The composition, structure, and electrochemical performance of the electrode made by the IP method were compared favorably with that made by the conventional method. The toxic and expensive organic solvent (NMP) was captured in coagulation bath instead of being released to the atmosphere. The IP electrodes show an excellent performance and durability at potentially lower cost and less environmental impact.

Thirdly, I have developed and demonstrated a solvent-free dry-powder coating process for making $LiNi_{1/3}Mn_{1/3}Co_{1/3}O_2$ (NMC) positive electrodes in lithium-ion

batteries, and compared the performance and durability of electrodes made by the dry-powder coating processes with that by wet-slurry coating processes. The technology that has been used is the electrostatic spray deposition (ESD) process. This process eliminates volatile organic compound emission, reduces thermal curing time from hours to minutes, and offers high deposition rates onto large surfaces. The long-term cycling shows that the dry-powder coated electrodes have similar performance and durability as the conventional wet-slurry made electrodes.

KEYWORDS: Lithium-Ion batteries, Solvent-free, Dry-powder-coated, Immersion Precipitation, Mixing sequences

Author's signature: Mohanad AL-Shroofy

Date: July 24, 2017

UNDERSTANDING AND IMPROVING MANUFACTURING PROCESSES FOR MAKING LITHIUM-ION BATTERY ELECTRODES

By

Mohanad AL-Shroofy

Director of Dissertation: Dr. Yang-Tse Cheng

Director of Graduate Studies: Dr. Thomas Dziubla

Date: July 24, 2017

Dedicated to my country (Iraq) and family

ACKNOWLEDGMENTS

This Ph.D. work would be not possible without the support of many people in my working and private life. First, I would like to gratefully and sincerely thank my advisor Prof. Yang-Tse Cheng for his continuous encouragement and support throughout my doctoral research in the past five years at the University of Kentucky. Without his patient, professional guidance, and financial and emotional support, this work would be impossible to finish.

I am grateful to all the members of my dissertation committee, Dr. Kozo Saito, Dr. Stephan Rankin, Dr. Mona Shirpour, and Dr. Janet Lumpp for their time, academic support, efforts, suggestions, and discussions on my research and dissertation.

I sincerely thank my former and current group members Jiagang Xu, Qinglin Zhang, Jie Pan, Baleegh Alobaid, Tao Chen, Long Zhang, Yikai Wang, Jiazhi Hu, Ming Wang, Yan Jin, Dingying Dang, Peizhen Li, and Dawei Li for their support and help with my research.

I would like to acknowledge Renata Arsenault, Oujung Kwon, and Mohan Karulkar from Ford Motor Company for helpful guidance, valuable discussions, and technical support.

I also would like to thank the Department of Chemical and Materials Engineering (CME) at the UK, and other colleagues and staff members, Lindsay Boehme, Kaur Aman, Azin Akbari, and Nancy Miller, who have provided me with experimental assistance.

I forever greatly appreciate my parents, wife, daughters, sons, brothers, sisters, and friends for their supports, encouragements, and love.

I want to express my gratitude to the Iraqi Government and the higher committee for education development in Iraq (HCED), for the scholarship support, the US National Science Foundation (Award No.: 1355438, Powering the Kentucky Bioeconomy for a Sustainable Future), and Ford Motor Company for their financial support.

TABLE OF CONTENTS

LIST OF FIGURES

LIST OF TABLES

Chapter 1 Introduction

Numerous research groups have been focusing on improving manufacturing processes and developing new materials for lithium-ion batteries (LIBs) since LIBs were commercialized by SONY in the 1990s. LIBs have been widely used in hybrid and electric vehicles, portable electronics, and medical devices due to their long cycle life, high energy, high voltage, good cycling performance, and high power density [1-3].

Today's LIB research activities involve lots of effort in developing novel materials and new manufacturing processes [2, 4], with little attention given to the profound effect of the mixing process on performance and long-term durability of LIBs. Our studies focus on addressing two questions: (1) can "conventional" LIB electrodes be made by dry powder-coating and immersion precipitation processes?; And (2) can electrode structures that are unattainable by the conventional wet slurry-coating method be made using the new manufacturing processes?

For a given electrode system, there is a set of optimum mixing process parameters that will deliver the best performance and durability. This set of optimum mixing process parameters can be obtained by establishing a correlation between mixing parameters, slurry material characteristics, and finished battery performance and durability through rigorous application of mixing theory, rheology and surface morphology for multi-component suspension systems, supported by both classic and novel analytical approaches. Different mixing sequences have been investigated to produce well-mixed slurries for various electrode materials. Kim et al. [5] found that the best capacity and stability of charge and discharge cycle can be obtained by dry mixing the active materials ($LiCoO_2$) and conductive agent (graphite) then adding the solution of the binder polyvinylidene fluoride (PVDF) and the solvent n-methyl-2-

pyrrolidone (NMP) to obtain a slurry. The weight ratio of $LiCoO_2$:graphite:PVDF was 89:6:5. Yang et al.[6] have prepared a positive electrode by mixing the active material ($LiCoO_2$) with a binder (PVDF) and a conductive agent as a dry powder first, then dispersed the mixture in a solvent (NMP) to produce a slurry. They found that this mixing sequence can increase the cycle life of the LIBs. Recently, Bauer et al. [7] reported the fabrication of a positive electrode by mixing the dry powders of $LiNi_{1/3}Mn_{1/3}Co_{1/3}O_2$ (NMC) and conductive agent carbon black (CB, Super C65)) with a mixture of PVDF solution and a fraction of CB. The additional CB particles are associated with the binder and provide conductive paths in the electrode.

The key objective of this work is to determine the best predictors (measured during electrode fabrication) of final cell robustness and quality, thereby shortening subsequent development cycles by compressing the development and scale-up phases. After the first round of coin cell results, a second iteration will be repeated using coin cells with more replicates per condition. We are focusing the work here on how the battery electrodes are made, and the key mission is to make the slurry uniform and coat it evenly.

Immersion precipitation (IP), a demixing process, is one of the phase inversion methods which has been widely used to make commercial porous polymeric membranes [8, 9]. Recently, the IP method has also been used to make polymer electrolyte membranes and separators for LIBs [10-12]. The demixing process can be achieved by solvent and non-solvent phase exchange in multicomponent mixtures [13]. The IP method can replace the wet slurry-based manufacturing process by capturing the toxic and expensive organic solvent and reduce the manufacturing time and the energy cost for drying.

Solvent-free coating process using dry particles is an alternative solution to replace the wet slurry-based manufacturing process, as it eliminates the cost of solvents as well as the cost of their removal and recovery. Solvent-free manufacturing has been achieved through pulsed-laser deposition, a method in which a laser is focused on to-be-deposited electrode components. This technique requires high vacuum (10^{-6} Torr) and high annealing temperature (>600 ºC), producing only thin films of cathode material (<500 nm) [14, 15] and is therefore impractical for large-scale electrode fabrication. While radio frequency (RF) magnetron sputtering can be used with lower temperature substrates (350 ºC), it requires expensive instrumentation and inert atmospheres, and again is impractical for large-scale electrode fabrication [16].

Another method of dry-powder coating is electrostatic spray deposition (ESD), a solvent-free technology that has been used in coating industries for over 30 years to create decorative and functional paints and coatings. This method eliminates the release of volatile organic compounds (VOCs), reduces energy consumption, increases paint material transfer efficiency, and improves painted-surface quality. In ESD, particles are charged as they pass through a charging gun and are deposited onto a grounded surface [17]. This method can be used on large particles and is scalable, offering high deposition rates onto large surfaces [18].

This dissertation focuses on understanding and improving manufacturing processes for LIBs electrodes. The content of this dissertation includes:

(1) Establish a correlation between key process parameters with battery durability and quality (consistency), thus enabling battery manufacturing process optimization.

(2) Develop a method for establishing above correlation between process parameters and battery attributes that can be applied to other battery chemistries.

(3) Quantify the effects of the mixing process on finished battery quality through rigorous application of mixing theory, rheology and surface morphology.

(4) Optimize the slurry mixing step of lib manufacturing. Specifically, quantitative correlations will be established between process parameters and slurry material characteristics and LIB performance and durability, leading to tangible battery cost savings due to over-design reduction.

(5) Develop a low-cost and environmentally friendly manufacturing method to fabricate LIBs.

(6) Demonstrate the preparation of high performance LIB cathodes by laboratory scale solvent-free dry powder coating and immersion precipitation processes.

Chapter 1 gives a brief introduction and the purpose of this dissertation, covering the literature review of LIBs, electrochemical mechanisms of LIBs, positive electrode, negative electrode, the cost and environmental effect, electrostatic spray method, immersion precipitation method, and motivation and goals of this dissertation.

Chapter 2 discusses the experimental study of using different mixing sequences to improve the performance and durability of lithium-ion batteries. Chapter 3 reports a new method of making LIB electrodes by adapting an IP technology commonly used in membrane manufacturing. Chapter 4 reports a solvent-free dry powder coating process for making $LiNi_{1/3}Mn_{1/3}Co_{1/3}O_2$ (NMC) positive electrodes in LIBs. Chapter 5 summarizes the conclusions and future research work.

1.1 Lithium-Ion Batteries

The Li-ion cell consists of positive (cathode) and negative (anode) electrodes that are separated by a polymeric separator and organic electrolyte. The electrodes fabrication involves the mixing of active material, polymer binder, and conductive agent in a solvent. The cathode and anode composite materials are cast on aluminum and copper foil current collector, respectively.

A polymeric film (separator) such as polyethylene (PE) or polypropylene (PP) [19] is immersed in the electrolyte and separate the anode from the cathode to prevent short circuit of the electrochemical cells. The separator should be porous, electrolyte permeable, mechanically durable, ionically conductive, electronic insulator, and good thermal and chemical stability to produce a battery with good performance, cost, safety, and durability [20].

The electrolyte consists of organic solvent and lithium salts such as ethylene carbonate (EC) and $LiPF_6$ respectively. The pathway of the Li-ion has to be provided by the electrolyte. It should be ionically conductive, chemically stable, electronically insulator, and able to transfer the Li-ions between the electrodes [21]. Several research groups have proposed additives to the electrolyte to improve lithium transfer and the rate performance of the Li-ion battery such as vinylene carbonate (VC) [22] and fluoroethylene carbonate (FEC) [23].

1.2 Electrochemical Mechanisms of Li-Ion Batteries

The electrochemical potential difference between the positive and negative electrodes leads to the movement of Li-ions during charge/discharge process. Assume a full cell battery consists of graphite as the negative electrode and $LiCoO_2$ as the positive electrode as shown in Figure 1.1. During charging, the Li-ions move from the

cathode through the separator and organic liquid electrolyte and insert into the anode. During discharging, the direction of the Li-ion movement will be reversed, and the chemical energy is converted into electrical energy, providing power. The electrode reactions are [24, 25]:

$$\text{Negative electrode: } C + xLi^+ + xe^- \leftrightarrow Li_xC$$

$$\text{Positive electrode: } LiMO_2 \leftrightarrow Li_{1-x}MO_2 + xLi^+ + xe^-$$

$$\text{Overall: } C + LiMO_2 \leftrightarrow Li_xC + Li_{1-x}MO_2$$

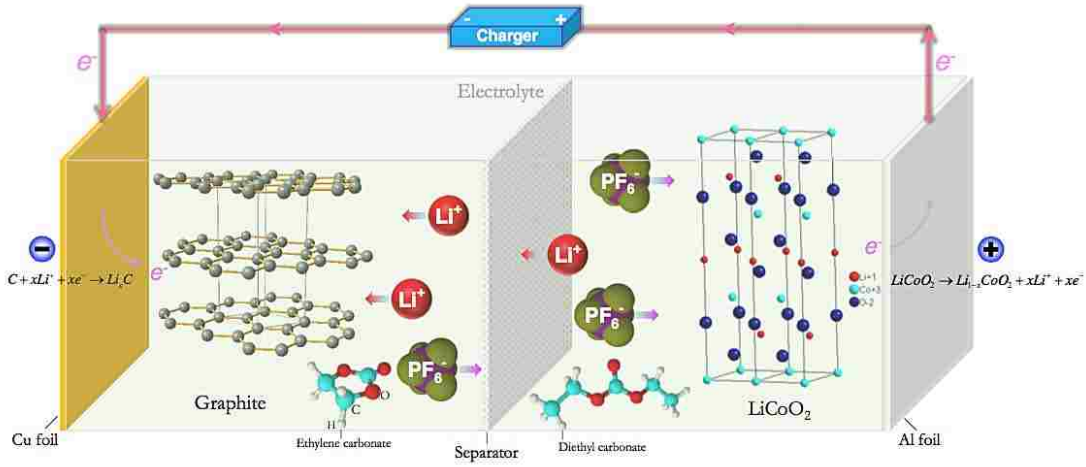

Figure 1.1: Schematic of the principle of the Li-ion battery during charging [25].

The energy released during discharge/charge can be calculated using the following equation [26, 27]:

$$Energy = \int V\, dq$$

where V and q are the voltage and the amount of charge transferred respectively. The chemical potential difference between the positive and negative electrodes is the LIB cell voltage [3].

The theoretical open circuit voltage (OCV) (E) is determined by the following equation [3, 25]:

$$\Delta G = -nFE$$

where G is the free energy, n is the charge number of the electrons, and F is Faraday constant.

1.3 Positive Electrode

The cathode electrode fabrication involves the mixing of active material, polymer binder, and conductive agent in a solvent. To achieve energy, power, and life performance, most research efforts of the last 20 years have been devoted to the aspects of developing new structures and new compositions of the electrochemically active material (AM), engineering of their particle size, morphology, surface coatings, and better understanding of their electrochemical behavior. Layered, olivine, and spinel are three main structures of lithium metal oxide. The layered Li metal oxide is in the form of $LiMO_2$ and M could be Mn, Co, or Ni [28]. The structure and the potential depending on the concentration and the type of the metal component [28].

$LiCoO_2$ is a layered material used in most commercial positive LIB electrodes, and it has good cycling and high voltage (~ 4 V). Due to the chemical reaction of the Co with the electrolyte which changed the structure, the capacity of $LiCoO_2$ usually drops from 274 mAh g^{-1} to 140 mAh g^{-1} as the theoretical and practical capacity respectively. The strong influence in the structure, toxicity, and cost of Co leads to studies of new material such as $LiNi_xMn_yCo_zO_2$. The NMC can deliver capacity of 150 mAh g^{-1} at voltage window between 2.5 V to 4.2 V [29] with very good performance, and the composition of x, y, and z can be varied for different purposes. Increasing the amount of Ni and Mn can lower the cost but lower the rate capability at a high state of charge [29].

1.4 Negative Electrode

To prepare negative electrodes, active material, binder, conductive agent, and solvent are mixed together to form a slurry that is cast on Cu foil. The most commonly used active material is graphite with the layered structure. Graphite has a theoretical

capacity of 372 mAh g^{-1} [30]. During charge/discharge, lithium is stored between the carbon layers [31]. Styrene butadiene rubber (SBR), carboxymethyl cellulose (CMC), and PVDF are the most commonly used binders in graphite anode to bond the particles together and adhere the prepared composite onto Cu foil [32]. Moreover, carbon black is the commonly used conductive agent to increase the electrical conductivity and improve the cycling efficiency.

1.5 Cost and Environmental Effect

Developing a low-cost and environmentally friendly process to fabricate batteries for electrification of the transportation sector is important in manufacturing of LIBs. The Department of Energy suggests that energy-storage systems must meet a cost target of \$125 kWh^{-1} to meet the requirements for widespread adoption, which would require a three- to four-fold reduction in system costs [33]. By 2020, it is assumed that more than 14 million hybrid and electric vehicles will be on the road, and the price will drop significantly. Today, most electricity used is generated by nonrenewable energy [34]. Using LIBs driven vehicles instead of gasoline driven cars requires very fast recharging in about 10 to 15 minutes, materials availability [35], safety, and lower production cost.

The cost of the battery consists of the cost of the material and production as following: (1) positive and negative electrodes material such as active material, conductive agent, binder, current collector, and solvent, (2) separator, (3) electrolyte, (4) cell packing, and (5) labor and overheads cost [36]. To reduce the cost and environmental impact, several approaches have been investigated such as using water-based solvent [37] or completely dry manufacturing processes to eliminate the toxic and costly NMP solvent in electrode fabrication [2], using new materials [38], using

bio-derived materials [4], reducing electrode drying time [39], reducing production cost [40], and improving battery performance [37, 38, 41]. During heat drying, the NMP will consume a large amount of energy to evaporate. The NMP vapor must be captured instead of being released to the atmosphere. Eliminating the release of VOCs and reducing energy consumption will eliminate the cost of solvents as well as the cost of their removal and recovery.

Quantitative correlations will be established between process parameters, material characteristics and LIB performance and durability, leading to tangible battery cost savings through over-design reduction, shortened development time, reduced cell-to-cell variation, and lower warranty costs. Assuming cell to cell variation reduction of 2-3% resulted from described process optimization, the associated de-rating (overdesign to account for variation and degradation) amount could be reduced.

Replacing the conventional wet slurry-based electrode manufacturing process with a lower cost, higher throughput, and more environmentally friendly dry powder coating process will lower electrode fabrication cost by 90%, lower VOCs emission to zero, and reduce electrode drying time from hours to minutes.

The high cost, toxicity, safety hazards, and chemical instability of the traditional electrode materials, and the overheating during quick charge lead the researchers to investigate new materials, environmentally friendly elements, and new manufacturing processes to develop new, cheap, and powerful LIB electrodes [36, 42, 43].

1.6 Immersion Precipitation (IP) Method

IP, a demixing process, is one of the phase inversion methods which has been widely used to make commercial porous polymeric membranes [8, 9]. Recently, the IP method has also been used to make polymer electrolyte membranes and separators for LIBs [10-12]. The demixing process can be achieved by solvent and non-solvent phase

exchange in multicomponent mixtures [13]. In this process, the polymer solution is cast on a suitable support which is then immersed into a non-solvent bath [8, 13]. Two mechanisms would operate as soon as the cast homogeneous polymer solution is exposed to a non-solvent bath: mass transfer and phase separation, resulting in transferring of the solvent molecules from the polymer solution to the non-solvent bath. As a result, a two phase mixture consisting of a solid polymer matrix and a non-solvent phase would grow and develop. After removing the non-solvent phase, porous structure forms [44-46]. The structure and the porosity of the solid porous polymer film depend on the properties of the materials and the processing conditions such as the composition of the materials, the concentration of polymer in solution, the pH and the temperature of the non-solvent bath, and the exposure time in the gelation bath [47-50].

1.7 Electrostatic Spray Method

Electrostatic spray painting is one of the applicable methods used recently in a wide range of applications [51-53]. This method is based on the voltage difference between the surface being painted and the electrostatic gun, which has the coated material. To create the voltage difference, an electrical charge is applied to the coated material while the target material is grounded or vice versa where the target surface is charged and the spray gun is grounded [54]. In other words, either the spray gun or the target surface must be negatively charged while the other side will be positively charged. The different charges between the spray gun and the target surface create an electric field, which will help to transfer the coating material from the spray gun to the target surface. The electric field helps to create the electrostatic force, which will work to transfer the charged coating material from the gun to the target surface creating high transfer efficiency. The high transfer efficiency is created because of the strong

electrostatic force between the gun and the target surface, which overcomes other barrier forces such as the momentum and airflow, which works to deviate the atomized materials from the electrostatic gun [54-56].

Some factors determine the electrostatic force strength such as the particle size and the particle moving speed. The high transfer efficiency created by the electrostatic force helps direct the atomized coating materials, which reduces the over-spraying and by that reduces the cost. Moreover, high efficiency also works to form a uniform coating, reduce the VOC and lower the cost of disposal of hazardous wastes [43].

1.8 Motivation and Goals

Optimization efforts in the battery industry typically focus on formulation modification and do not harness the vast potential of mixing science. Understanding of the various stages of mixing (wetting, dispersion, stabilization), as well as key underlying interfacial and surface phenomena, offers a powerful optimization tool that can lead to superior product quality and reproducibility. Deficits in this understanding are of particular detriment in the battery industry where the specific challenges of high-cost, rheological complex, non-Newtonian, and temperature sensitive dispersions would most benefit from a rigorous, first-principles approach.

This work brings together two “spheres” of knowledge: (1) industrial mixing, structured liquids, rheological complex liquids on the one side together with (2) lithium-ion slurry manufacturing on the other side. The former body of knowledge has seen more rigorous application in other coatings (pigments), pharmaceutical and detergents industries, but has been less actively exploited in lithium-ion applications, and thus holds promising opportunities. Figure 1.2 shows the project strategy of using different mixing sequences. The properties of the slurry made here will irrevocably

determine most aspects of the cell's electrochemical performance, longevity and critically the reproducibility of these attributes.

The objectives and motivation of using different mixing sequences to prepare LIBs are: (1) quantify link between electrode slurry mix parameters and finished product quality using mixing theory, rheology, morphology, conductivity, and mechanical and electrochemical properties, (2) identify slurry characterization techniques that are the best predictors of final battery robustness, (3) improve durability and product quality, shorter development times, and reduce over-design and cost, and (4) establish groundwork for more focused work on subset of sequences and investigate which sequences are best and why.

Developing and demonstrating a low-cost and environmentally friendly manufacturing process to fabricate batteries for electrification of the transportation sector by using solvent-free dry powder coating process and immersion precipitation method for manufacturing of cathodes in LIBs. Because of NMP's high cost and potential as an environmental pollutant, solvent recovery is necessary in commercial applications, adding further costs to battery fabrication [40]. The typically used NMP solvent is toxic, flammable, and expensive [57, 58]. During heat drying, the NMP will consume a large amount of energy to evaporate. The NMP vapor must be captured instead of being released to the atmosphere. The capturing of the toxic and expensive organic solvent is one of the motivations for this work. A further motivation is to reduce the manufacturing time and the energy cost for drying.

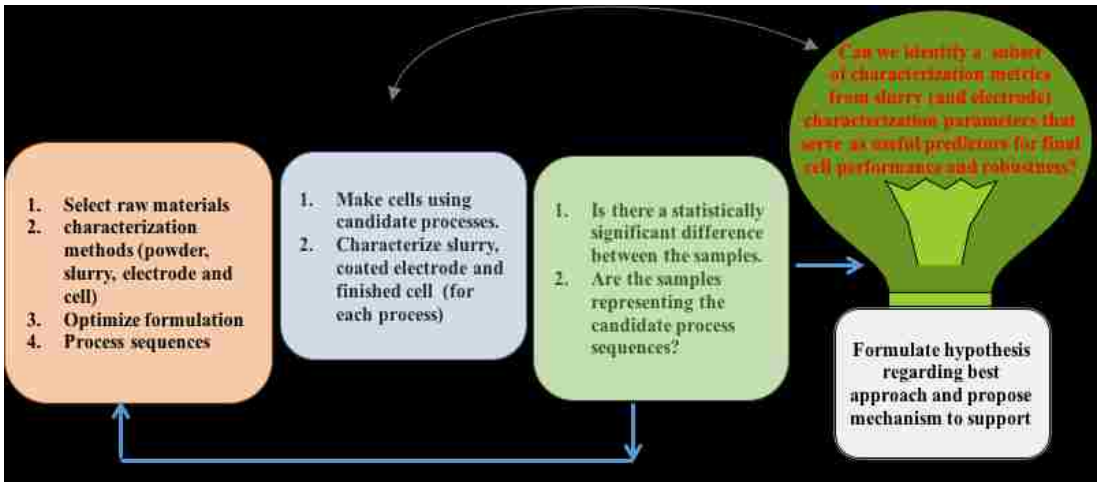

Figure 1.2: Project strategy of using different mixing sequences to improve the performance and durability of Li-ion batteries.

Chapter 2 Using Different Mixing Sequences to Improve the Performance and Durability of Lithium-Ion Batteries

2.1 Introduction

Secondary Lithium-ion batteries (LIBs) have been widely used as the most popular rechargeable energy storage and power sources in today's portable electronics, electric vehicles, and plug-in hybrid electric vehicles [59-62]. The market for LIBs has increased over the last decade because of LIBs' high energy density, good rate of charge and discharge, high voltage, reliability, long cycle life, and design flexibility [24, 63-65].

In the last three decades, a lot of work has been done to improve the performance and durability of LIBs, including 1) exploring new compositions, morphologies, particle sizes, and surface coatings; and 2) using various methods of characterization to understand the electrochemical behavior [66].

The first step in LIBs manufacturing is mixing high solid-content slurries for both the positive and negative electrodes. For a given electrode system, which consists of active material, polymer binder, carbon black, and solvent, the mixing process parameters, such as the order of introducing materials (sequence) [67] and the intensity and duration of each mixing step, can strongly affect the subsequent steps in battery manufacturing, including coating and drying processes [68]. The mixing process is, therefore, critical in determining the quality and electrochemical performance of the battery [69]. Different mixing sequences have been investigated to produce well-mixed slurries for various electrode materials. Kim *et al.* [5] found that the best capacity and stability of charge and discharge cycle can be obtained by dry mixing the active materials ($LiCoO_2$) and conductive agent (Graphite) then adding the solution of the binder (PVDF) and the solvent (NMP) to obtain a slurry. The weight ratio of

$LiCoO_2$:graphite:PVDF was 89:6:5. Yang *et al.* [6] have prepared the positive electrode by mixing the active material ($LiCoO_2$) with a binder (PVDF) and a conductor as a dry powder first, then dispersed the mixture in a solvent (NMP) to produce a slurry. They found that this mixing sequence can increase the cycle life of the LIBs. Recently, Bauer *et al.* [7] reported the fabrication of a positive electrode by mixing the dry powders of $LiNi_{1/3}Mn_{1/3}Co_{1/3}O_2$ (NMC) and conductive agent carbon black (Super C65)) with a mixture of PVDF solution and a fraction of CB. The additional CB particles were associated with the binder to provide conductive paths in the electrode.

Optimization efforts in the battery industry typically focus on formulation and modification of electrode composition and structure with less emphasis on harnessing the vast potential of mixing science and technology. Understanding of the various stages of mixing (wetting, dispersion, stabilization), as well as key underlying interfacial and surface phenomena, offers a powerful tool that can lead to superior product quality and reproducibility. By establishing a correlation between mixing parameters, slurry material characteristics, and finished battery performance and durability, the mixing process parameters can be optimized.

We have investigated four mixing sequences to prepare the slurries for making the positive electrode. Here, we report the structure, performance, and durability of positive electrodes made from these slurries.

2.2 Experimental

2.2.1 Slurry preparation

The cathode materials were purchased from several suppliers given in Table 2.1. Four mixing sequences have been used to prepare the slurries of the positive electrodes. Sequence 1 consists of three mixing steps, as shown in Figure 2.1a. In the

first step, the poly(vinylidene difluoride) (PVDF) was dissolved in a *N*-methylpyrrolidone (NMP) solvent by using a planetary mixer-deaerator (Mazerustar KK-50S, Kurabo). The Mazeruster planetary mixer has different levels of rotation and revolution, and the maximum processing capacity of this machine is 250 g. To dissolve PVDF in NMP completely, three cycles were used to mix the samples at 680 rpm rotation and 1140 rpm revolution with a total time of 360 seconds. The second mixing step was adding carbon black (CB) (Super p C65) to the binder solution and mixing at 4000 rpm for 45 min. The third mixing step was adding active material NMC to the mixture and blending at 4000 rpm for 1h. In the second and third mixing steps, a homogenizer (Polytron PT 10-35 GT) was used. The homogenizer has a maximum speed of 30,000 rpm and volume of 0.1 to 10,000 ml.

To prepare a slurry using mixing sequence 2 as shown in Figure 2.1b, the dry powders of NMC and CB were pre-mixed using the planetary mixer. The mixture was then added to the binder solution and blended at 4000 rpm for 1h in the homogenizer. The binder solution was prepared as mentioned in the first mixing step of sequence 1.

Table 2.1 The materials, chemical names and abbreviations, and supplier of the cathode electrode.

	Materials	**Chemical Name and Abbreviation**	**Supplier**
Cathode			
	Active Material	NMC $LiNi_{1/3}Mn_{1/3}Co_{1/3}O_2$, 111 type	UMICORE
	Binder	PVDF (kf 1100) Poly(vinylidene dfluoride)	KUREHA AMERICA
	Conductive Carbon	Carbon Black (Super p C65)	TIMCAL
	Solvent	NMP *N*-Methyl-2-pyrrolidone	BASF

For sequence 3 shown in Figure 2.1c, the first and second mixing steps were the same as sequence 2 steps. The third step was adding NMP solvent to the pre-mixed (NMC and CB) and mixing the mixture in the planetary mixer. The final step was to add the binder solution to the mixture as a fourth mixing step at 4000 rpm for 1h.

Sequence 4 was prepared using the steps shown in Figure 2.1d. CB was mixed with NMP to wet the CB nanoparticles first in the planetary mixer. The CB/NMP mixture was then mixed with the PVDF solution which was prepared using the same mixing steps as in sequence 1. Finally, NMC was added and blended using the homogenizer at 4000 rpm for 1 h.

Two cycles in the planetary mixer were used to blend the materials in the second step of sequence 2 and second and third of sequence 3 and 4 at 680 rpm and 1140 rpm for rotation and revolution respectively with total time of 600 s. The amount of NMP was different for each sequence to adjust the viscosity of the final slurries, while the weight ratio (92 NMC:4 CB:4 PVDF) was the same.

2.2.2 Electrode preparation

The prepared slurries were rested in a vacuum chamber for 5 min to remove the gas bubbles formed during mixing then cast onto a 15 μm thick aluminum foil using a compact tape casting film coater with dryer and vacuum chuck (MTI Corp.) at a casting speed of 0.2 m/min. The thickness of the coated layer was adjusted using a doctor blade of a specified gap to control the mass loading of the electrodes. The coated electrodes were pre-dried at the ambient temperature overnight then calendered in a compact electrical rolling press (MTI Corp.) with adjusted clamping force to control the packing density, porosity, and adhesion of the electrode [70]. The calendered electrodes were punched to 12 mm diameter discs using a Precision Disc Cutter (MTI Corp.) and placed

in a vacuum oven at 130°C for 12 h then transferred directly to a glove box for cell assembly.

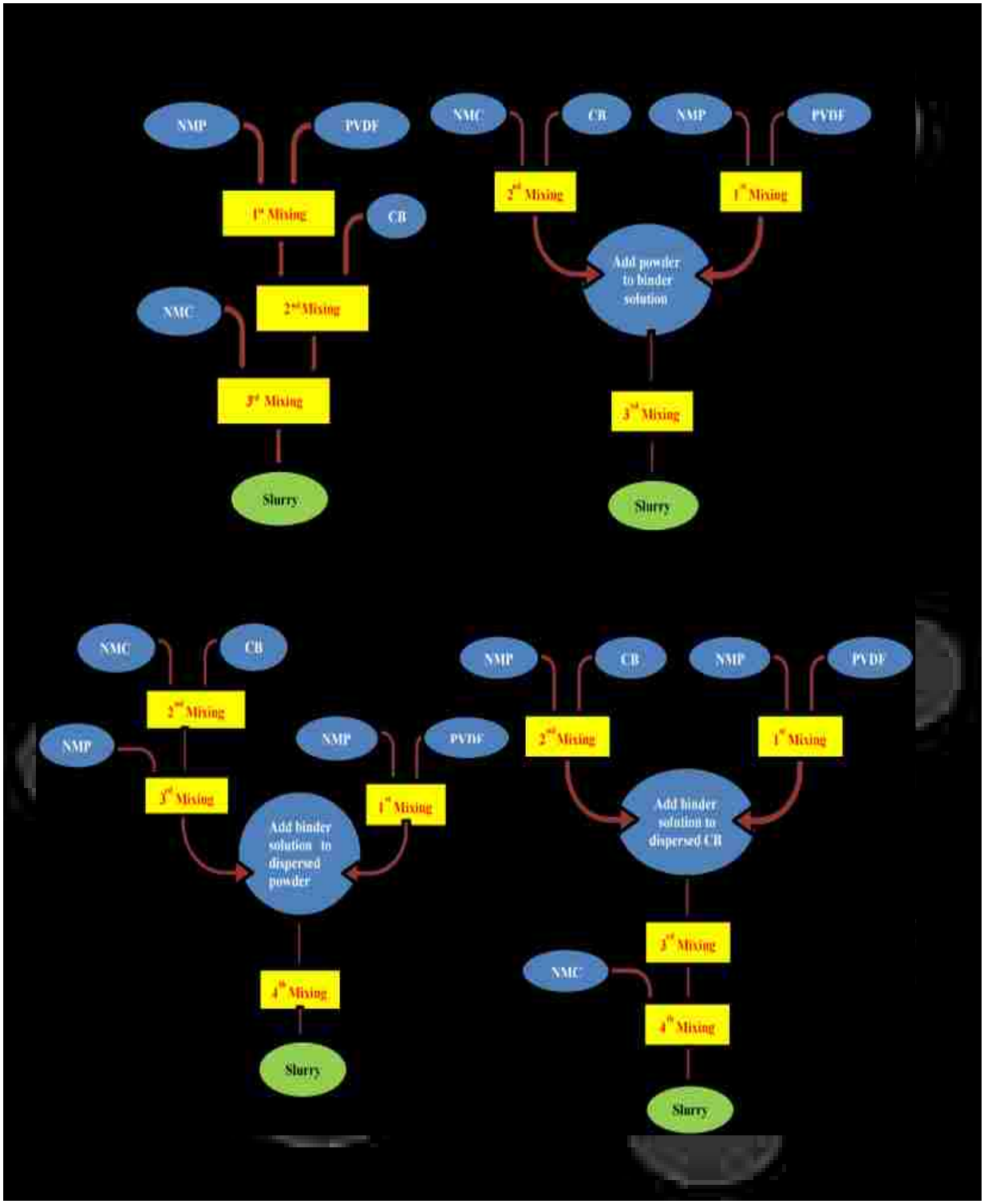

Figure 2.1: Illustration of the mixing sequences for preparing the electrode slurries, (a) sequence 1, (b) sequence 2, (c) sequence 3, and (d) sequence 4.

2.2.3 Characterization

2.2.3.1 Rheology Measurement

Rheological tests were carried out in both steady state flow and oscillatory modes in an AR-1000 rheometer (TA instrument) to help understand the interaction between binder, active materials (AM), and conductive agent (CA), as well as the dispersion of the agglomerate carbon [71]. Rheological measurements can also help achieve the correct viscosity of the slurries before casting them onto the Al foil.

Freshly prepared slurries were measured in the steady state flow mode, followed by the oscillatory mode of measurements. From the oscillatory mode, complex viscosity (G*), storage modulus (G'), and loss modulus (G") were obtained over a range of frequencies. Prior to running the rheology test, two minutes of equilibrium were applied.

2.2.3.2 Morphology

The surface morphology and cross-section view of the electrodes were investigated using an Environmental Scanning Electron Microscopy (ESEM) with Energy Dispersive Spectroscopy (EDS) (Quanta, FEG 250). To prepare cross-section samples the following steps were used: (1) cut 12 mm diameter samples from the electrodes, (2) mount the sample in epoxy and leave it for 12 h for solidification, (3) cut the mounted sample after drying with diamond saw, (4) rough then fine polishing with sheet grinding silicon carbide, (5) clean the samples using ethanol and dry at room temperature, and (6) deposit gold on the surface and fold the sample with Cu tape to increase the conductivity.

2.2.3.3 Mechanical measurements

To compare the cohesion between electrode particles and the adhesion between the electrode film and current collector (Al foil), a NanoTest Vantage (Micro Materials Ltd) was used. In the micro-indentation, a grid of 4 x 4 indentations was used, and the spacing between indents was fixed at 250 μm to avoid the influence of neighboring indentation marks. The load was ramped until the depth reached 20 μm, and then unloaded. In the scratch test, a diamond indenter was lowered onto the sample by increasing the load as the indenter tip moves across the surface of the sample. The applied load was between 30μN-500 mN. The hardness and Young's modulus were calculated as a function of load using the Oliver-Pharr method [72].

2.2.3.4 Conductivity

The four-point resistivity and conductivity type measurement (Signatone) was used to measure the conductivity of a dry film electrode. The two outside probes were used to pass the current, while the two inside probes were used to measure the voltage difference [73]. To avoid the influence of the Al conductor, the slurry was cast onto a glass substrate. The average conductivity was calculated using [74].

$$\sigma_e = \frac{I}{4.532\ t\ V} \qquad 2.1$$

where σ_e is electronic conductivity, I is the current, t is the thickness of the film electrode, the number (4.53) is $\frac{\pi}{\ln 2}$, and V is the voltage.

2.2.3.5 Porosity and Packing Density

Electrode porosity is an important parameter for cell performance. The porosity of the dried laminate electrode without Al foil was determined according to the following equations [50, 75]:

$$\text{Electrode true density} = \frac{1}{\left(\frac{\text{Materials wt \%}}{\text{Materials density}}\right)} \quad 2.2$$

$$\text{Packing density} = \frac{\text{Calendered electrode weight loading}}{Electrode\ thickness} \quad 2.3$$

$$\text{Porosity} = 1 - \frac{\text{Packing density}}{\text{Electrode true density}} \quad 2.4$$

The wt% and the theoretical density of each material (active material (NMC), conductive agent (CB), and binder (PVDF)) are 4.8, 1.94, and 1.7 (g/cm^3), respectively.

The measurement of electrode thickness is critical due to its porous structure which influences the packing density and the performance of the Li-ion batteries. Measuring the thickness of the electrode film will help evaluate the uniformity of the electrode during casting. The laminate electrode thickness was measured using a digital micrometer with an accuracy of ±1 μm. The electrode film is punched into small discs with diameters 10 to 14 mm after totally dried and calendered. Attention should be paid during the measurements to avoid damaging the electrode film. More than 10 thickness measurements were performed at different spots to check the uniformity of the electrode, which is helpful to control the quality. Each electrode was weighted using METTER TOLEDO with 4 digits analytical scale.

2.2.3.6 Coin Cell Fabrication and Electrochemical Tests

Electrodes were tested in a coin cell type CR2025 (20 mm diameter and 2.5 mm thick) (Hohsen) using lithium metal as the counter electrode. The coin cells were assembled using an automatic coin cell crimper (KTE-20S-D, Hohsen) inside the glovebox (MB-20-G, MBraun). The glovebox was filled with argon, and the level of moisture and oxygen was less than 0.1 ppm. Pure lithium metal foils (99.9%, Sigma–Aldrich) were used as the counter electrode. The electrodes were punched to 12mm diameter discs by using precision disc cutters (MTI Corp.). Poly-propylene (Celgard 2400) was used as separators between the lithium foil and the cathode. The electrolyte was 1M LiPF6 in a mixture of ethylene carbonate/ ethyl-methyl carbonates (EC/EMC 3:7 by volume) with 2% vinylene carbonate (VC, BASF). To achieve good contact and obtain a uniform current distribution, a stainless steel spacer and spring were placed on Li metal. During the charging process, the lithium ion moves from the cathode (positive) into the anode (negative), while during discharge the movement is reversed. The electrolyte serves as a carrier to the lithium ions between the two electrodes [76]. The electrochemical performance of assembled half-cells was measured by multi-channel Bio-logic potentiostats (VMP-2) and (VMP-3) under galvanostatic mode at room temperature. Before starting the test, the coin cells were rested for 2 hours. The cyclic voltammetry tests were carried out at several rates of C/R (R in hour) between 3 V and 4.3 V with a constant voltage holding period at 4.3 V until the current dropped below C/20.

2.3 Results and Discussion

To achieve the capacity close to the theoretical capacity of NMC (150-200 mAh g^{-1}), the NMC, CB, and PVDF component with a weight ratio of 90:5:5 respectively were mixed together in a NMP solvent using the homogenizer at 4000 rpm for 1h. After preparing the slurry and casting on a current collector (Al foil), the electrode films were totally dried and assembled to coin cells. The long-term cycling performance was carried out at rates of 0.5C and 1C between 3 V and 4.3 V followed by constant voltage holding of 4.3 V with current limitation of 0.05C at the end of each charge and rate of 1C between 2.5 V and 4.2 V without hold. The cells with low C-rate (0.5C) and holding during charge at C/20 as shown in Figure 2.2 have the highest specific capacity (158 mAh g^{-1}) and stable cycle life up to 210 cycles.

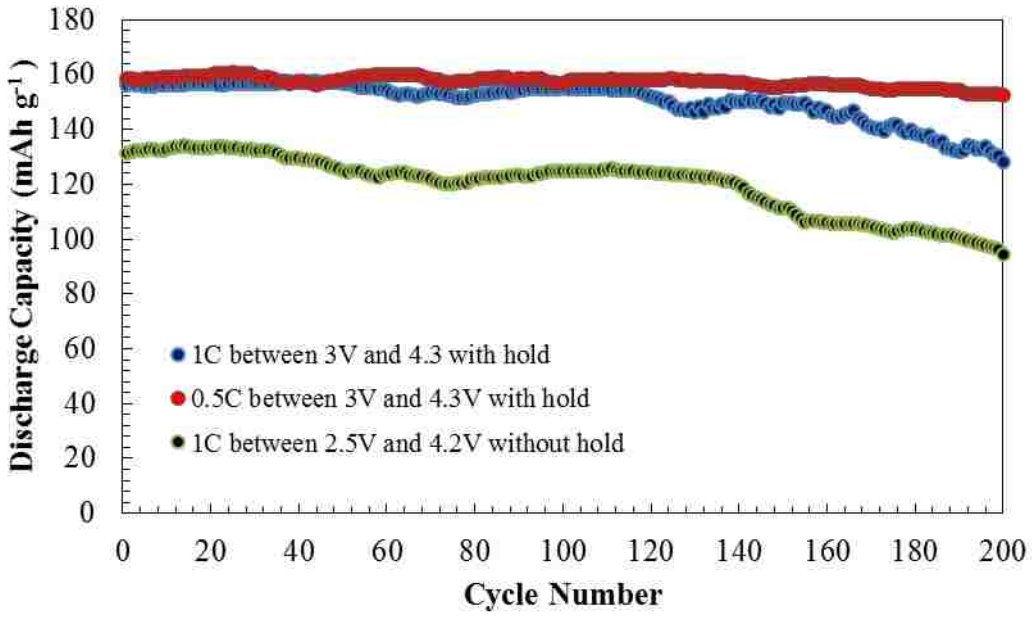

Figure 2.2: Potential vs. capacity profiles of electrodes with C-rates of 1C and 0.5C and voltage window from 3 V to 4.3 V followed by constant voltage holding with current limitation of 0.05C, and C-rate of 1C between 2.5 V and 4.2 V without holding step.

To optimize sequence 1 and achieve the target loading (~ 2 mAh cm^{-1}) with high specific capacity, several electrode batches, coating gaps, and amount of NMP solvent were made, while the weight ratio, mixing time, and mixing speed were the same. At 200 µm initial blade gap, the theoretical capacity of NMC (160.69 mAh g^{-1}) and the loading level of (2 mAh cm^{-2}) have been achieved as shown in Table 2.2 sample 2. The cells were charged and discharged between 3.0 V and 4.3 V followed by constant voltage holding with current limitation of C/20 at the end of each charging step.

Table 2.2 Initial blade gap casting, the mass of NMC and NMP, loading, and the specific capacity of different samples made from different batches.

Samples	Initial blade gap (µm)	Coated electrode thickness (µm)	Mass of the electrode (mg)	Amount of NMC (g)	Amount of NMP (g)	Loading	
						Weight (mg/cm^2)	Calculated capacity (mAh/cm^2)
1	127	80	11.88	2	2.5	15.12	2.13
2	200	80	11.20	4	4	14.26	2
3	100	50	6.47	6	5	8.32	1.16
4	100	50	6.25	6	5	7.95	1.12
6	185	50	5.78	2	3	7.36	1.04
7	185	50	5.78	2	3	6.19	0.98

The porosity and packing density do not seem to depend on mixing time, but are strongly affected by calendaring as shown in Table 2.3. Figures 2.3a and b show the discharge capacities at various current densities 0.2C, 1C, 10C, and 1C for the electrodes prepared by different mixing times with calendering and without calendering process. The mixing time and calendering process have a strong influence on capacity at the high C-rate of 10C. However, the capacity *vs.* cycle number result shows that the samples with (30 min) mixing time have a higher specific capacity over 90 cycles, while the samples with longer mixing time (90 min) have lower capacity retention. The

calendered electrode shows more degradation than the ones without calendering. The specific capacity decreases by redusing the porosity % which affect the volume change of the NMC during lithiation and delithiation [77] .

Table 2.3 Porosity, packing density (P.d), loading, and thickness of electrode samples that prepared by different mixing time with and without calendering process.

Samples	P.d (g/cm^3)	Porosity (%)	Loading (mAh/cm^2)	Thickness (µm)
Without Calender				
(30min)	1.80	58	1.94	71
(60min)	1.65	61	2.08	83
(90min)	1.69	60	2.03	79
With Calender				
(30min)	2.71	36	2.06	50
(60min)	2.60	39	2.03	52
(90min)	2.64	38	1.99	49

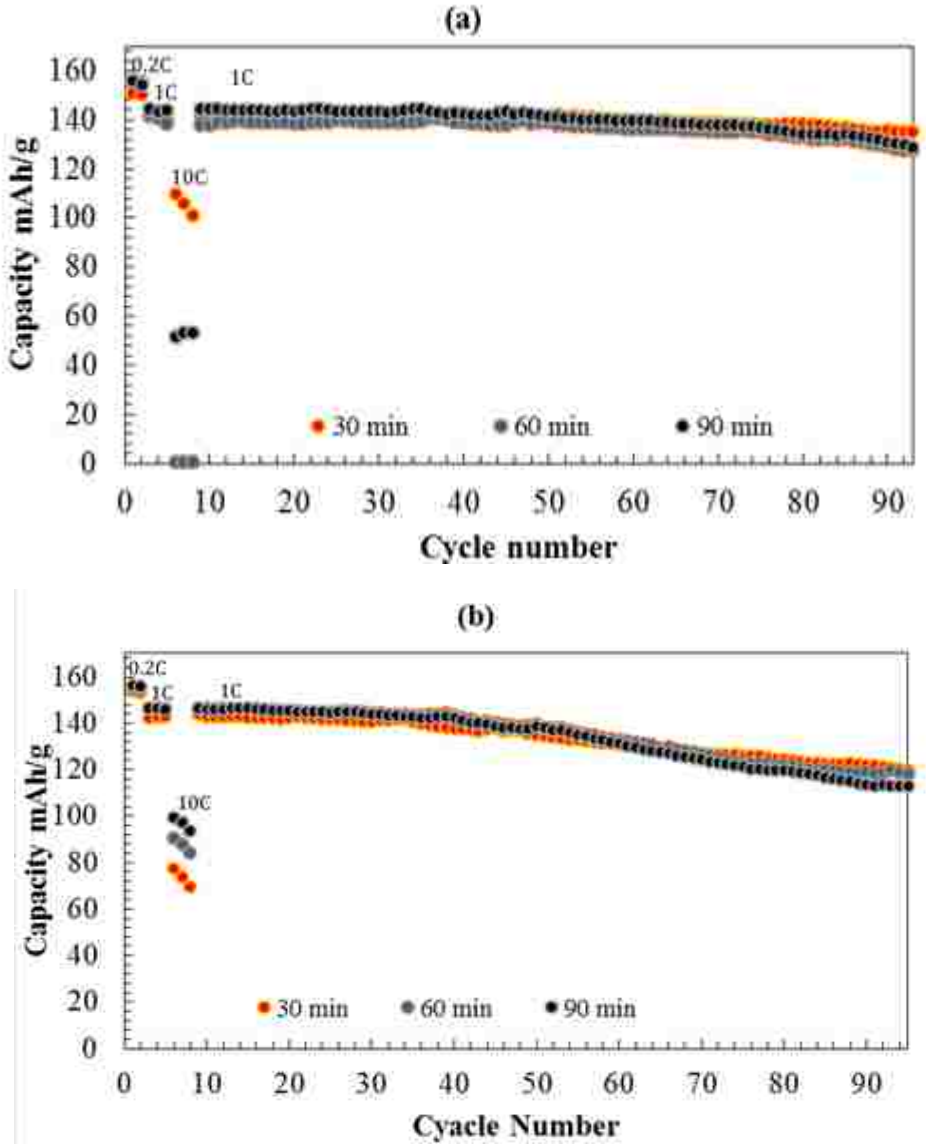

Figure 2.3: Discharge specific capacity at a variable charging rate of 0.2C, 1C, 10C, and 1C of electrodes made by different mixing times in the voltage range from 3 V to 4.3 V followed by constant voltage with current limitation of 0.05C at charging step: (a) without calendering, (b) with calendering.

To identify each material in the component electrode (NMC, CB, and PVDF), SEM images in Figure 2.4a and b were taken for the samples prepared by mixing NMC with the binder solution and dried at 130 °C for 12 h. The NMC in secondary particles has irregular morphology [78]. Figure 2.4c shows the distributions of CB in the binder solution after drying in a vacuum oven at 130 °C for 12 h.

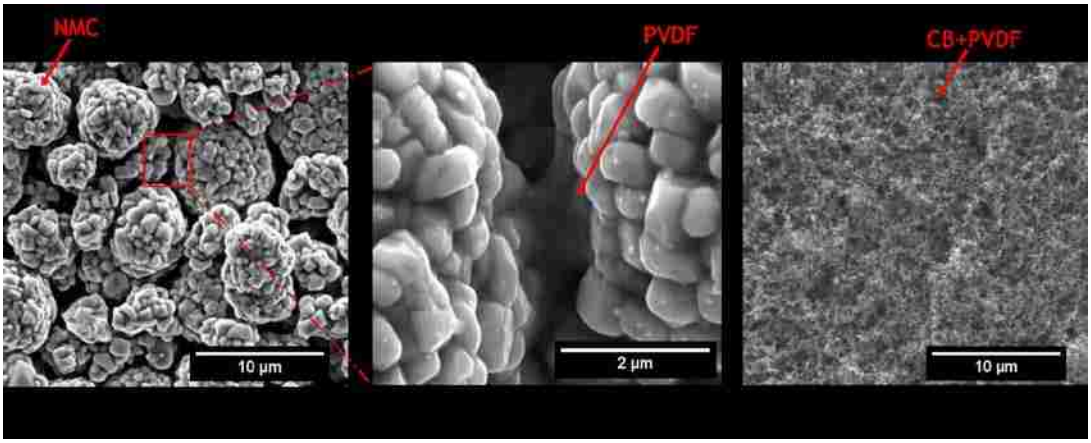

Figure 2.4: The scanning electron microscopy (SEM) images of the films that cast and dried at 130 C for 12 h; (a) NMC and PVDF, (b) high magnification of NMC and PVDF, (c) CB with PVDF.

Electrodes of several film thicknesses have been made to study the effect of the gap spacing on the mass loading, porosity, and packing density of the prepared electrodes. The electrodes were dried in vacuum oven at 130 °C for 12 h and calendered with 40 µm calender machine gap. The electrodes thickness, loading, and packing density increased with increasing the gap spacing, while the porosity decreased as shown in Table 2.4.

Table 2.4 Coating gap, thickness, porosity, packing density (P.d), and loading of the electrodes with various coating blade gap.

Coating Gap (µm)	Thickness (µm)	P.d (g/cm^3)	Porosity (%)	Loading (mg/cm2)
140	41	2.3	45.5	9.5
170	52	2.5	39.6	13.5
200	53	2.6	39.8	13.6
230	55	2.7	36.1	14.8

Long-term cycling of the electrodes made with gap spacing 140, 200, and 230 µm at C-rate of 0.2C, 1C, 10C, and 1C is shown in Figure 2.5. The initial capacity (157 mAh g^{-1}) of the 200 µm casting gap electrode was higher than the capacities (155 mAh

g^{-1}) and (150 mAh g^{-1}) of 140 µm and 230 µm electrodes, respectively. At low and high rates the 200 µm cast electrode has a better capacity than the other electrodes.

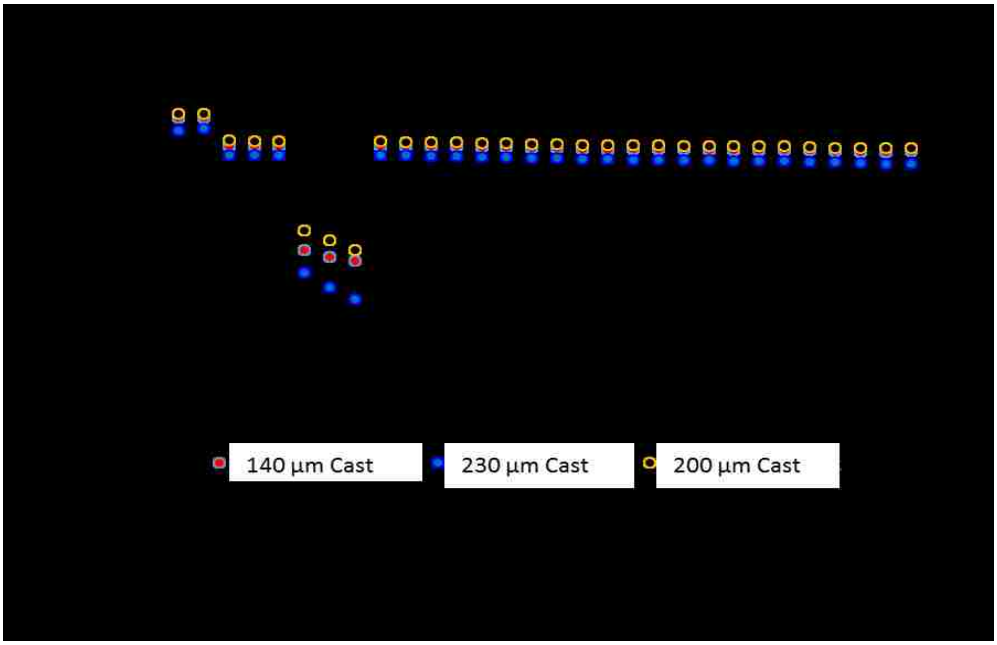

Figure 2.5: Rate capability of electrodes with different coated gap thickness (140, 200, and 230 µm) at C-rate of 0.2C, 1C, 10C, and 1C in a half-cell with 3 V and 4.3 V followed by constant voltage with current limitation of 0.05C at charging step.

The cell-to-cell and batch-to-batch reproducibility are critical in many applications since a battery pack consists of hundreds or thousands of cells. A pack's performance is limited by its weakest cell. If cell-to-cell variation can be reduced, less overdesign is required which can lead to the elimination of one or more cells per pack without impacting performance. Two batches of electrodes were prepared using the same conditions and studied the viscosity and electrochemical performance.

In contrast to a Newtonian fluid such as water and an elastic-plastic material such as steel, many materials and notably structured liquids, such as battery slurries, are viscoelastic. Storage modulus relates to the elastic portion, and the loss modulus relates to the viscous portion of viscoelasticity [79, 80]. The steady-state flow tests were used to obtain the shear stress and shear rate of the slurries. Oscillatory measurements were used to obtain more information about how the particles disperse and when the

sedimentation will occur [81]. Figure 2.6a shows that we can achieve the same viscosity of the slurries at a shear rate between (3 to 8 s^{-1}), and the slurries have shear thinning behavior. Figure 2.6b shows the result of frequency sweeps using oscillatory shear measurements. The storage modulus (G′) dominates over the loss modulus (G"), which suggests that the slurries are gel-like rather than liquid-like.

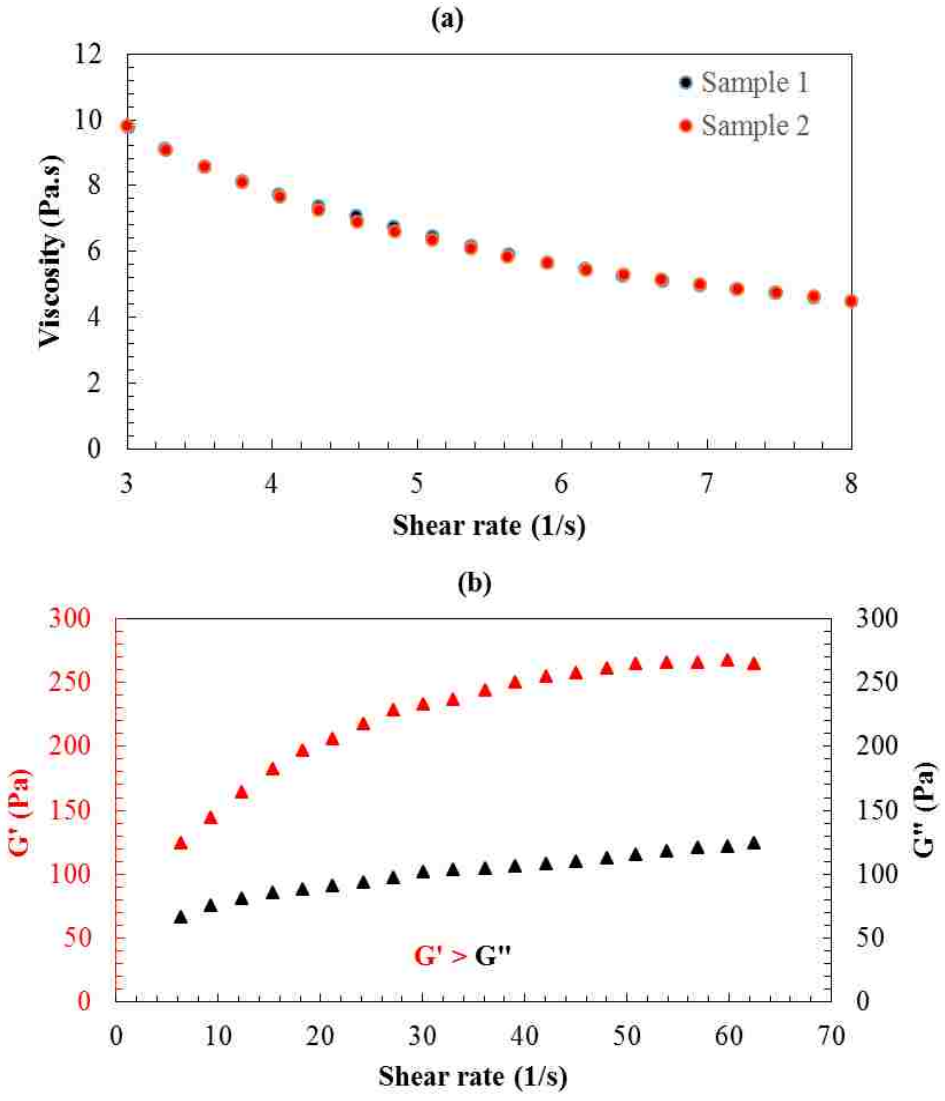

Figure 2.6: Rheology measurements using Flow test of viscosity as a function of shear rate between 3 s-1 to 8 s-1 (a), and oscillatory shear measurements as a function of frequency sweeps (b).

Statistical analysis using ANOVA was carried out for some samples after cutting them to discs and measuring the mass of the coated electrode as shown in Figure 2.7. We found the P-value of 0.2067 (Table 2.5) which indicates that there is no significant difference between the samples.

Two batches of electrodes were prepared under the same condition, and coin cells of three samples from each batch were used to test the electrochemical properties. The cycling performance at different C-rates rate (0.2C, 1C, 10C, and 1C) in Figure 2.8 shows that the samples have almost the same capacity during charge and discharge at various current rates. The results approved that the cell to cell and batch to batch were reproducible.

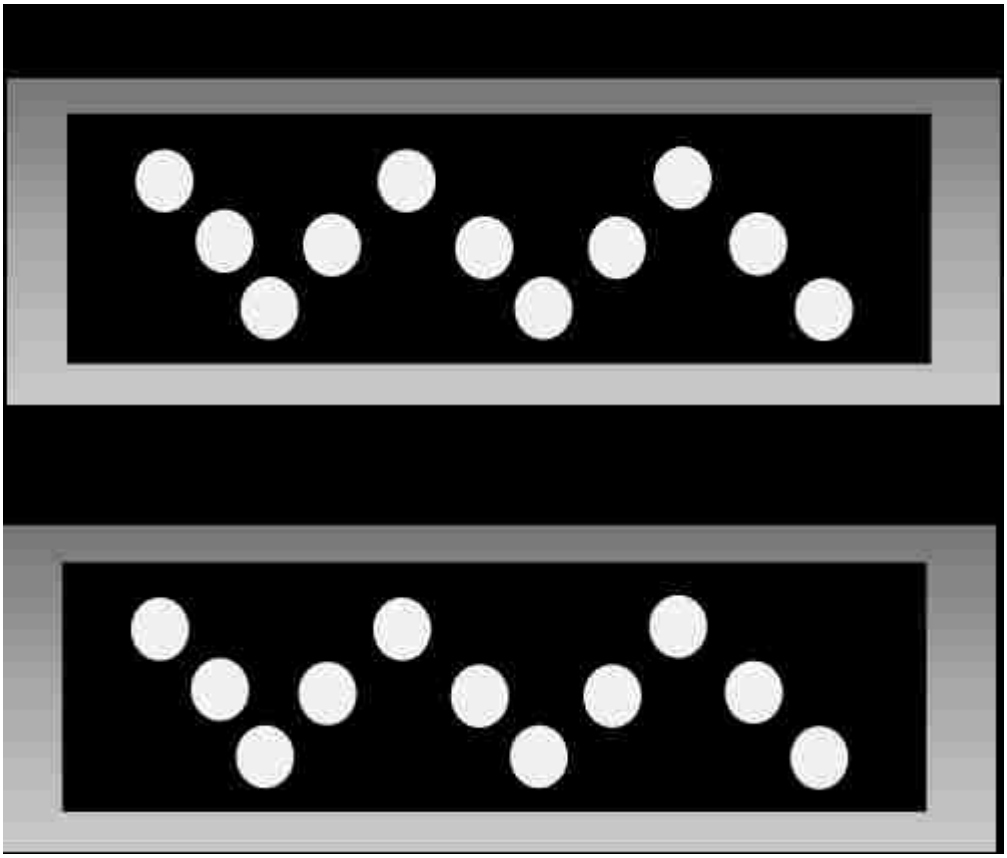

Figure 2.7: The way of cutting the samples from electrodes.

Table 2.5 Statistical ANOVA table to show the P-value

Source of Variation	SS	df	MS	F	P-value

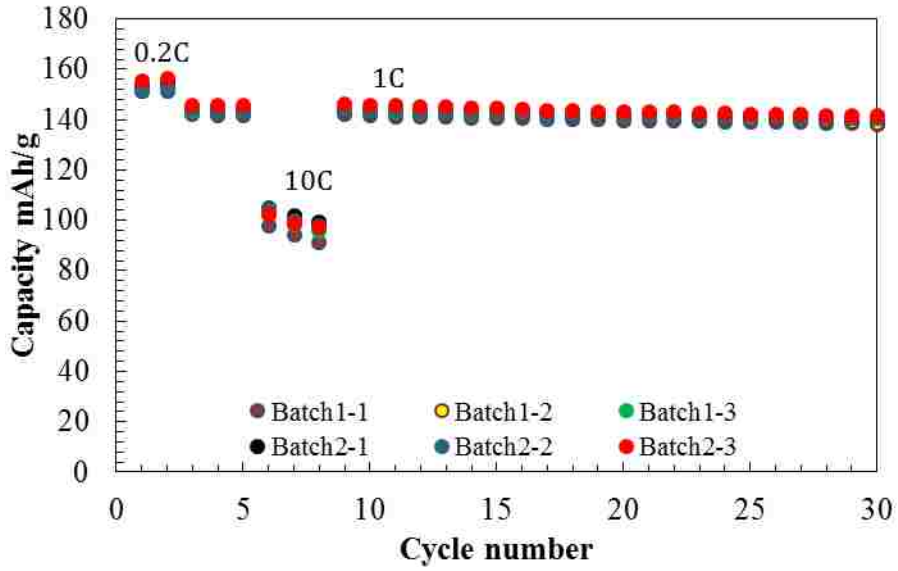

Figure 2.8: Cycling Performance at Different C-rates for 6 samples from two batches of electrodes made under the same conditions.

To help understand the distributions of the electrode components, the morphology of the electrodes prepared using sequence 1 was studied. Figures 2.9a and b show a SEM images of the electrode in cross-section, and Figures (2.9c-e) show the EDS maps of carbon, oxygen, and fluorine, respectively. CB appears evenly dispersed throughout the sample and form a network with PVDF between the NMC particles.

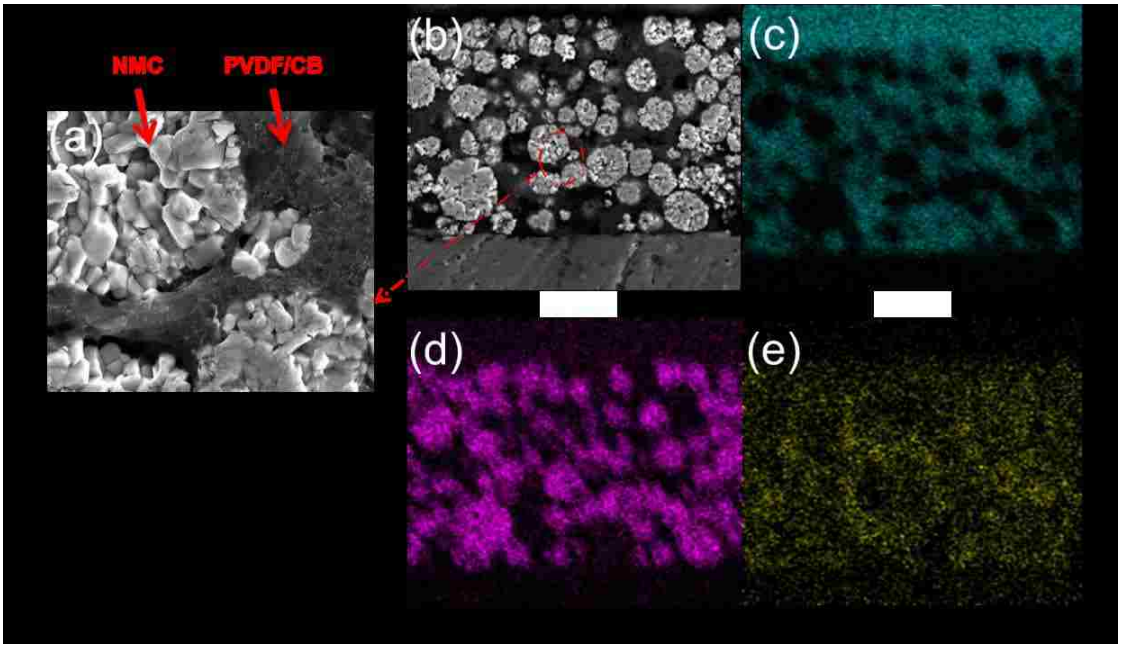

Figure 2.9: The SEM images of the cross-section electrode that prepared by sequence 1 (a) and (b). Energy dispersive spectroscopy (EDS) maps of the elements carbon (c), oxygen (d), fluorine (e) from the image (b).

Comparing with sequence 1, the viscosity of slurries prepared in sequence 2 was lower, and the rheological behavior was different if the same amount of NMP solvent was used. To optimize sequence 2 and achieve the same viscosity as that in sequence 1, different amount of NMP and the same weight ratio, mass, and mixing speed were used. Figure 2.10a shows that the viscosity increases with decreasing the amount of NMP. The loss modulus G" dominates over the storage modulus G′ as shown in Figure 2.10b. This behavior is of liquid-like similar to what Bauer *et al.* reported [7].

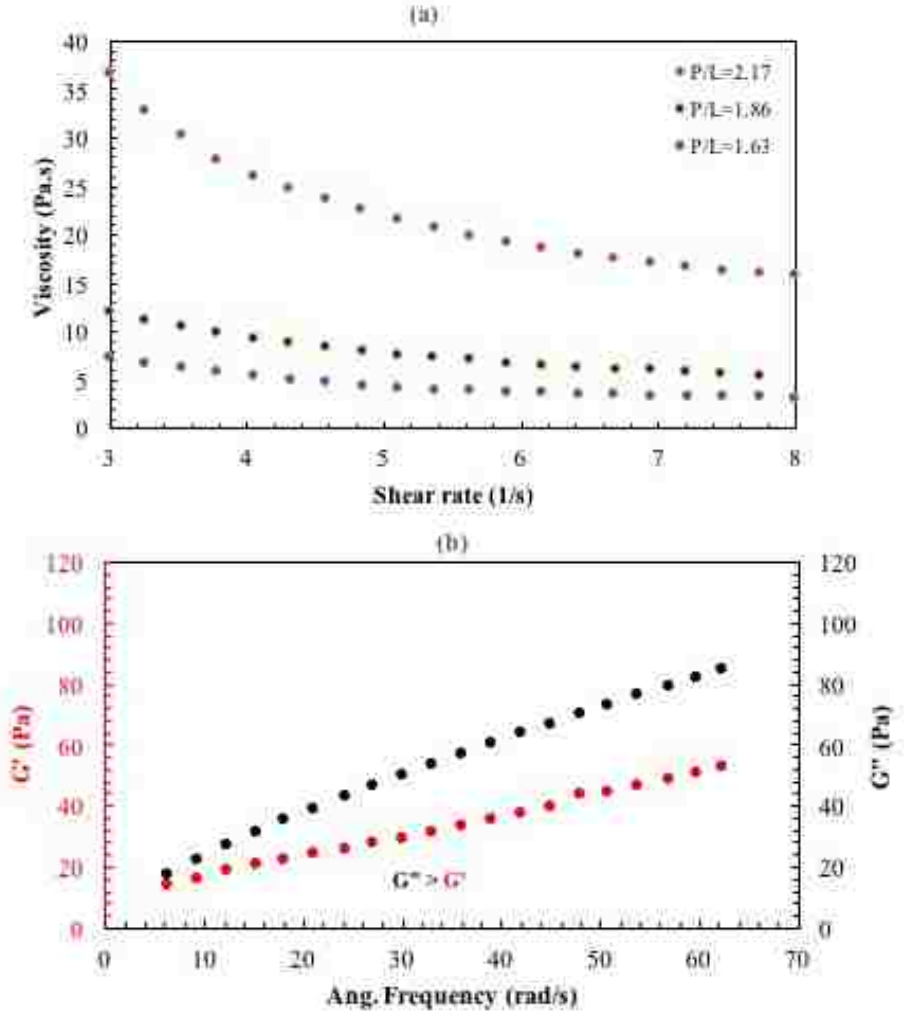

Figure 2.10: Viscosity as a function of shear rate of slurries prepared by using a different amount of NMP solvent (powder to liquid ratio) (a), and oscillatory shear measurements as a function of frequency sweeps (b).

The SEM images of the top surface and cross-section of the as-prepared electrode after the curing and calendering steps in Figures 2.11a and b respectively show the distribution of NMC and CB particles with PVDF binder. Some of the CB particles were left on the surface of the NMC, and that was a result of the trapping by the PVDF solution [26]. The cross-section images and the EDS maps show that the NMC particles were covered with the mixture of CB particles and PVDF (Figure 2.11c and d).

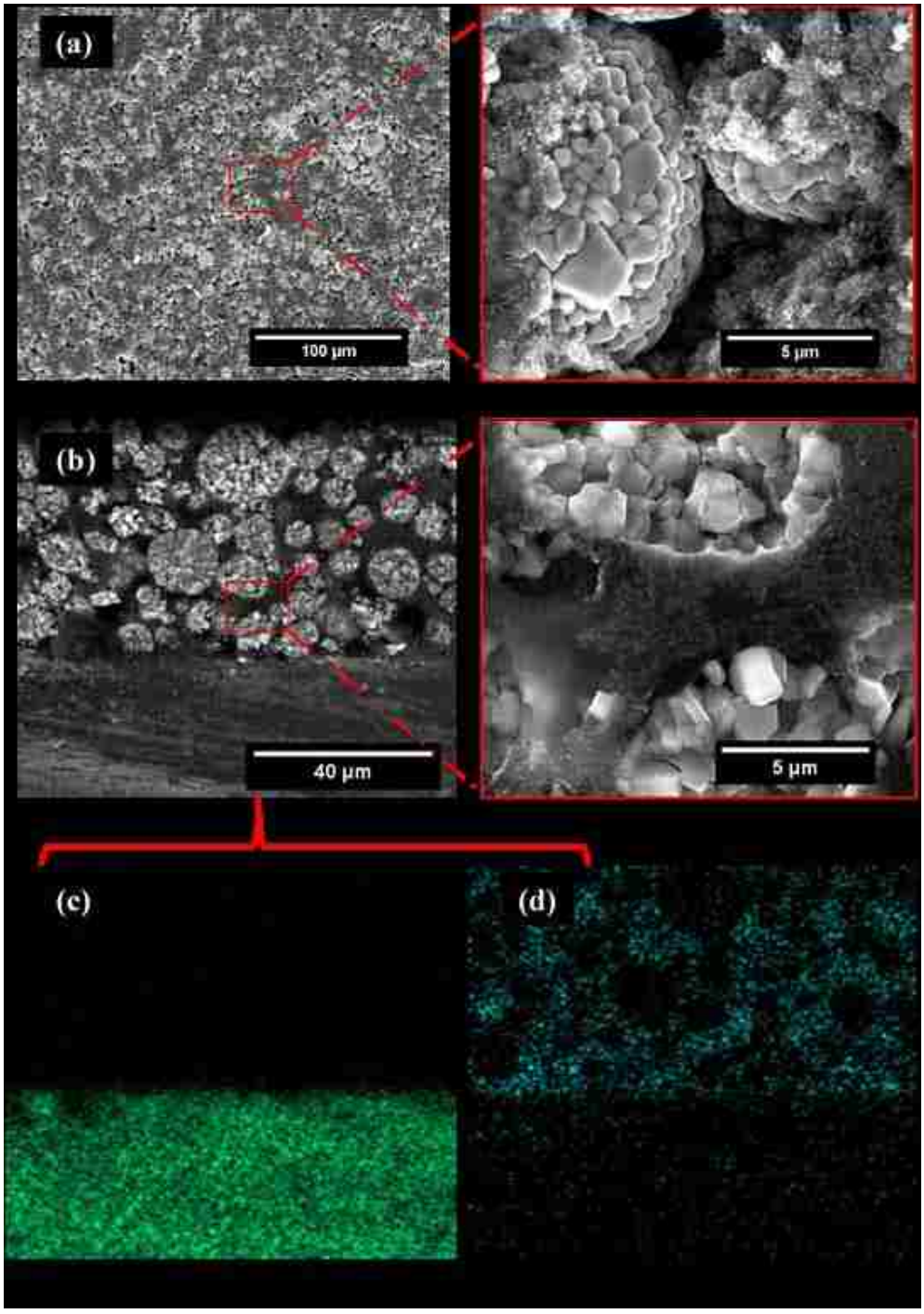

Figure 2.11: SEM images show the distribution of NMC and CB particles with PVDF binder in surface cathode electrode after dried in a vacuum oven with two different magnification (a), the cross-section of the electrode (b), and the EDS maps of the elements Aluminum (c) and carbon (d) from the cross-section image (b).

To optimize sequence 3, the amount of NMP solvent was investigated, while the weight ratio, mass, and mixing speed and time were fixed. Oscillatory measurements show that the loss modulus G" dominates over the storage modulus G′, and the slurry behaved as liquid-like. A change in the surface tension of the slurry was also observed. This behavior happened when a part of PVDF contacted with the solid particles and adsorbed at the surface while the other part extended in the solvent [80]. The NMC particles were covered with CB and PVDF, as shown in the cross-section SEM and EDS images in Figures 2.12a-d. Figure 2.13 shows the particle distribution of sequence 4 electrodes with different magnification.

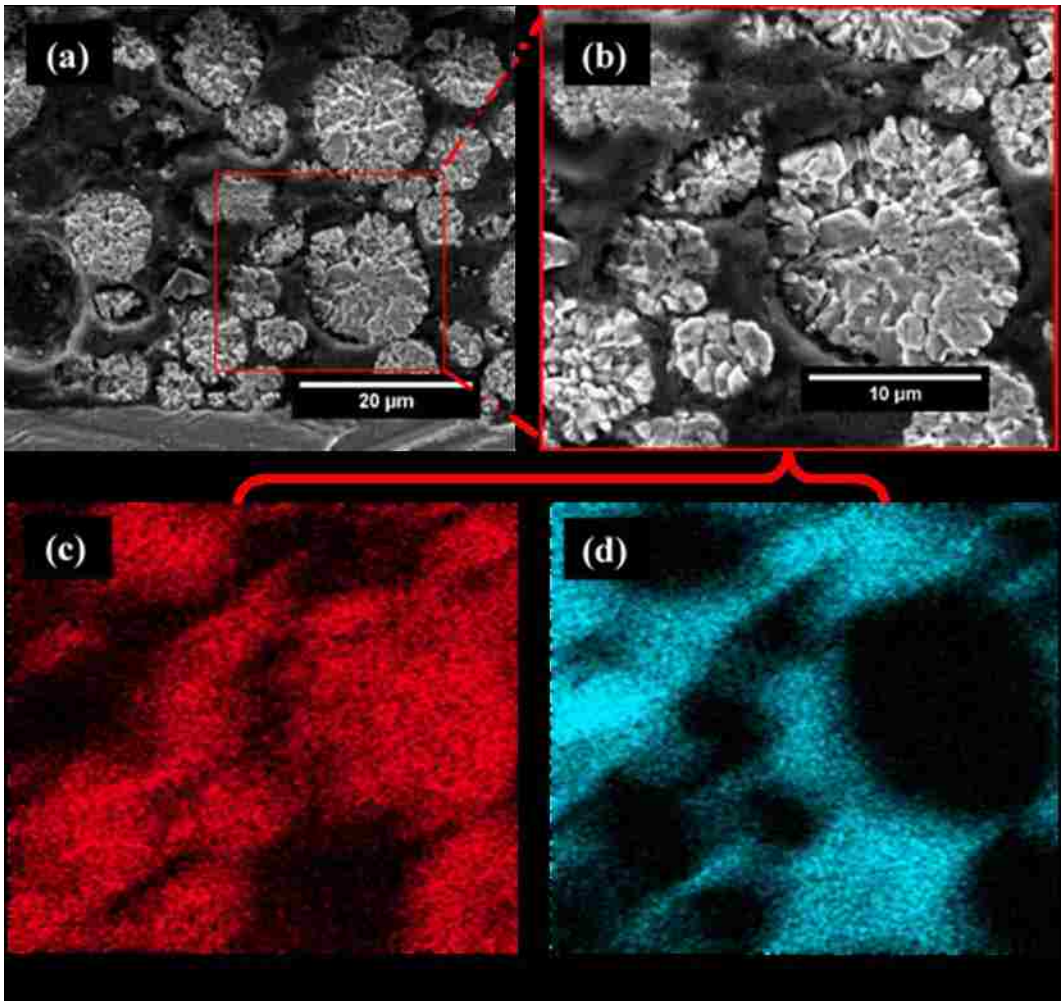

Figure 2.12: SEM images of the cross-section electrode with two different magnification (a) and (b), and EDS maps of the elements oxygen (c) and carbon (d) from the image (b).

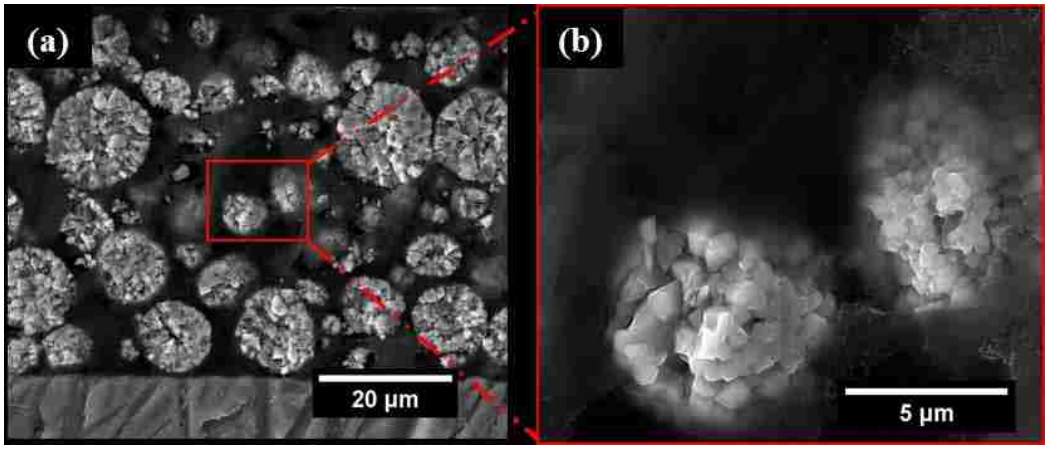

Figure 2.13: SEM images of the cross-section electrode as-prepared by using the sequence 4 with two different magnification (a) and (b).

Over a wide range of shear rate, the viscosity measurements of the four sequences were measured, as shown in Figure 2.14a, to investigate the behavior of the slurries at the same share rate (50 s^{-1}) that was applied during casting of the slurries onto the Al foil.

The viscosity measurements of the slurries over lower shear region show that the shear thinning behavior became stronger in sequence 2 and 3. The sequences with a higher ratio of powder to liquid exhibit higher shear thinning behavior [82] as shown in Figure 2.14b and Table 2.6. Less drying time for electrodes prepared by sequence 2 was required because of the high concentration of the solid particles [83].

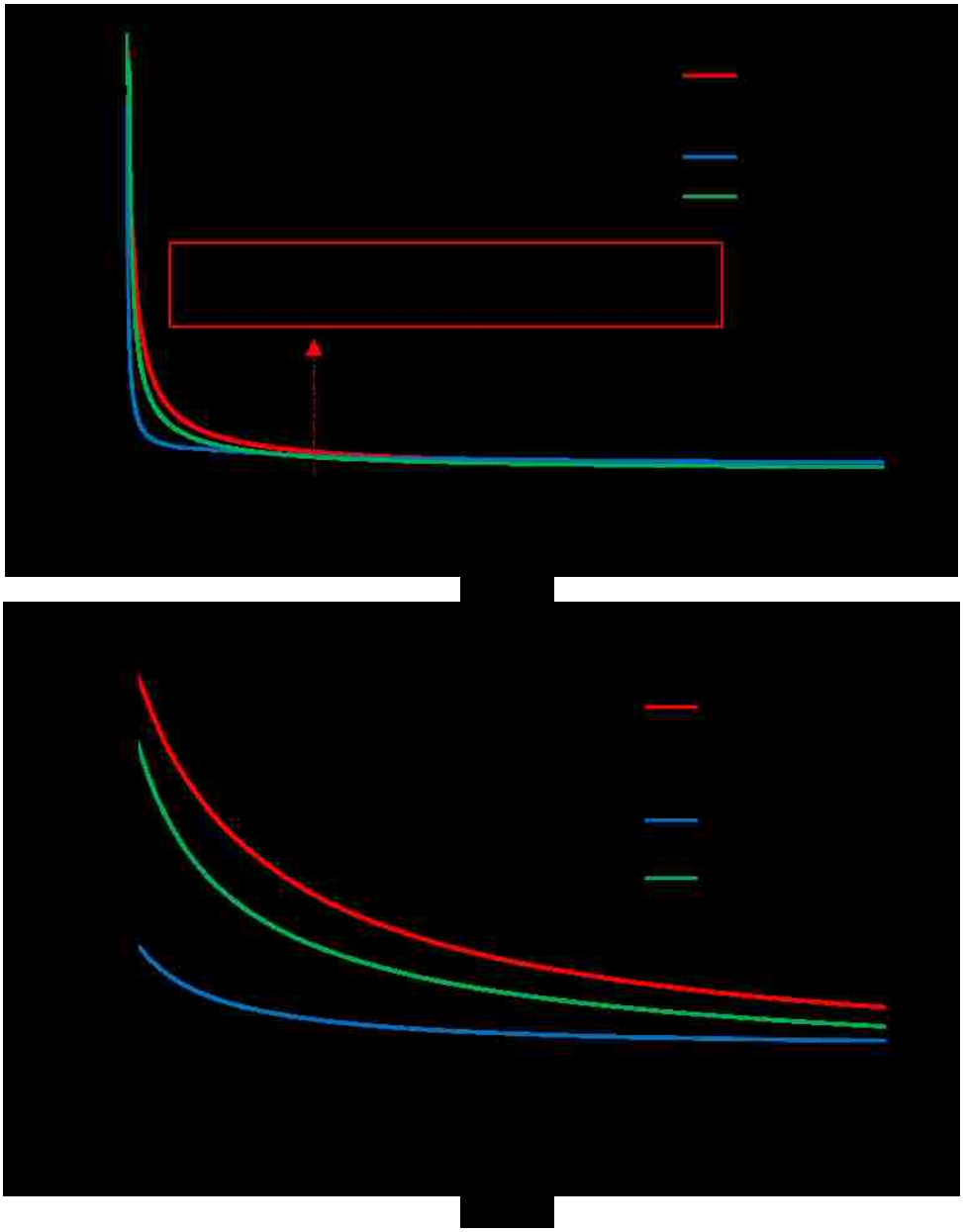

Figure 2.14: Flow rheology measurements of the viscosity as a function of shear rate of slurries prepared by using different mixing sequences; the red line shows the shear rate used in the doctor blade coating device 50(1/s) (a), and over the lower shear region (b).

Table 2.6 The NMC, CB, PVDF, NMP, and powder to liquid weight ratio of the four mixing sequences.

Sequence	NMC (g)	CB (g)	PVDF (g)	NMP (g)	Powder/Liquid (P/L)
1	6	0.26	0.26	5.5	1.19
2	6	0.26	0.26	2.75	2.37
3	6	0.26	0.26	2.9	2.25
4	6	0.26	0.26	5.25	1.24

In Figure 2.15, we propose a structural model to explain the rheological measurement results. For sequence 1, NMC particles were partially covered with the mixture of CB and PVDF solution and formed a network as shown in Figure 2.15a. The composite network increased the conductivity (26.8 S m^{-1}) of the electrodes and created a path for Li-ion during charging and discharging. In sequence 2 as shown in Figure 2.15b, after adding the binder solution to the mixture of dry powder, the binder surrounded the particles and prevented the composite network between the NMC and CB. This order of mixing showed a decrease in the conductivity (8.7 S m^{-1}) of the electrodes. For sequence 3, after adding the NMP solvent to the powder mixture, the CB particles were trapped and agglomerated as shown in Figure 2.15c. The agglomeration of the CB affected the distribution of the electrode materials and decreased the conductivity (9.6 S m^{-1}). In sequence 4 as shown in Figure 2.15d, the electrodes showed different morphology and higher conductivity (21.2 S m^{-1}) than sequences 2 and 3. NMC and CB were combined without PVDF in sequence 1 and 4, while in sequence 2 and 3 NMC and CB were combined with PVDF.

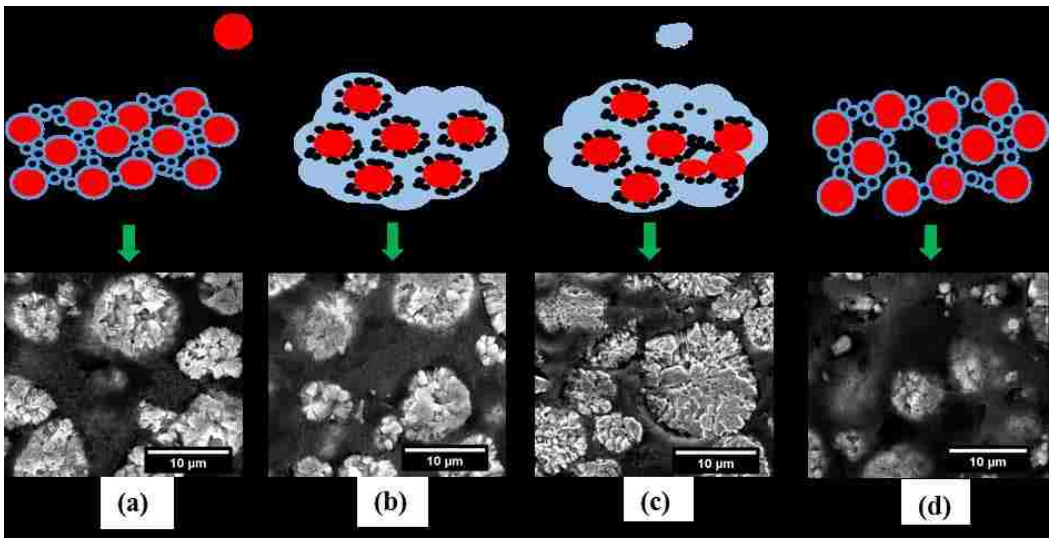

Figure 2.15: Schematic illustration and cross-section SEM images of the composition of electrodes NMC, CB, and PVDF after prepared by using; (a) sequence 1, (b) sequence 2, (c) sequence 3, and (d) sequence 4.

The oscillatory measurement was the additional rheology test that was used after the flow steady state test to obtain more information about the particle dispersion and the sedimentation [7]. The storage modulus (G') dominates over the loss modulus (G") for sequences 1 and 4 as shown in Figure 2.16a, and the slurries behave as gel-type. Sequences 2 and 3 behave like liquid-type because of the loss modulus G" dominates over the storage modulus G′ as shown in Figure 2.16b.

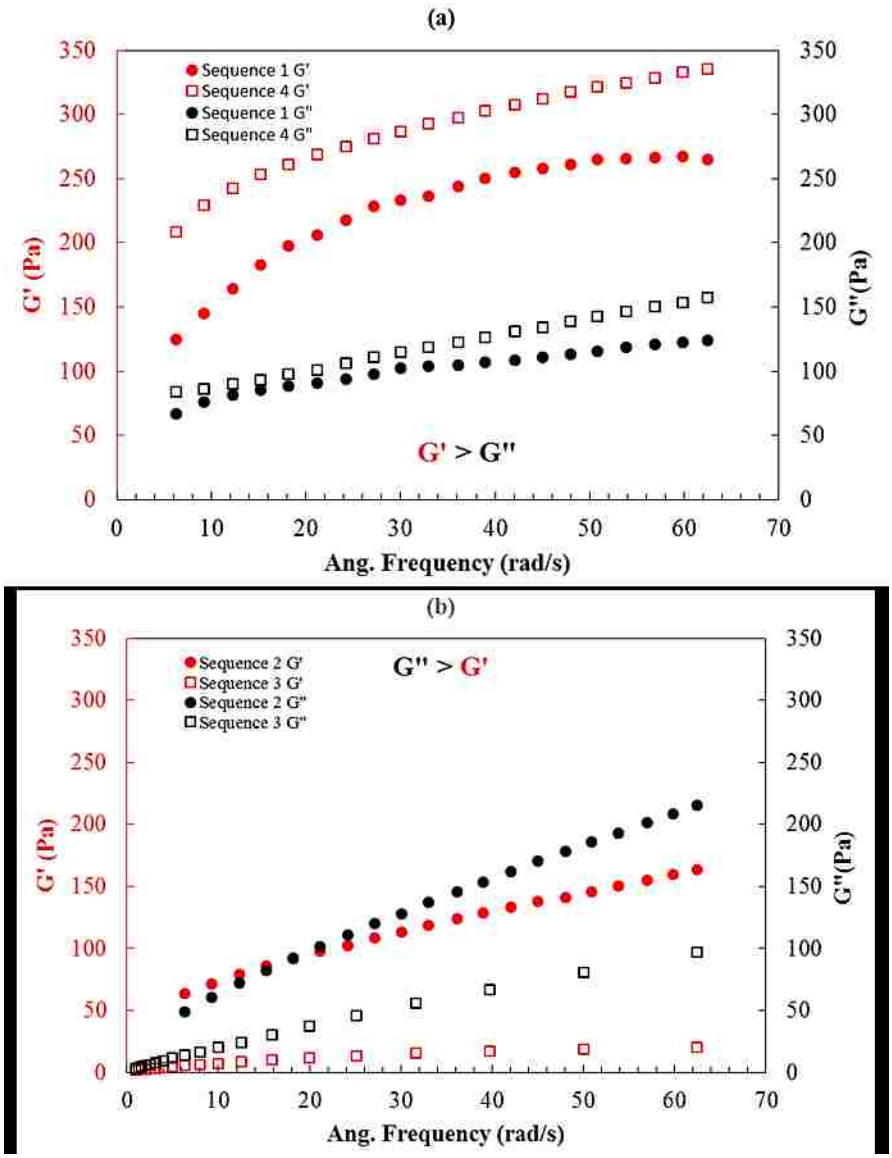

Figure 2.16: Rheology tests using oscillation measurement for the slurries that prepared by sequences 1 and 4 (a), and sequences 2 and 3 (b).

The hardness and elastic modulus of the samples were measured using a micro indenter with a diamond Berkovich tip during loading and unloading at a constant rate of 4 mN s^{-1} with a dwell period of 10 s at maximum load. The 20 µm depth was chosen to allow sufficient penetration into the electrodes to avoid surface roughness effect on the hardness and modulus measurement. A grid of 4 x 4 indentations and 250 µm spacing between indents were used to avoid the influence of neighboring indentation

marks as shown in SEM images Figure 2.17. The mean and standard deviation of the hardness and elastic modulus of sequences 2 and 3 were higher than that of sequences 1 and 4 as shown in Figure 2.18 a and b, respectively and Table 2.7. The scratch test indicates that the particle cohesion of the electrode in sequences 2 and 3 was stronger than that of sequences 1 and 4 as illustrated in figure 2.19. The cohesion and adhesion of the electrodes resulted from the interaction between the electrode materials. The interaction between PVDF and CB was stronger than that between PVDF and NMC [84].

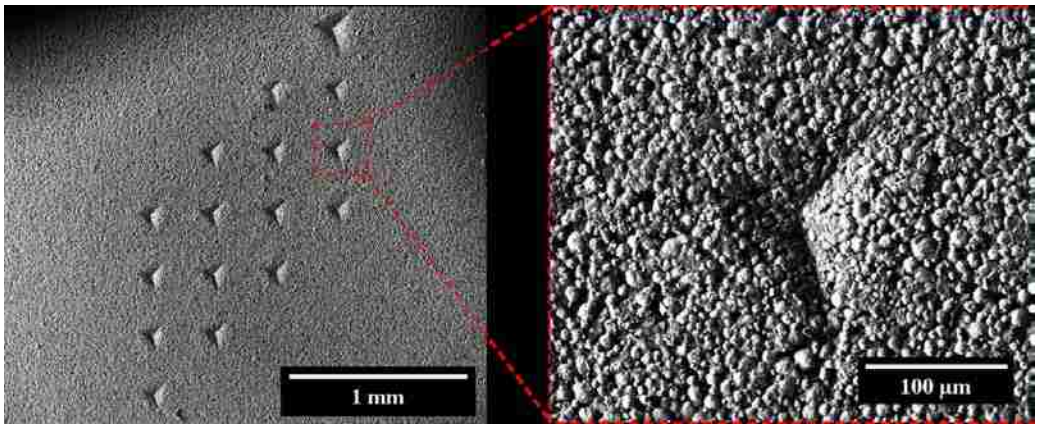

Figure 2.17: SEM image of the targeted indentation on the NMC cathode electrode (a) and magnified indent image (b).

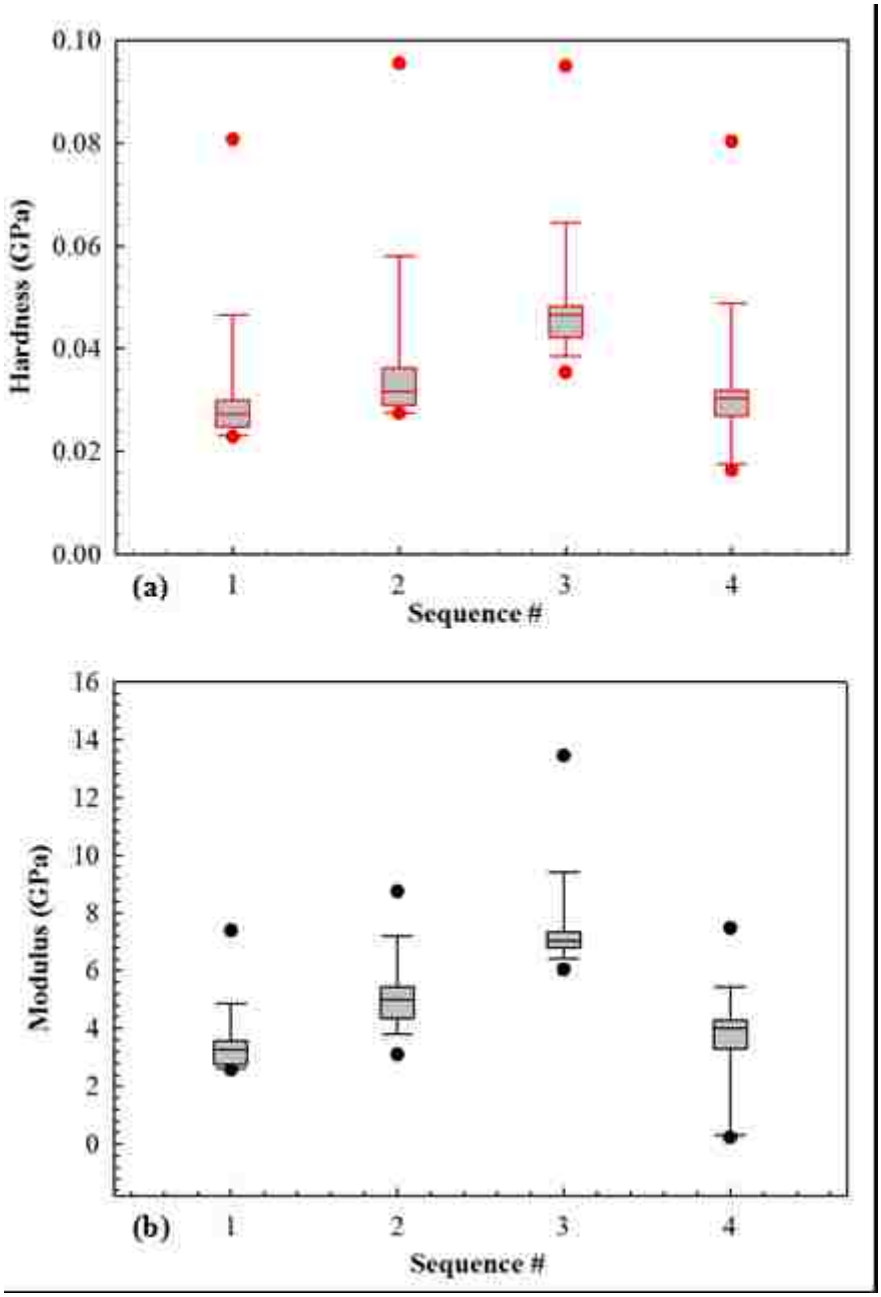

Figure 2.18: (a) Hardness and (b) Young modulus of the electrodes that prepared by different mixing sequences measured at control depth 20µm and grid of 4 x 4 indentations.

Table 2.7 Elastic modulus (E) and Hardness (H) of the different mixing sequences electrodes. The values reported are mean ± standard deviation.

Sequence	Control Depth	
	H (MPa)	E (GPa)
1	30±13	3.45±1.12
2	37±16	5.11±1.25
3	48±13	7.41±1.66
4	31±13	3.59±1.73

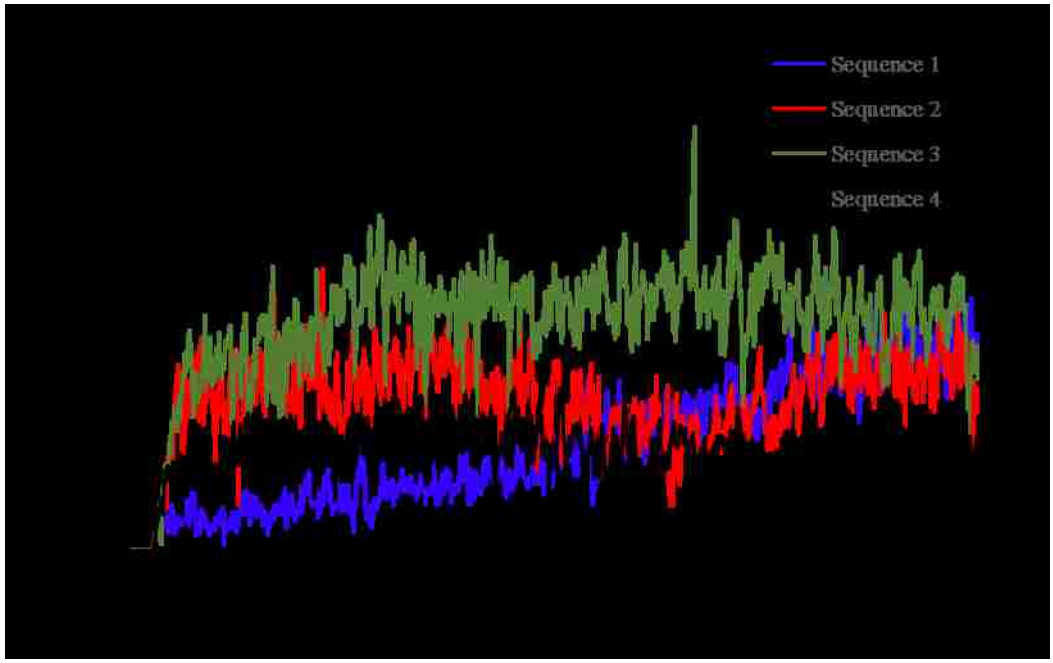

Figure 2.19: The scratch test of electrodes prepared by sequences 1, 2, 3, and 4.

The galvanostatic cycling measurement was conducted to compare the cycling performance of the electrode that was prepared by the four mixing sequences. Half cells were cycled at different C-rates (0.2C, 1C, 5C, and 1C) and long-term cycling at 0.5C as shown in Figure 2.20a and b respectively in a voltage range of 3V and 4.3 V followed by constant voltage with a current limitation of 0.05C at charging step. Sequence 4 has

better capacity at high rate (5C) as shown in Figure 2.20a, and sequences 1 has superior cycle results over sequences 2, 3 and 4 with long time cycling.

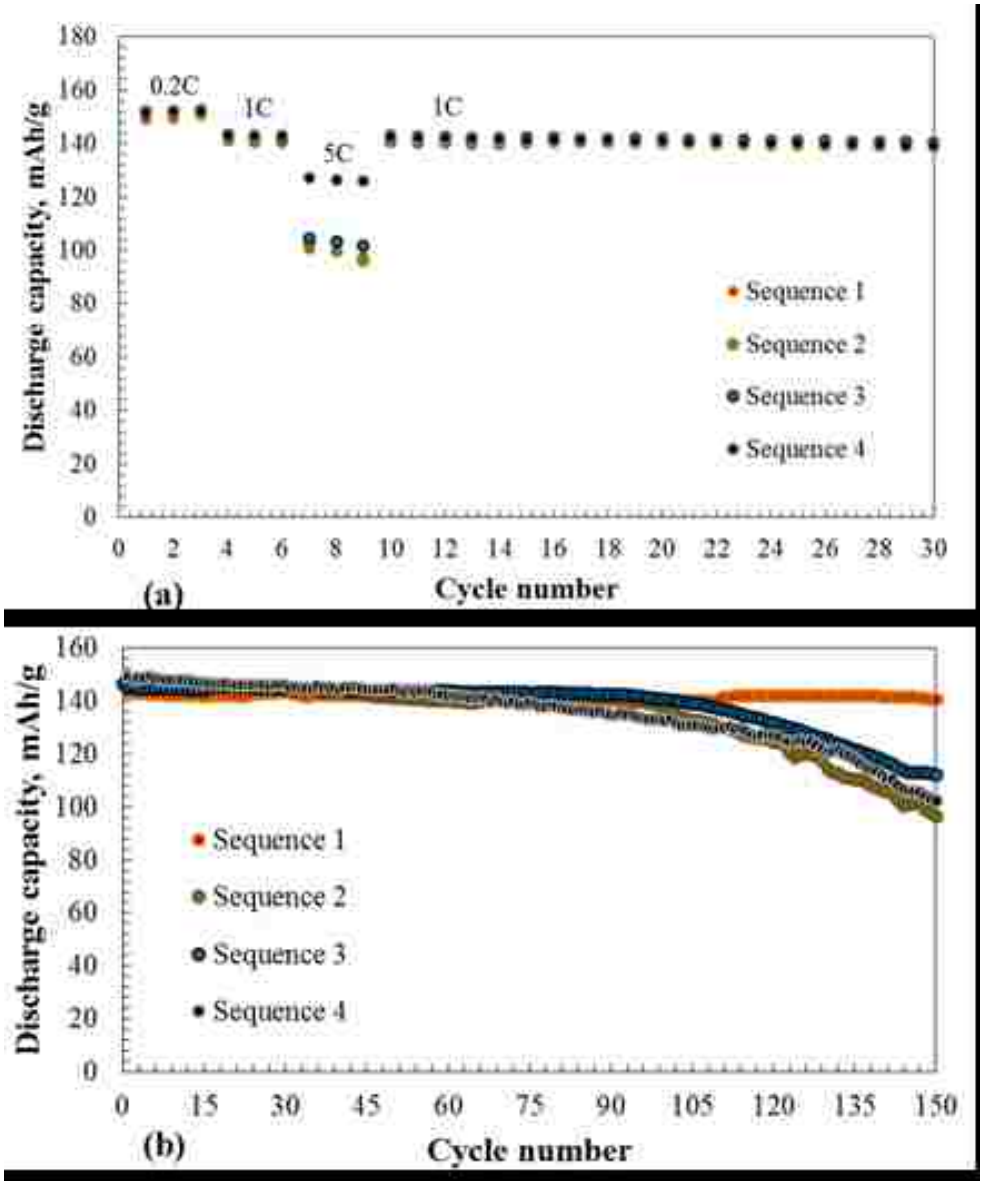

Figure 2.20: The discharge specific capacity vs. cycle number at a variable charging rate of 0.2C, 1C, 5C, and 1C (a) and long-term cycling at 0.5C (b) of NMC electrodes that made of sequences 1-4 in the voltage range from 3 V to 4.3 V followed by constant voltage with current limitation of 0.05C at charging step.

2.4 Conclusions

Specific capacity close to the theoretical capacity of NMC and stable cycle life were achieved by using voltage range from 3 V to 4.3 V and low C-rate (0.5C) followed by constant voltage with current limitation of 0.05C at charging step. For sequence 1, by using initial blade gap of 200 μm, the loading level of (2 mAh cm^{-2}) and the theoretical capacity of NMC (161 mAh g^{-1}) were achieved. The porosity and packing density do not seem to depend on mixing time but are strongly affected by calendaring. The mixing time of 30 min in the second mixing step and calendering have a strong influence on cell capacity at high C-rate.

The mixing sequences 1, 2, 3, and 4 were optimized, and the rheological behavior of the slurries, morphology, conductivity, and mechanical and electrochemical properties of electrodes were investigated. Using the same amount of NMP to prepare the slurries of sequences 2, 3, and 4, the viscosity was lower than the viscosity of sequence 1. Reproducible results within each sequence as evaluated by slurry, electrode characterization, and coin cell performance were achieved, and there were no significant differences between the samples. Slurries from sequences 1 and 4 have different rheological properties from 2 and 3, and the rheological characterization classifies them as 'gel-like' systems (dominant storage modulus). Conversely, sequences 2 and 3, exhibit 'fluid-like' rheology (dominant loss modulus). Some of the characterizations and observations appear to correlate with the gel or fluid-like behavior. Specifically: (1) Gel-like (Sequence 1 and 4): Lower viscosity at the same NMP:solids level than fluid-like (Sequence 2 and 3). More importantly, Sequence 4 has better capacity at high rate (5C), and sequences 1 has superior cycle results over sequences 2, 3 and 4 with long time cycling.

The key sequence-related factor determining fluid or gel-type behavior appears to be whether the NMC and CB are mixed in the presence of or prior to the introduction of the binder solution. The conductivity measurements show that electrodes from sequence 1 have higher conductivity than the other sequences. The mechanical property tests using micro-indentation indicate that the electrodes from sequence 3 have the highest hardness and elastic modulus. This result is consistent with scratch test results, which were used to understand the cohesion between the particles. Interestingly, hardness and elastic modulus do not translate directly to better cycle life.

Chapter 3 Adapting Membrane Manufacturing Technology to Making Lithium Ion Battery Electrodes

3.1 Summary

We report a new method of making lithium-ion battery electrodes by adapting an immersion precipitation (IP) technology commonly used in membrane manufacturing. Specifically, a lithium-ion battery positive electrode consisting of $LiNi_{1/3}Mn_{1/3}Co_{1/3}O_2$ (NMC), carbon black (CB), and Poly(vinylidene difluoride) (PVDF) was made by first preparing a slurry using *N*-Methyl-2-pyrrolidone (NMP) as a solvent. The slurry was next cast onto an aluminum foil which was then immediately immersed in a coagulation bath to remove the NMP solvent. The composition, structure, and electrochemical performance of the electrode made by the IP method were compared favorably with that made by the conventional method. This study demonstrates that the IP method can be adapted to make LIBs with excellent performance and durability at potentially lower cost and less environmental impact.

3.2 Introduction

Lithium-ion batteries (LIBs) have been commercially available since the early 1990s [85-87]. Many researchers worldwide are focusing on improving the performance and durability while reducing the cost of advanced LIBs for applications such as hybrid and pure electric vehicles, portable medical devices, and consumer electronics [2, 88-92]. The US Department of Energy has set the performance and cost targets for LIBs to meet the demand for hybrid and electric vehicles [93]. To reduce the cost and environmental impact, several approaches have been investigated such as using water based solvent [38] or completely dry manufacturing processes to eliminate the toxic and costly NMP solvent in electrode fabrication, using bio-derived materials

[4], reducing electrode drying time [40], reducing production cost [37], and improving battery performance [38, 41].

The conventional manufacturing process of making LIB electrodes consists of: (1) mixing active materials, conductive agent, and binder in a solvent, (2) casting the slurry onto Al foil for making the positive electrode or Cu foil for making the negative electrode, (3) drying at high temperature, and (4) calendering the electrode to control its porosity and packing density. The typically used NMP solvent is toxic, flammable, and expensive [57, 58]. During heat drying, the NMP will consume a large amount of energy to evaporate. The NMP vapor must be captured instead of being released to the atmosphere. The capturing of the toxic and expensive organic solvent is one of the motivations for this work. A further motivation is to reduce the manufacturing time and the energy cost for drying.

Immersion precipitation (IP), a demixing process, is one of the phase inversion methods which has been widely used to make commercial porous polymeric membranes [8, 9]. Recently, the IP method has also been used to make polymer electrolyte membranes and separators for LIBs [10-12]. The demixing process can be achieved by solvent and non-solvent phase exchange in multicomponent mixtures [13]. In this process, the polymer solution is cast on a suitable support which is then immersed into a non-solvent bath [8, 13]. Two mechanisms would operate as soon as the cast homogeneous polymer solution is exposed to a non-solvent bath: mass transfer and phase separation, resulting in transferring of the solvent molecules from the polymer solution to the non-solvent bath. As a result, a two phase mixture consisting of a solid polymer matrix and a non-solvent phase would grow and develop. After removing the non-solvent phase, a porous structure forms [44-46]. The structure and the porosity of the solid porous polymer film depend on the properties of the materials

and the processing conditions such as the composition of the materials, the concentration of polymer in solution, the pH and the temperature of the non-solvent bath, and the exposure time in the gelation bath [47-50].

Several similar requirements exist in polymeric membrane manufacturing and LIB electrode fabrication. Both involve PVDF and NMP, and both require high porosity and well-defined thickness. Unlike PVDF membranes, however, LIB electrodes must have a high loading of solid particles, which makes translating the IP method to electrode fabrication nontrivial. Nevertheless, we hypothesize that successfully translating the mature membrane manufacturing technology to electrode fabrication will reduce the cost and environmental impact of making LIB electrodes. This work is the first attempt to demonstrate the possibility of adapting the IP method for LIB electrode manufacturing.

For commercial LIBs, one of the most promising materials for a positive electrode is $LiNi_{1/3}Mn_{1/3}Co_{1/3}O_2$ (NMC). NMC has structural stability and high specific capacity comparing with other cathode materials [94]. PVDF, widely used in making porous membranes, is a typical binder for LIBs [58]. Indeed, several studies have shown that the PVDF is one of the most popular binders for cathode and anode fabrication [38], microporous polymer electrolyte [95], and separator in LIBs [8]. PVDF is inert and acid resistant [96]. It can also help improve adhesion between active materials, conductive agent, and current collector in LIBs [38].

In this paper, we (1) develop and demonstrate a new method of making LIB positive electrodes by an immersion precipitation (IP) process, (2) characterize the electrode structure, including particle distribution and porosity, and (3) compare the performance and cycle life of electrodes made by the IP and conventional methods.

3.3 Experimental part

3.3.1 Electrode preparation

The weight ratios of NMC to CB to PVDF binder were fixed at 92:4:4 wt.% respectively. CB and PVDF were dried in a vacuum oven for 24 h before use. The mixing steps are shown in Figure 1a. First, PVDF was dissolved in NMP in a (Mazerustar KK-50S, Kurabo) planetary mixer-deaerator operated at 680 rpm rotation and 1140 rpm revolution with a total time of 360 s. Second, CB was added to the binder solution followed by mixing at 4000 rpm for 45 min in a (Polytron PT 10-35 GT) homogenizer. Third, NMC was added to the homogenizer, and the mixture was mixed at 4000 rpm for 1 hour. Finally, the homogeneous slurry was rested in a vacuum chamber for 5 min to remove bubbles and then transferred out of the chamber to cast at room temperature onto 15 μm thick aluminum foil with an automatic compact film coater with built-in dryer and vacuum chuck (MTI Corp). For casting, the adjustable doctor blade gap was set at 200 μm and the casting speed was 0.2 m/min. The above fabrication steps are the same for both IP and the conventional method of making electrodes.

Adapting the IP method for membrane fabrication, the casted electrode was immediately immersed in a deionized (DI)-water bath at 25°C for 2 min followed by a pre-drying step by exposing the electrode in dry air for 5 min. The electrodes were left to dry at room temperature overnight. The IP method of making electrodes is schematically illustrated in Figure 3.1a-d.

The electrode was calendered with a 40 μm rolling gap using a compact electric rolling press (MTI Corp.) at room temperature to improve the adhesion of electrode materials with the Al foil and control the porosity and packing density [97]. The calendered electrode was punched to 12 mm diameter discs by a Precision Disc Cutter

(MTI Corp.) and further dried in vacuum oven for 12 h at 130°C. For comparison, positive electrodes of the same composition were prepared by the conventional slurry method using the same mixing sequence and parameters without the IP step. Coin cells of CR2025 type (Hohsen) were made in a glove box using electrodes made by IP and the conventional slurry method. The 12 mm diameter NMC positive electrodes discs were assembled by automatic coin cell crimper (KTE-20S-D, Hohsen) in inert argon-filled glove box (MBRAUN MB-20-G) with oxygen and moisture level of (<0.1 ppm). Pure lithium metal foils (Sigma Aldrich) were used as counter and reference electrodes. The electrolyte was added on the poly-propylene (Celgard 2400) microporous separator film to carry the Li-ions between the electrodes. Stainless steel spacer and waved spring were placed on lithium discs to increase the pressure on the electrode to achieve good electrical contact.

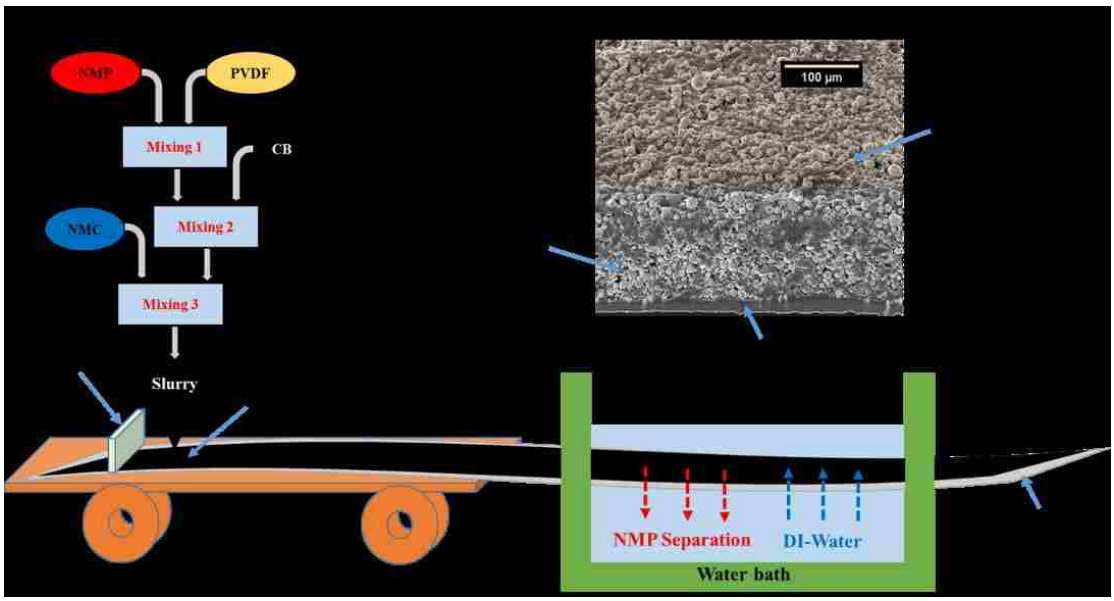

Figure 3.1: Schematic illustration of the immersion precipitation (IP) process for making LIB positive electrodes: (a) mixing, (b) casting, (c) immersion precipitation, and (d) cross-section and top-view SEM images of NMC electrode made by the IP method.

3.3.2 Characterization

3.3.2.1 Morphology

Scanning electron microscopy (SEM) images were collected in an environmental scanning electron microscopy (ESEM) (Quanta FEG 250, FEI) to observe the surface structure of PVDF membranes and the structure of the surface and cross-section of the positive electrodes made by the IP and conventional methods. The cross-section sample preparation described in chapter 2 section 2.2.3.2, and the calculation of porosity and packing density of the electrodes described in section 2.2.3.5.

3.3.2.2 Electrolyte uptake

Using the equation (1) [95, 98, 99], we can calculate the electrolyte uptake of the prepared electrodes.

$$Electrolyte\ uptake = \frac{W_{\mathrm{w}} - W_{\mathrm{d}}}{W_{\mathrm{d}}} \times 100\% \qquad (1)$$

where W_{d} is the weight of the dry electrode and W_{w} is the weight of the wet electrode with electrolyte. The procedure was done by measuring the mass of the dried electrodes, soaking the electrodes with the electrolyte (1M LiPF6 in ethylene carbonate/ethyl-methyl carbonates (EC/EMC 3:7 by volume) with 2% vinylene carbonate (VC) for 1 h, and then taking the electrodes out of the electrolyte and measuring the weight again.

3.3.2.3 Electrochemical measurements

More than 16 coin cells from 3 batches were made to test the electrochemical performance of the prepared electrodes by the IP process and conventional methods in half-cells with pure lithium as the counter electrode. The coin cells were connected to a Potentiostat/Galvanostat (Bio-Logic MPG-2) or (Bio-Logic VMP-3) with

galvanostatic mode at room temperature to provide charging and discharge profiles. The lower and upper voltage limited for NMC cathodes were 3 and 4.3 V, respectively. The C-rate is the cycling rate of the electrodes at a different rate of C/R (R hours per charge or discharge).

3.3.2.4 Electrochemical Impedance Spectroscopy

Electrochemical impedance spectroscopy (EIS) measurements were done using the Bio-Logic Potentiostat/Galvanostat (VMP-3) with a frequency range from 10 mHz to 100 kHz and potential amplitude of 5 mV at room temperature. The coin cells were rested for 24 h before running the impedance measurement.

3.4 Results and discussion

The scanning electron microscope (SEM) images in Figure 3.2a-c show a top view of the PVDF alone at different magnification. The PVDF/NMP solution was cast onto the Al foil with a 200 μm blade gap. It was immediately immersed in DI-water for 2 min and then removed from the DI-water bath to dry at room temperature overnight. Finally, it was dried in a vacuum oven for 12 h at 130°C. To show the difference in the final structure of PVDF film that made by IP and the conventional electrode manufacturing methods, a PVDF/NMP solution was cast and dried at room temperature overnight before drying in the vacuum oven for 12 h at 130°C (designated as the "conventional PVDF"). The formulation of PVDF and NMP (weight ratio %) and casting condition were the same to ensure that the PVDF films only differ in the IP step. Figure 3.2d shows that the "conventional PVDF" film has a dense structure with small holes that formed after NMP evaporation, while the IP method PVDF film at the same magnification, shown in Figure 3.2c, has a uniformly distributed microporous structure with larger holes formed after water evaporation.

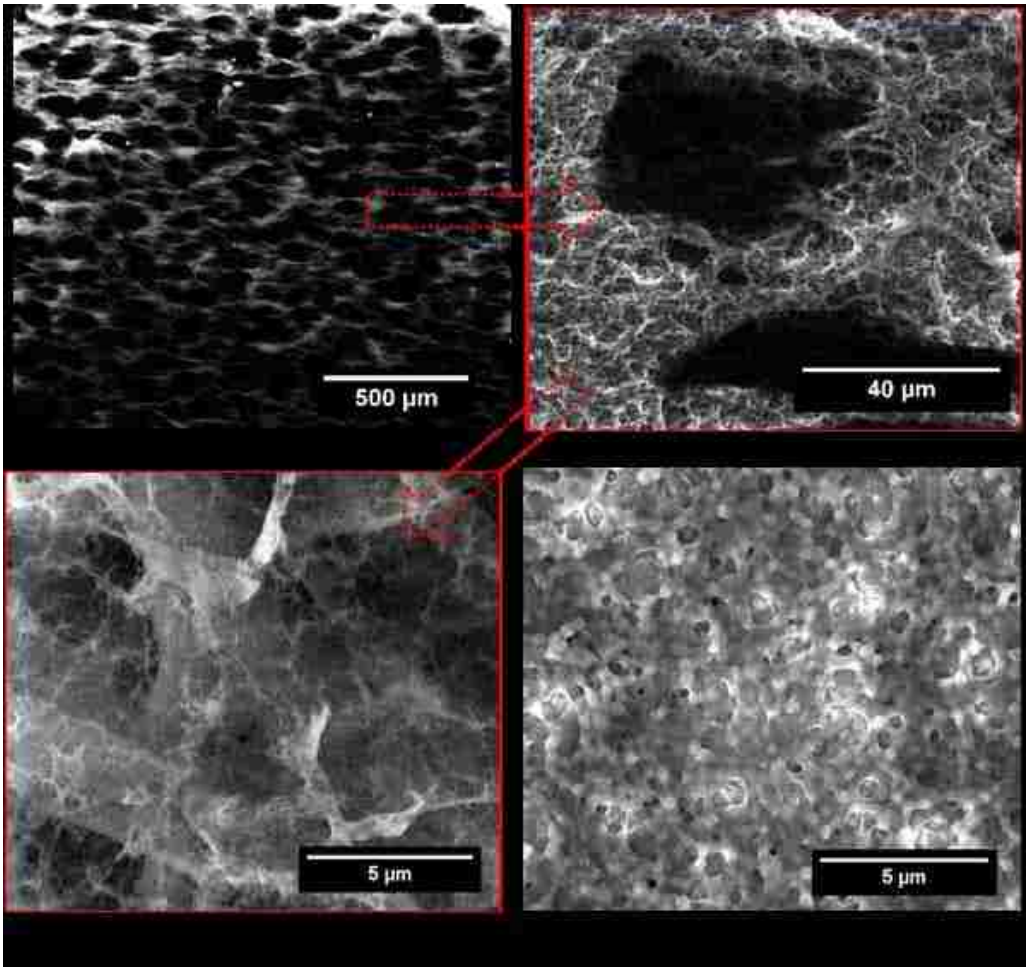

Figure 3.2: Scanning electron microscope (SEM) images of top surface of PVDF film formed by the IP method with different magnifications (a), (b), and (c), and by the "conventional PVDF" (d).

SEM images, Figures 3.3a and b, show the top surface of conventional and IP created electrodes after calendering respectively. The cross-section of the conventional electrode after calendering is shown in Figure 3.3c, while Figure 3.3d shows the IP electrode after calendering. The electrode components are observed as bright gray (NMC), dark gray (CB & PVDF), and black (porous regions). From the SEM images in Figure 3.3, the electrode particles are stacked together to form the electrode, and the PVDF binder coats the surface of the particles and bridges them together. Some of the particles fill the pores of the PVDF structure which is formed by evaporating the DI-water [12]. The cross-section images of the IP method in Figures 3.3d shows a more

homogeneous distribution of NMC particles without sedimentation, and fewer agglomerated particles than that of the conventional electrode shown in Figure 3.3c.

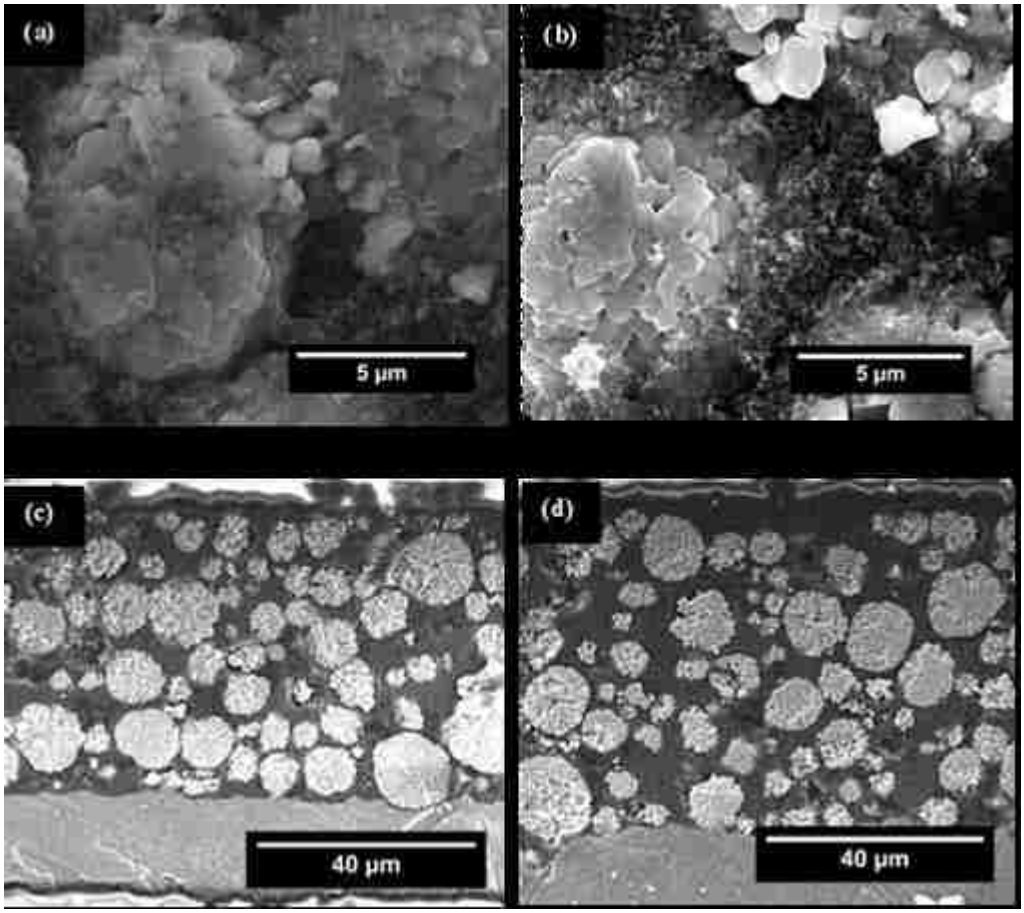

Figure 3.3: Scanning electron microscope (SEM) images of NMC electrodes after calendering: top surface of conventional made electrode (a) and IP method electrode (b), the cross-section of the conventional electrode (c), and the cross-section of the IP method electrode (d).

To understand the differences between the IP and conventional electrode fabrication methods, the electrolyte uptake was calculated which shows that the electrodes made by the IP method without calendering have more electrolyte uptake (34%) than the electrodes made by conventional method (29%). The electrolyte can fill the pores and swell into the PVDF structure because of the microporous structure in the PVDF membrane [12] which greatly increases the electrolyte uptake [99]. The

electrolyte uptake for the electrode that made by IP and conventional methods after calendering was (17%) and (16%), respectively.

The galvanostatic cycling measurement was carried out to compare the capacity and cycling performance of the electrodes made by the IP and conventional methods. To observe the differences between the behaviors of NMC cathodes, half cells were cycled at 0.5C in the voltage range of 3 to 4.3 V followed by a constant voltage step with a current limitation of 0.05C at the charging step. The discharge capacity was calculated based on the NMC mass. Figure 3.4a shows the discharge specific capacity versus the cycle number for both positive electrodes without calendering. IP and conventional made electrodes show initial capacity of (147 mAh g^{-1}) and (148 mAh g^{-1}). After 163 cycles, their capacities are (117 mAh g^{-1}) and (109 mAh g^{-1}) with capacity retention of 80% and 74%, respectively. The results are consistent based on tests conducted on multiple cells from several batches. Thus, electrodes made by the IP and conventional methods have slightly different initial and long-term cycling capacities.

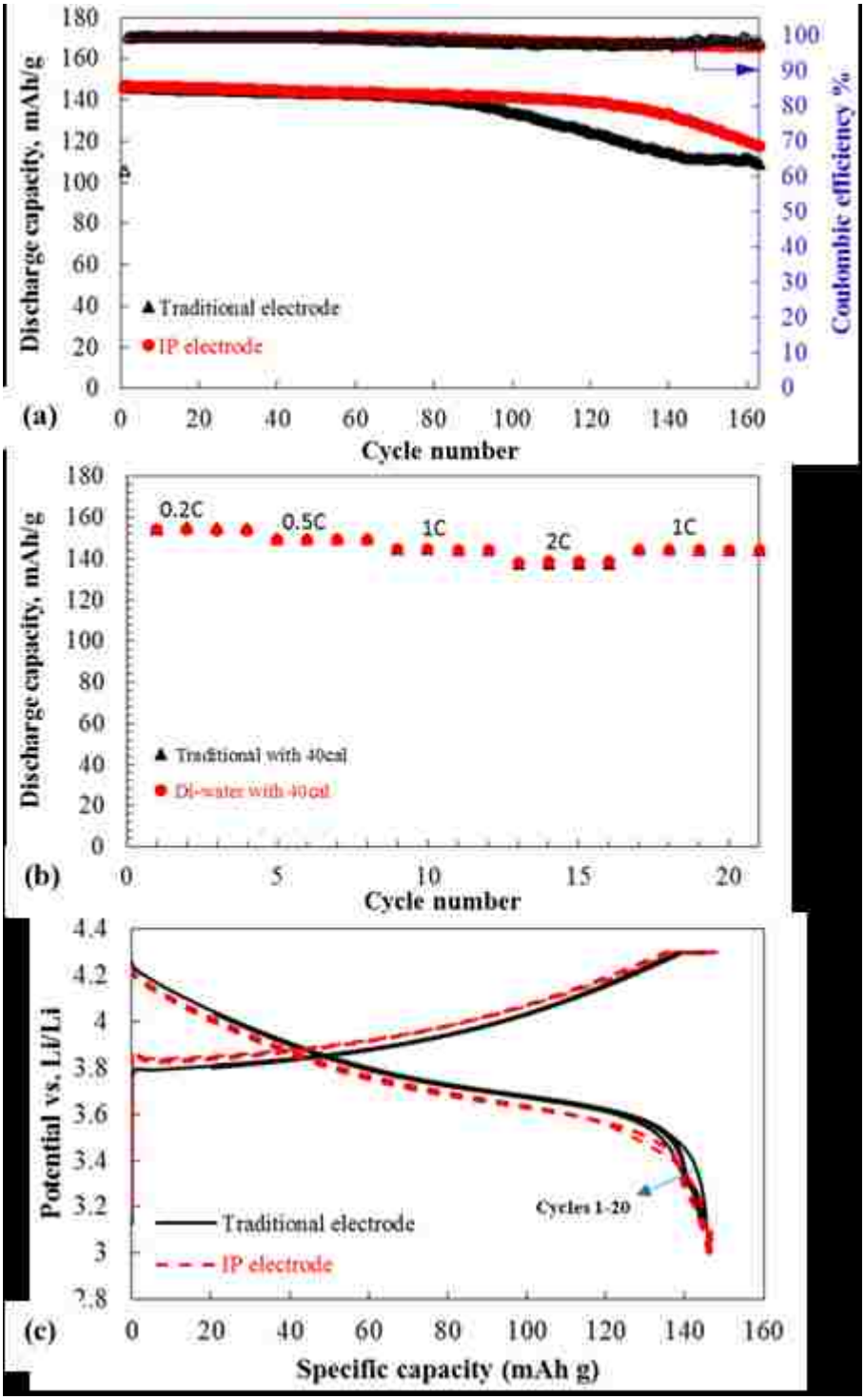

Figure 3.4: Electrochemical characteristics of NMC electrodes made by IP and conventional methods without calendering in the voltage range from 3 to 4.3 V followed by a constant voltage charging step with current limitation of 0.05C: the discharge specific capacity on the left side and the coulombic efficiency on the right side versus cycle numbers (a), discharge specific capacity at variable charging rate of 0.2, 0.5, 1, and 2C then back to 1C (b), and charge-discharge profile for the cycles 1st, 5th, 10th, and 20th under 0.5C rate (c).

The rate capability of the NMC electrodes, summarized in Table 3.1, was measured with various charge and discharge rates of 0.2, 0.5, 1, and 2C then back to 1C between 3.0 and 4.3 V followed by a constant voltage charging step with a current limitation of 0.05C. At low rates, both electrodes have a similar discharge capacity, while at high rates (2C) the IP electrode (136 mAh g^{-1}) has a higher capacity than the conventional electrode (126 mAh g^{-1}) as shown in Figure 3.4b. The difference in discharge capacity at a higher rate of 2C is referred to the difference in electrode/electrolyte contact area which is expected to be larger in the more porous IP electrodes, leading to faster ionic transport and reduced polarization [100]. The improvement in cycle life, capacity retention, and rate performance at the high rate of 2C for an electrode made by the IP process suggests that by using this method the structure of the PVDF [50], the porosity, and the homogeneous distribution of the NMC particles may be better than that by the conventional method.

Table 3.1 The rate capability of the NMC electrodes without calendering at a various charge and discharge rates of 0.2, 0.5, 1, and 2C then back to 1C.

Electrode without calendering	**Capacity (mAh g^{-1}) at 0.2C**	**Capacity (mAh g^{-1}) at 0.5C**	**Capacity (mAh g^{-1}) at 1C**	**Capacity (mAh g^{-1}) at 2C**	**Back to capacity (mAh g^{-1}) at 1C**
IP method	153	148	143	136	143
Conventional method	148	146	139	126	138

Figure 3.4c shows the comparison of the 1st, 5th, 10th, and 20th charge and discharge curves of the NMC electrodes which were prepared by conventional and IP methods. The red dashed lines show the results for electrodes made by the IP method, while the solid black lines show the result for the conventionally made electrode. All the curves exhibited the same behavior with smooth charge-discharge curves.

To control the porosity and the packing density, we have calendered the electrodes and measured the cycling performance with the same cycling rates as the electrodes that were tested without calendering. The IP made electrodes have higher porosity, slightly thicker, and lower packing density than the conventional electrodes as shown in Table 3.2. The cycling performance in Figure 3.5a shows that the capacity of IP electrode degraded from (148 mAh g^{-1}) to (128 mAh g^{-1}) after 163 charge/discharge cycles with capacity retention of 85%, while the capacity of conventional electrode decayed from (151 mAh g^{-1}) to (92 mAh g^{-1}) after 163 cycles with capacity retention of 62%. Long-term cycling has shown that the IP made electrode has a cycle life and capacity retention better than the conventionally made electrode.

Table 3.2 The porosity, thickness, loading, packing density, and initial discharge capacity of both electrodes made by conventional and IP methods.

Electrodes	**Thickness (µm)**	**loading (mAh cm^{-2})**	**Porosity (%)**	**Packing density (g cm^{-3})**	**Discharge initial capacity (mAh g^{-1})**
Without calendering					
IP	90	2.31	60	1.69	147
Conventional	88	2.32	59	1.73	148
Calendering with 40µm gap					
IP	62	2.62	35	2.78	151
Conventional	55	2.33	34	2.79	148

The rate capacity for both electrodes has similar behavior as shown in Figure 3.5b. The IP electrodes have a higher cycling stability than the conventional electrodes which indicates that the IP method may be better than the conventional method.

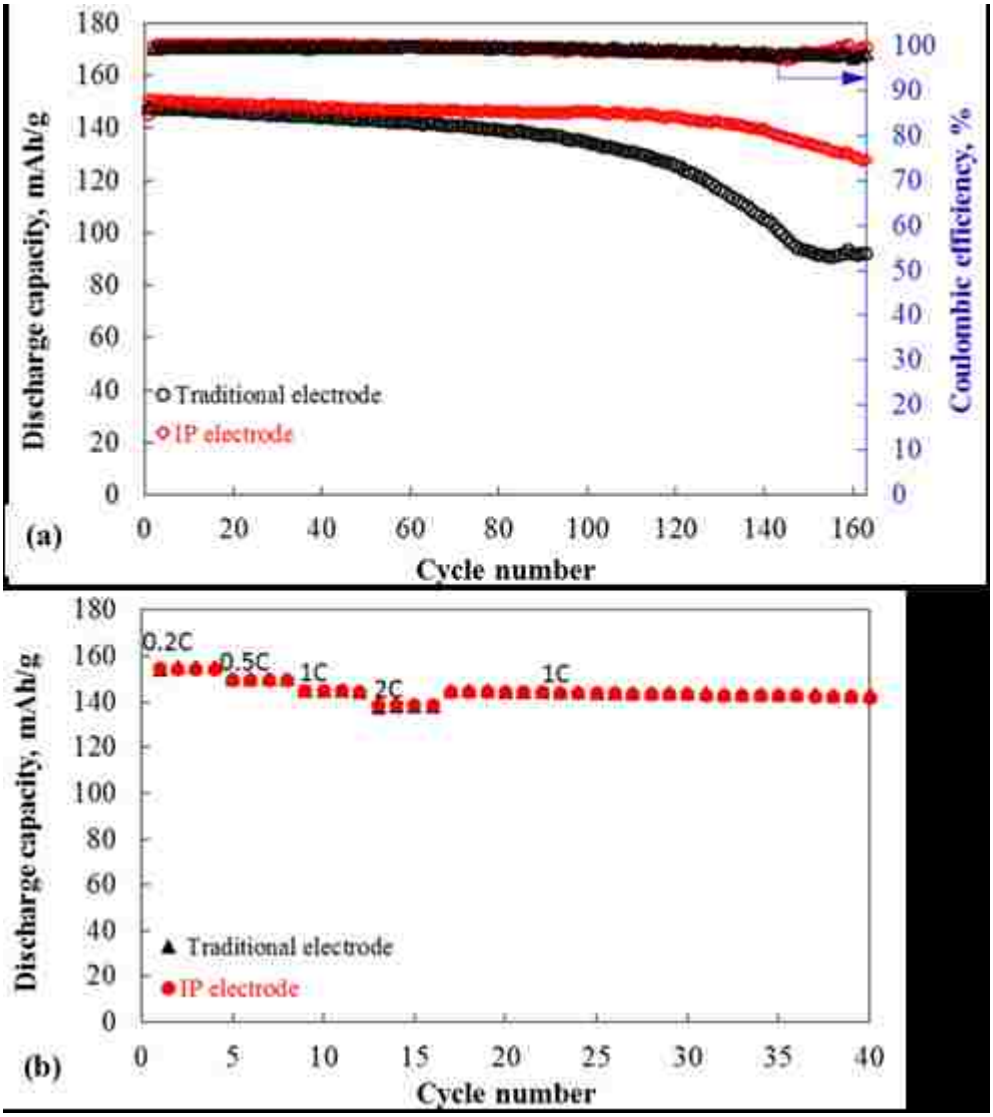

Figure 3.5: Long-term cycling performance and coulombic efficiency of NMC cathodes made by IP and conventional methods with 40 µm calendering at a rate of 0.5C and voltage range from 3 to 4.3 V followed by constant voltage during charging process with current limitation of 0.05C (a) and the rate capability at 0.2, 0.5, 1, and 2C then back to 1C (b).

To compare the electrochemical resistance of the electrodes made by the traditional and the IP method, the electrochemical impedance spectroscopy (EIS) was used. The experimental impedance and the well fitted equivalent circuit as shown in Figure 3.6 were used to explain the internal impedance of the cells before and after cycling. The Nyquist plots for the electrodes at the initial state consist of mainly three contributions. The displacement of the semicircle plot from the origin at the highest

frequency represents mainly the electrical resistance of electrolyte, separator, and electrode (Re). The intermediate-frequency semicircle can be assigned to charge transfer resistance (R1) and its associated the constant phase elements (CPE1), and the low-frequency tail is attributed to Warburg effect (W_o) that characterizes the diffusion of Li-ions on the active material particles/electrolyte interface [100-102]. Using the Zview software, the fitted equivalent circuit shown in the inset Figure 3.6a were used to fit the plots. The electrodes without calendering show that the IP method electrode before cycling has semicircle smaller than the traditional electrode as shown in Figure 3.6a. The numerical values of the elements are given in Table 3.3 which indicated that the IP electrode has lower resistance. We believed that the lower interfacial resistance (R1) in IP electrodes results from the formation of microporous structure of PVDF after immersed in DI-water and the difference in material distributions and fabrication [102] as shown in cross-sectional SEM image Figure 3.3d. After the solvent-non solvent exchange occurs and NMP leaves the PVDF, the PVDF forms pores around NMC and CB particles within a few seconds. The porous structure of PVDF in the IP electrode can host more electrolyte than the traditional one and that will ensure an easy path for the Li-ions to reach the NMC particles and lower the resistance. In the traditional method, the PVDF formed layers with less porosity, and that reduced the uptake of the electrolyte and the kinetic of the Li-ions.

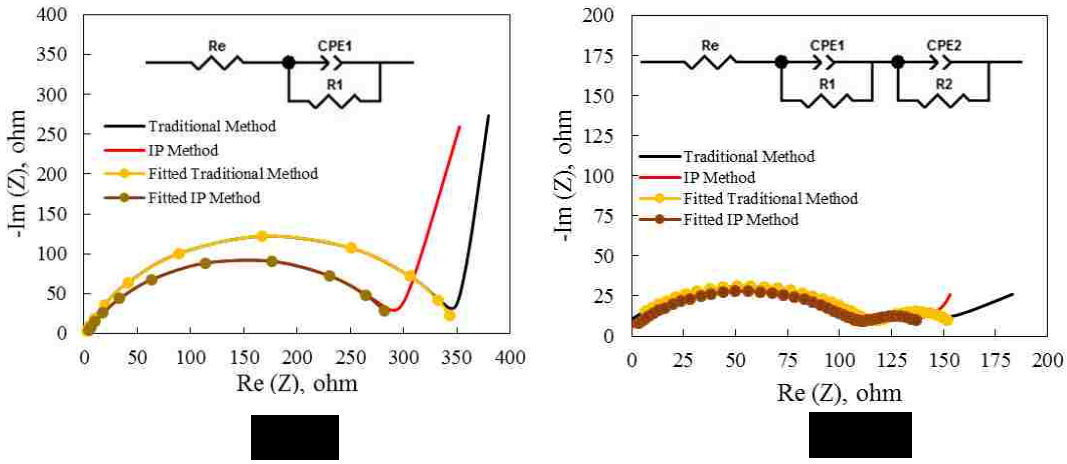

Figure 3.6: Electrochemical impedance spectroscopy (EIS) of traditional and IP electrodes: Nyquist plots and equivalent circuit of the electrodes before cycling (a), and after 160 cycles (b).

Table 3.3 The fitting numerical values of the equivalent circuit elements at the initial states.

Sample	Re (ohm)	R1 (ohm)	CPE1 (F)
Traditional method	1.4	352.4	1.2E-5
IP method	2.3	297.8	1.6E-5

The Nyquist plots of the electrodes with calendering as shown in Figure 3.6b were changed to one semicircle in the high frequency range and another semicircle at lower frequency range after cycling to 160 cycles. After cycling, we observed the second semicircle at low frequency which we believe it's attributed to SEI layer formed. The resistor (R1 and R2) and the constant phase elements (CPE1 and CPE2) values after cycling as shown in Table 3.4 were obtained from the fitting of the equivalent circuits in the inset Figure 3.6b. R1 is the SEI film impedance, and R2 is the faradic charge-transfer resistance. It should be noted that the (W_o) is not taken into account, and the capacitors are now replaced by constant phase elements (CPE1 and CPE2) to

better fit the depressed semicircles [103]. It can be found that the IP electrodes have resistance smaller than the traditionally made electrodes.

Table 3.4 The fitting numerical values of the equivalent circuit elements after cycling.

Sample	Re (ohm)	R1 (ohm)	CPE1 (F)	R2 (ohm)	CPE2 (F)
Traditional method	48.6	130.3	3.2E-5	38.8	4.9E-3
IP method	13.5	118	7.2E-5	32.3	1.3E-2

To identify the morphology of the electrodes that prepared by the IP and traditional methods after 160 cycles, the post-cycling SEM and EDS images shown in Figure 3.7a-g were obtained. The SEM images show that both electrodes exhibit cracks after cycling. The microporous PVDF structure in IP electrode reduced the size of the cracks in Figures 3.7a and b comparing with the traditional electrodes in Figures 3.7c and d. The distributions of the NMC and PVDF throughout the electrode are shown in the EDS images which are presented by the elements oxygen, fluorine, and carbon in Figures 3.7a-c, respectively. The PVDF effectively maintained the structure of the electrode, and the cracks may help explain the capacity fading during cycling.

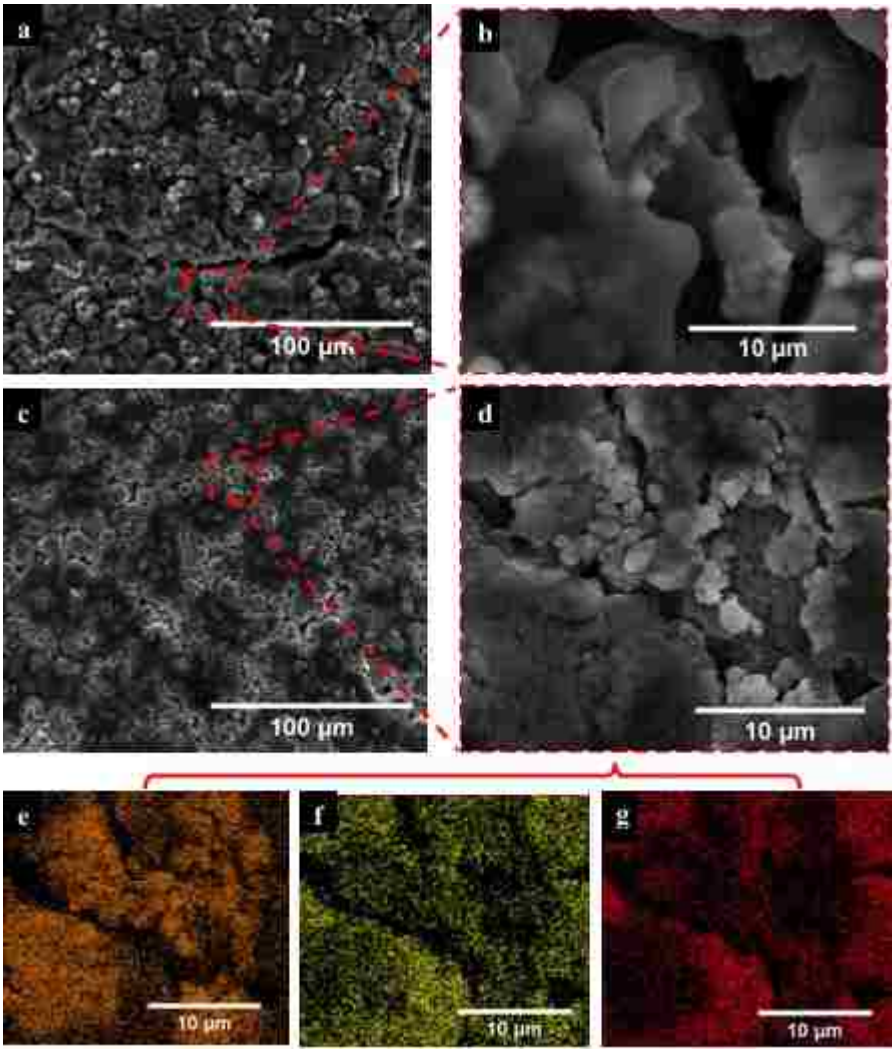

Figure 3.7: SEM images of the top surfaces of the electrodes after 160 cycling at 0.5C cycled between 3.0 V to 4.3 V: (a) the traditional electrode, (b) magnified traditional electrode, (c) the IP electrode, (d) magnified IP electrode. EDS maps of the IP electrode of the elements oxygen (e), fluorine (f), and carbon (g) from the image (d).

3.5 Conclusions

Half-cells of NMC electrodes made by the IP and conventional methods were characterized and tested. The results show that the IP process can be used to manufacture the LIB positive electrodes. The morphology shows that the electrodes made by the two methods have a similar microstructure with a slight difference in the material distribution, which leads to similar electrochemical performance and cycling life.

The exchange of NMP in the slurry with the DI-water can solidify the electrode fast without generating toxic and volatile NMP vapor that occurs during the drying step in conventional electrode manufacturing. The IP process may, therefore, reduce the energy cost and shorten the time for drying. Furthermore, since NMP is dissolved in water instead of forming NMP vapor in the IP process, distillation may be used to extract and reuse NMP in battery manufacturing. This work demonstrates that the IP method can be adapted to prepare LIB positive electrodes, which opens a new direction of making electrodes faster and at lower cost.

Chapter 4 Solvent-Free Dry Powder Coating Process for Low-Cost Manufacturing of $LiNi_{1/3}Mn_{1/3}Co_{1/3}O_2$ Cathodes in Lithium-Ion Batteries

4.1 Summary

We report a solvent-free dry powder coating process for making $LiNi_{1/3}Mn_{1/3}Co_{1/3}O_2$ (NMC) positive electrodes in lithium-ion batteries. This process eliminates volatile organic compound emission and reduces thermal curing time from hours to minutes. A mixture of NMC, carbon black, and poly(vinylidene difluoride) was electrostatically sprayed onto an aluminum current collector, forming a uniformly distributed electrode with controllable thickness and porosity. Charge/discharge cycling of the dry-powder-coated electrodes in lithium-ion half cells yielded a discharge specific capacity of 155 mAh g^{-1} and capacity retention of 80% for more than 300 cycles when the electrodes were tested between 3.0 and 4.3 V at a rate of C/5. The long-term cycling performance and durability of dry-powder coated electrodes are similar to those made by the conventional wet slurry-based method. This solvent-free dry powder coating process is a potentially lower-cost, higher-throughput, and more environmentally friendly manufacturing process compared with the conventional wet slurry-based electrode manufacturing method.

This chapter is reproduced from the work that published as: Al-Shroofy, Mohanad, Qinglin Zhang, Jiagang Xu, Tao Chen, Aman Preet Kaur, and Yang-Tse Cheng. "Solvent-free dry powder coating process for low-cost manufacturing of $LiNi_{1/3}Mn_{1/3}Co_{1/3}O_2$ cathodes in lithium-ion batteries." *Journal of Power Sources* 352 (2017): 187-193.

4.2 Introduction

Lithium-ion batteries (LIBs) dominate the market of energy-storage systems utilized in portable consumer electronic devices due to their high operating voltage, good rate capability, and long cycle lifetime [103-108]. While LIBs are popularly used in portable devices, state-of-the-art LIBs are behind the target needed for widespread adoption in vehicular applications and large-scale stationary storage systems. The Department of Energy suggests that energy-storage systems must meet a cost target of \$125 kWh^{-1} to meet the requirements for widespread adoption, which would require a three- to four-fold reduction in system costs [34]. In a recent publication, Wood and coworkers suggest (1) reducing electrode processing costs associated with organic solvents and their drying time and (2) increasing electrode thickness without compromising power density as two ways to significantly reduce system costs in LIBs [40].

The most commonly employed wet slurry-based coating method for electrode fabrication involves the mixing of active material, polymer binder, and conductive additive in a solvent. The slurry is then coated onto current collectors, dried, and calendered. *N*-methylpyrrolidone (NMP) is the most commonly used organic solvent to dissolve the poly(vinylidene difluoride) (PVDF) binder in electrode fabrication. Evaporation of NMP requires a significant energy investment, as electrodes must be dried for several hours at temperatures as high as 120 ºC to remove this solvent [109]. Because of NMP's high cost and potential as an environmental pollutant, solvent recovery is necessary in commercial applications, adding further costs to battery fabrication [40]. Numerous research groups have explored the possibility of removing organic solvents from electrode fabrication to reduce costs and environmental impact.

By replacing traditionally utilized PVDF with polymer binders such as carboxymethyl cellulose (CMC) [110, 111], alginate [112], and fluorine acrylic latex (TRD 202A) [113], water can be used instead of NMP as the solvent for electrode preparation. In several publications, water-based slurries have been reported to create electrodes with comparable performance to those fabricated with NMP [113]. Using water as the solvent eliminates the use of organic solvents, however, the time-intensive and energy-demanding drying step can be further optimized to reduce the cost of battery fabrication. For these reasons, new methods of electrode fabrication have been explored to eliminate the use of solvents altogether.

Solvent-free coating process utilizing dry particles is an ideal alternative solution to replace the wet slurry-based manufacturing process, as it eliminates the cost of solvents as well as the cost of their removal and recovery. Solvent-free manufacturing has been achieved through pulsed-laser deposition, a method in which a laser is focused on to-be-deposited electrode components. This technique requires high vacuum (10^{-6} Torr) and high annealing temperatures (>600 ºC), producing only thin films of cathode material (<500 nm) [14, 15] and is therefore impractical for large-scale fabrication. While Radio frequency (RF) magnetron sputtering can be used with lower temperature substrates (350 ºC), it requires expensive instrumentation and inert atmospheres, again impractical for large-scale electrode fabrication [16].

Another method for dry-powder coating is Electrostatic Spray Deposition (ESD), a solvent free technology that has been used in coating industries for over 30 years to create decorative and functional paints and coatings. This method eliminates the release of volatile organic compounds (VOCs), reduces energy consumption, increases paint material transfer efficiency, and improves painted-surface quality. In ESD, particles are charged as they pass through a charging gun, and are deposited onto

a grounded surface [17]. This method can be used on large particles and is scalable, offering high deposition rates onto large surfaces [18].

Recently Hiroya *et al.* reported the fabrication of cathodes using a tribo-charging gun made of a polytetrafluoroethylene (PTFE), which produces mostly positively charged particles. The cathodes coated on aluminum current collectors at room temperature contained $LiCoO_2$ particles (LCO, ~2 μm in diameter) as the active material, carbon black particles (~40 nm) as the conductive agent, and poly(methyl methacrylate) particles (~100 nm) as the binder. These subsequently roll-pressed electrodes (ca. 70 μm thick) were reported to have a capacity of ca. 140 mAh g^{-1} in lithium half cells charged at 0.1C for one cycle [114]. More recently, Ludwig *et al*. reported the use of ESD, followed with hot-rolling treatment, to create 40-130 μm thick cathodes containing a 90:5:5 ratio of LCO:carbon additive:PVDF with ca. 30% porosity, which delivered specific capacity of 121 mAh g^{-1} at a charge rate of 0.1 C in lithium half cells. Similarly prepared cathodes containing $LiNi_{1/3}Mn_{1/3}Co_{1/3}O_2$ (NMC) as the active material were also reported, showing 138 $mAhg^{-1}$ in lithium half cells [115].

In this study, we sought to (1) further demonstrate laboratory scale solvent-free dry powder coating processes for making LIB cathodes, and (2) compare in detail the performance and durability of electrodes made by dry powder coating processes with that by wet slurry coating processes and to other cathodes prepared by this method.

4.3 Experimental

4.3.1 Electrode Fabrication

4.3.1.1 Dry-Powder-Coated Electrodes

To prepare the dry cathode mixture, NMC (Umicore) was mixed with carbon black (CB, Super P C65, TIMCAL) in a planetary mixer-deaerator (Mazerustar KK-50S, Kurabo) for 20 min. The NMC particle size is between 5.6 μm and 12 μm (D_{50}=10.0). The resultant mixture was combined with PVDF (kf 1100, Kureha America) to create a mixture of NMC:CB:PVDF with a weight ratio of 80:10:10, which was obtained after mixing in a ball mill (8000M Mixer/Mill, SPEX) for 30 min.

The electrostatic dry-powder-coating process for electrode fabrication utilized a corona-type electrostatic spray gun setup (Figure 4.1) inside a spray booth to capture loose powder, which was used to spray the powder mixture onto an electrically grounded Al foil (15 μm thick). The DC voltage between the gun and Al foil was set at 25 kV. Compressed air (15 psi) was used to transport the powder mixture from the hopper to the spray gun. The distance between the tip of the spray gun and the substrate was fixed at 20 cm. The angle between the spray direction and the normal of the Al foil was 45º. The thickness of the sprayed layer was controlled by keeping the spraying time to 1 min, and the size of the fabricated electrode layer was about 18 mm wide and 25 mm long. The dry-powder-coated electrodes were transferred to an oven and heated in air for 1 h at 170 ºC. Then the baked electrodes were calendered at room temperature with specified gap spacing by a compact electrical rolling press (MTI Corp.). The gap spacing was estimated to be between 10-25 μm during calendering. 12 mm diameter discs were cut using a Precision Disc Cutter (MTI Corp.) and transferred to a glove box.

4.3.1.2 Wet-Slurry-Coated Electrodes

For comparison, slurry-based electrodes were prepared from NMC, CB, and PVDF (90:5:5 wt. ratio) suspended in NMP (84% in volume, BASF). The slurry was blended in a homogenizer at 4000 rpm for 1 h (Polytron PT 10-35 GT) and afterward was casted onto Al foil (15 μm thick) using a compact-tape casting coater with integrated dryer and vacuum chuck (MTI Corp.). The adjustable doctor blade gap was set to 200 μm, and slurry was cast at a speed of 0.2 m min^{-1}. The electrodes were dried in air overnight and calendered in a compact electric rolling press (MTI Corp.) with adjusted clamping force at room temperature. After calendering, 12 mm diameter discs were cut using a Precision Disc Cutter (MTI Corp.) after which they were placed in a vacuum oven at 130 °C for 12 h.

4.3.2 Electrode Characterization

4.3.2.1 Morphology

Using an Environmental Scanning Electron Microscopy (ESEM) with Energy Dispersive Spectroscopy (EDS) (Quanta FEG 250, FEI), we investigated the morphology and composition of the powders, as well as the surface and cross section of the electrodes made by the electrostatic spray and wet slurry coating processes.

4.3.2.2 Thermogravimetric Analysis

Thermogravimetric Analysis (TGA) was used to determine the mass ratios of the powder mixtures consisting of NMC, CB, and PVDF before and after electrostatic spraying. TGA experiments were performed on a TA Q500 instrument, with a standard heating rate of 10 °C min^{-1} from ambient temperature to 800 °C under air.

4.3.2.3 Coin Cells Assembling and Electrochemical Tests

CR2025-type coin cells were assembled using an automatic coin cell crimper (KTE-20S-D, Hohsen) inside argon filled glovebox (MB-20-G, MBraun) with water and oxygen levels below 0.1 ppm. Lithium metal foil (99.9%, Sigma–Aldrich) was used as the counter/reference electrode. A piece of poly-propylene membrane (Celgard 2400) was used as the separator between the lithium foil and the cathode. 1M $LiPF_6$ in ethylene carbonate/ethylmethyl carbonate (EC/EMC 3:7 by volume, BASF) with 2% vinylene carbonate (VC, BASF) was used as the electrolyte. The electrolyte weight ratios were 12.5 wt% $LiPF_6$, 25.7 wt% EC, 59.9 wt% EMC, and 2.0 wt% VC. A stainless steel spacer and spring were placed on the lithium metal to obtain a uniform current distribution and served as a current collector. The electrochemical characterization of the assembled cells was performed using a multi-channel potentiostat (VMP-3, Bio-logic) operated in the galvanostatic mode. Cell cycling was performed at room temperature with a 2 h resting period before each test. Charge/ discharge tests were also performed at variable rates, ranging from 0.5C to 10C, cycling between 3.0 V and 4.3 V. At the end of each charge, the electrode was holding at 4.3 V until the current dropped below 0.05C. More than 20 coin cells from 3 batches were made to test the electrochemical performance of the prepared electrodes by the dry-process and wet-process methods in half-cells with pure lithium as the counter electrode.

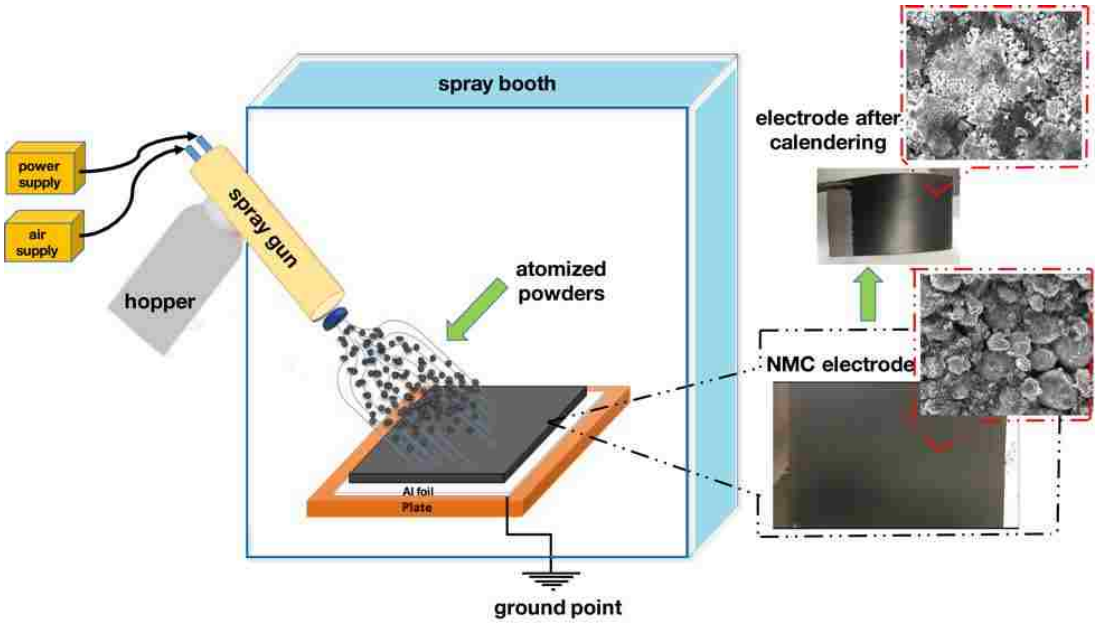

Figure 4.1: Illustration of an electrostatic dry-powder coating process for making cathodes containing NMC, carbon black, and PVDF.

4.4 Results and discussion

NMC was used as the cathode active material because of its high reversible specific capacity (150-200 mAh g^{-1}) [116], high energy density (140-180 Wh/kg) [117], and high charge and discharge rate capability [94]. The dry-powder-coated electrodes were transferred to an oven set at 170 ºC, close to the melting point of PVDF (177 ºC) and were heated in air for 1 h. The heating temperature was close to melting point of PVDF to build bonding between PVDF and the solid particles (NMC and CB), meanwhile maintain the porosity of electrodes during heating [118]. The baked electrodes were calendered at room temperature to increase the cohesion between the particles and the binder hence improve the integrity of the electrodes. The calendering process could also improve the adhesion between the coated materials and the Al foil, and control the porosity and the packing density of the electrodes.

To determine whether the dry-powder-coated electrodes contained the target ratio of NMC:CB:PVDF with as-prepared mixture of powders, we analyzed the pre-mixed powder and that deposited on the Al foil using TGA. For the powder mixture and coated electrodes, mass loss trends (Figure 4.2a) were nearly identical. Comparing the TGA plots of the mixtures to that of the components shown in Figure 4.2b, it is evident that the mass loss spanning ca. 400 to 460 ºC corresponds to PVDF [119, 120], whereas the loss from 500 to 600 ºC corresponds to CB. In the temperature window analyzed, NMC does not lose mass, which means it is thermally stable [121].

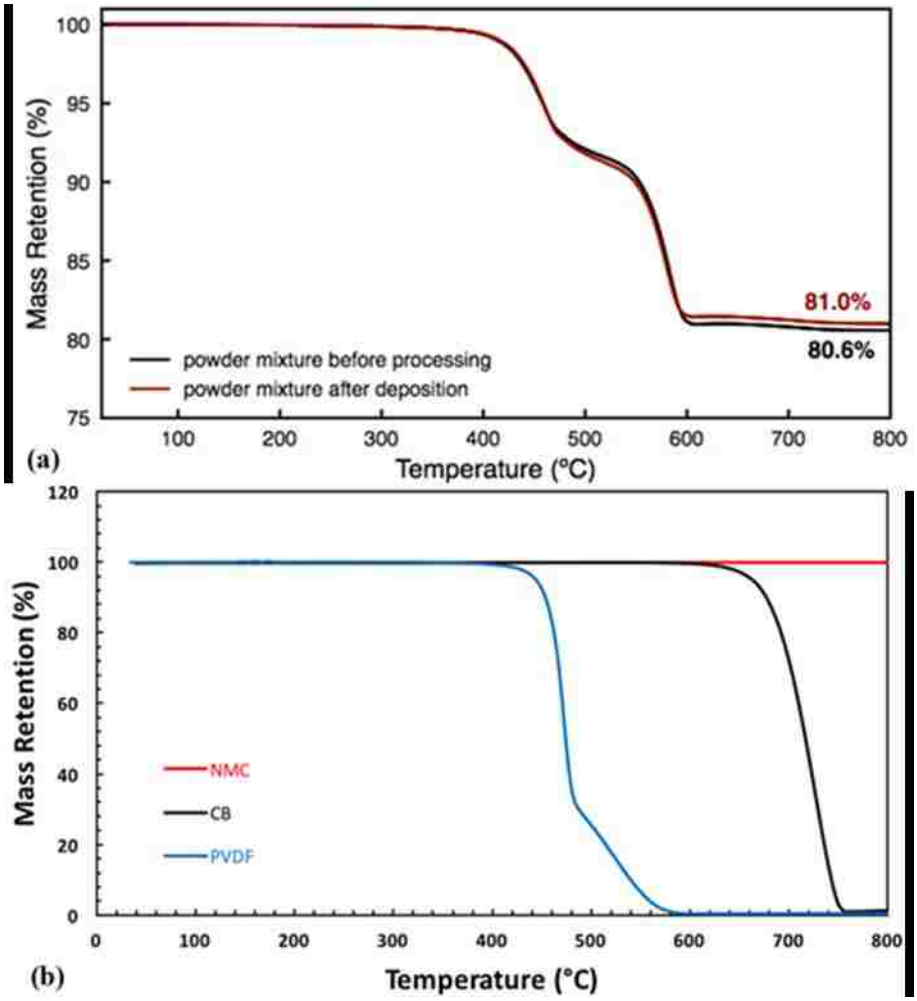

Figure 4.2: Mass retention vs. temperature of electrode mixtures before and after electrostatic dry-powder-coating, as determined by thermogravimetric analysis (TGA) under air atmosphere (a), and TGA for pure PVDF, CB, and NMC (b).

SEM was used to analyze the powder mixtures to determine whether the particles remained intact after electrostatic coating. SEM images (Figure 4.3a-b) indicate that the NMC particles are intact after processing, as no appreciable morphological difference is observed before and after coating. The SEM image of the top surface of the as-prepared electrode after the curing and calendering steps (Figure 4.3c) shows that the electrode is more dense after processing. Figure 4.4 shows the even

distribution of the electrode particles over a large electrode area. For comparison, a top view of a slurry-made electrode after drying and calendaring is shown in Figure 4.3d.

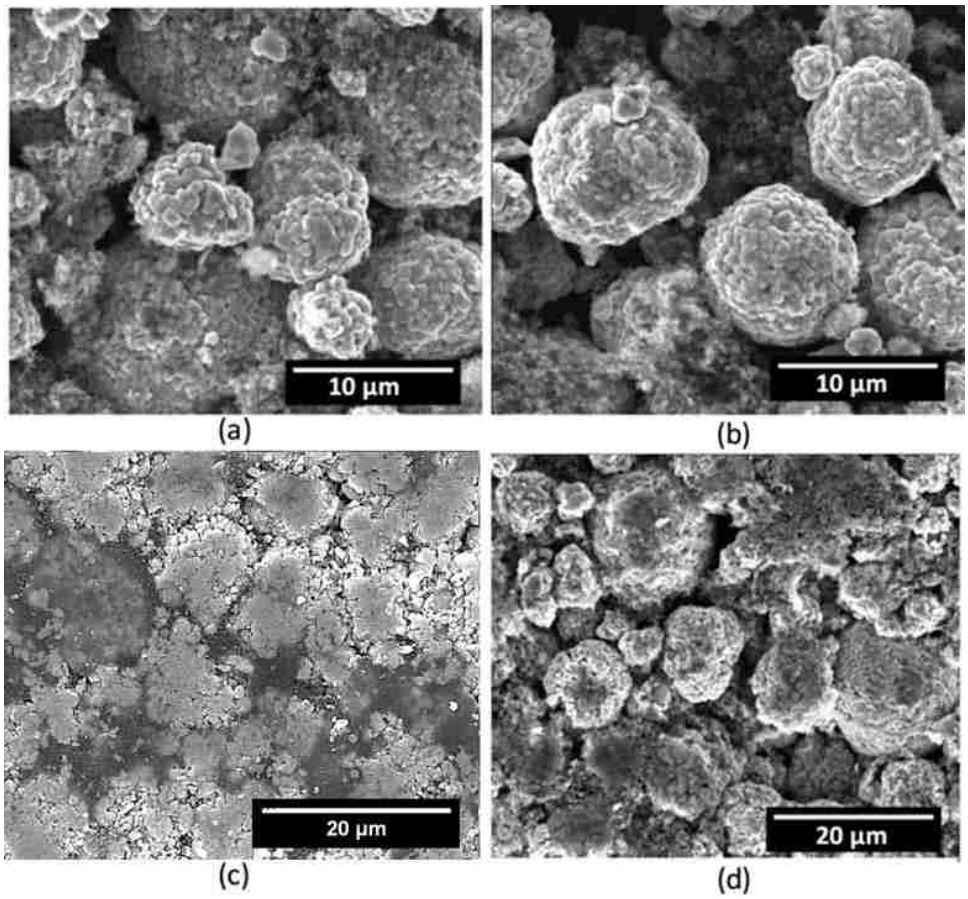

Figure 4.3: Top-view SEM images of: (a) Powder mixture before dry-powder coating. (b) Powder mixture after dry-powder coating. (c) Dry-powder-coated electrode after calendering. (d) Wet-slurry coated electrode after drying and calendering.

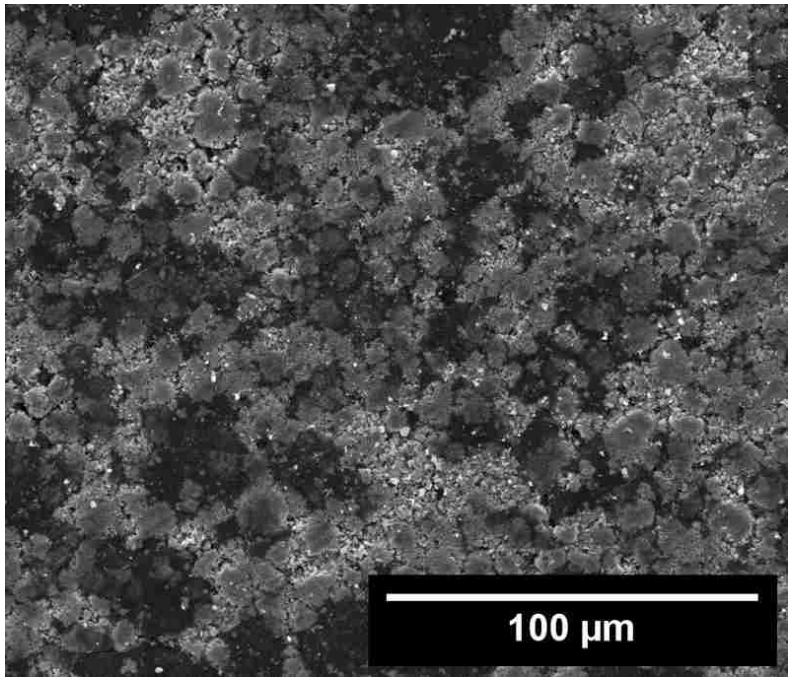

Figure 4.4: SEM image of the top surface of a dry-powder coated electrode to show the evenness of the electrode.

Cross-sectional SEM images of the dry-powder-coated electrodes after calendering are shown at two magnifications in Figures 4.5a and b. For comparison, the SEM cross-section image of an electrode made by the traditional wet-slurry method is shown in Figure 4.5c. The structures of the electrodes made by the two processes are similar. EDS was used to map the elements carbon, oxygen, and fluorine (Figures 4.5d-f). Based on the oxygen and fluorine maps, respectively, the EDS maps show that NMC and PVDF are dispersed throughout the sample. Although the carbon map shows the presence of carbon throughout the image, because carbon is present in both carbon black and PVDF, it is not possible to differentiate between these species.

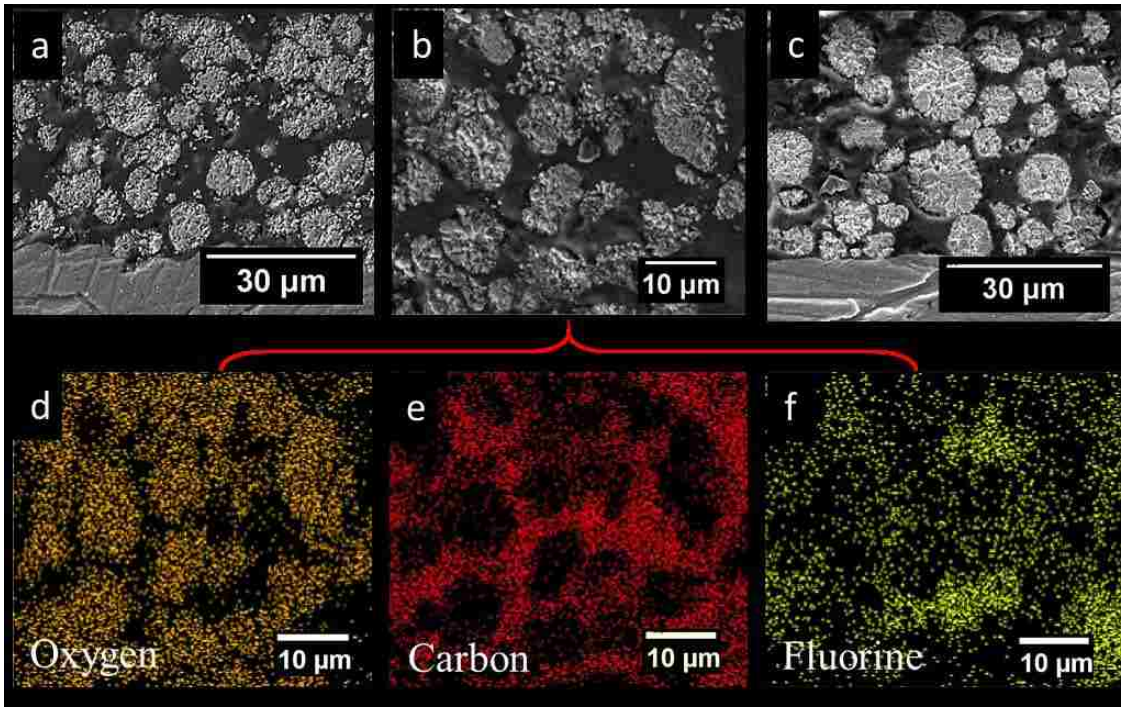

Figure 4.5: SEM images of the cross-section of the dry-powder-coated electrode after calendering (a) and magnified cross-sectional view (b). A cross-sectional view of the wet-slurry-coated electrode (c). EDS maps of the elements carbon (d), oxygen (e), fluorine (f) from image (b).

The calendering process compacts the electrodes, improves the cohesion between the particles and the adhesion of the composite materials with the Al foil, and controls the porosity and the packing density of the electrodes [97, 122]. The electrodes are well compacted after calendering with a porosity of 31% and packing density of 2.5 g cm^{-3}. For comparison, two conventional slurry-based electrodes with mass loading higher and lower than the dry-powder coated electrode were studied. (See Table 4.1)

Table 4.1 The thickness, mass loading, porosity, density, and discharge capacity of electrodes made by the dry and wet processes.

Process	Thickness (µm)	Mass loading (mg cm^{-2})	Porosity (%)	Packing density (g cm^{-3})	Discharge capacity (mAh g^{-1})
Dry-powder coating electrode	40.5	10.07	31	2.5	155
Wet-slurry-based electrode (higher loading)	52	14.27	35	2.7	156
Wet-slurry-based electrode (lower loading)	32.6	7.65	41	2.4	157

The electrochemical behavior of dry-powder-coated electrodes was analyzed in lithium half cells using 1M $LiPF_6$ in EC/EMC (3:7 by volume) containing 2 wt% VC as the electrolyte. VC was added to improve the rate performance [22]. Cell potential vs. state-of-charge plot for the first cycle of the dry-powder-coated electrode is shown in Figure 4.6a. For comparison, the first cycle electrochemical behavior of a wet-slurry made electrode is shown in Figure 4.6b. Evidently, the voltage profiles for charge-discharge cycles for the dry powder-coated electrodes are similar to that of the conventional slurry-coated electrodes.

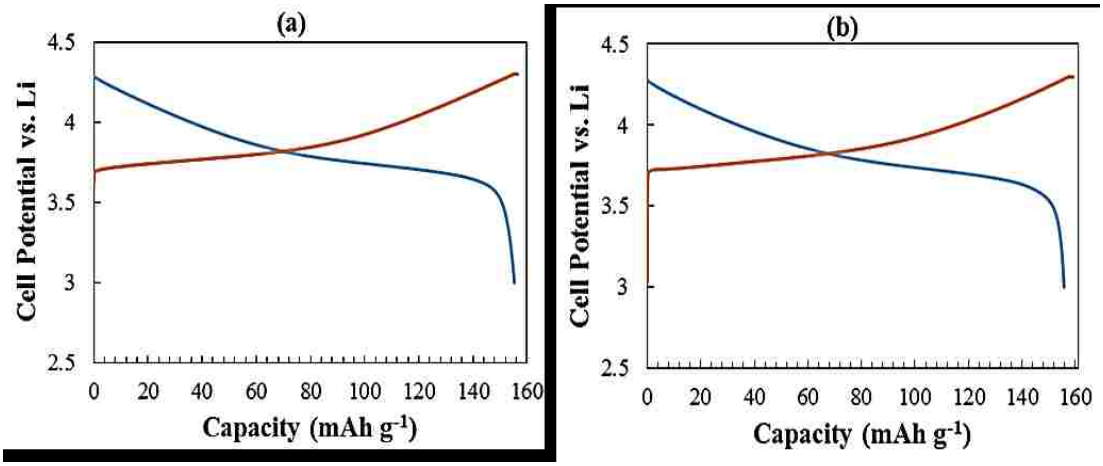

Figure 4.6: Cell potential vs. Capacity for the first charge and discharge cycles of the dry-powder-coated electrode (a) and wet-slurry-coated electrode (b).

Figure 4.7a shows the potential profile for cycles 1, 10 and 20 between 3.0 V and 4.3 V at 0.2C with a constant voltage holding with the current limitation of 0.05C at the end of the charge step. For dry-powder coated electrodes, the initial discharge capacities fade slowly during cycling and are 155 mAh g^{-1} and 153 mAh g^{-1} for cycles 1 and 20, respectively, while for wet-slurry-coated electrodes there is little capacity fade for the first 20 cycles.

To investigate the effect of different charge/discharge rates on the cycling performance of the dry sprayed and slurry electrodes, the NMC cells were charged and discharged between 3.0 V and 4.3 V at various cycling rates, in the order of 0.2C, 0.5C, 1C, 2C, 5C, 10C and 1C. For dry powder coated electrodes, the specific capacities were 156, 148, 139, 130, 96, 20, and 139 mAh g^{-1}, respectively, as shown in Figure 4.7b. When returned to 1C, the capacity recovered to the previous level. At high rates, the electrodes will polarize and the plateaus of the NMC become shorter when the charge and discharge current densities increase, causing a decrease in capacity [112]. For the wet-slurry-coated higher mass loading electrode the discharge capacities for the respective C-rates were 153, 149, 145, 140, 129, 46, and 145 mAh g^{-1}, while for the

wet-slurry-coated lower mass loading the electrode discharge capacities were 151, 145, 140, 133, 120, 90, and 139 mAh g^{-1}. The small difference in the discharge capacities between the dry-powder and wet-slurry coated electrodes for high charge/discharge rates may come from the differences in porosity and packing density of the electrodes.

Figure 4.7c shows the long term cycling performance of the dry sprayed (0.2C) and the conventional slurry-made electrode (0.5C) between 3.0 V and 4.3 V followed by constant voltage with current limitation of 0.05C after charge step. For the dry-powder-coated electrode, the first discharge capacity was 155 mAh g^{-1}, and the discharge capacity was 123 mAh g^{-1} after 300 cycles with a capacity retention of 80%. While for the wet-slurry-coated electrode, the first discharge capacities were 156 mAh g^{-1} and 157 mAh g^{-1} with capacity retention of 60% and 65% and discharge capacity of 97 mAh g^{-1} and 104 mAh g^{-1} after 300 cycles for higher and lower mass loading, respectively. The cycling performance of the dry sprayed NMC electrode is better than that of the traditional slurry-coated electrode by exhibiting stable performance and better capacity retention. These results suggest that (1) the internal resistances are comparable and (2) the NMC is fully utilized in both electrodes.

The post-cycling SEM images, Figures 4.8a-d, were obtained for the electrodes prepared using both methods after 300 cycles. The SEM images show that cracks appeared after cycling in both electrodes. At the end of discharge cycles, the dry-powder electrode images in Figure 4.8a and b showed that cracks appeared at the NMC grain boundaries, while in the wet-slurry electrode (Figure 4.8c and d), the crack appeared around the NMC particles and in the CB and PVDF mixture. The size of the cracks in the dry-powder electrode appeared larger than that in the wet-slurry electrode, though the difference in cracking does not seem to be responsible for the slight difference in performance and durability of electrodes made by the two processes.

As reported by Ludwig *et al*. [115], they used electrostatic spray deposition (ESD), followed by hot-rolling treatment and a mass wt. ration of 90:5:5, the discharge capacity was 121 $mAhg^{-1}$ in lithium half cells and the capacity retention was 87% at 0.5C after 50 cycles. In this work, we demonstrated that by heating the electrode film after spray and before calendering it at ambient temperature, the electrode showed an improvement in performance and cycle life. The difference in the performance may also be contributed to the mass ratio different (NMC:CB:PVDF=80:10:10 in this work vs. 90:5:5 in Ludwing *et at*. [115]. The PVDF will hold the NMC and CB particles and improve the cohesion among the electrode components and the adhesion between the electrode and the Al foil.

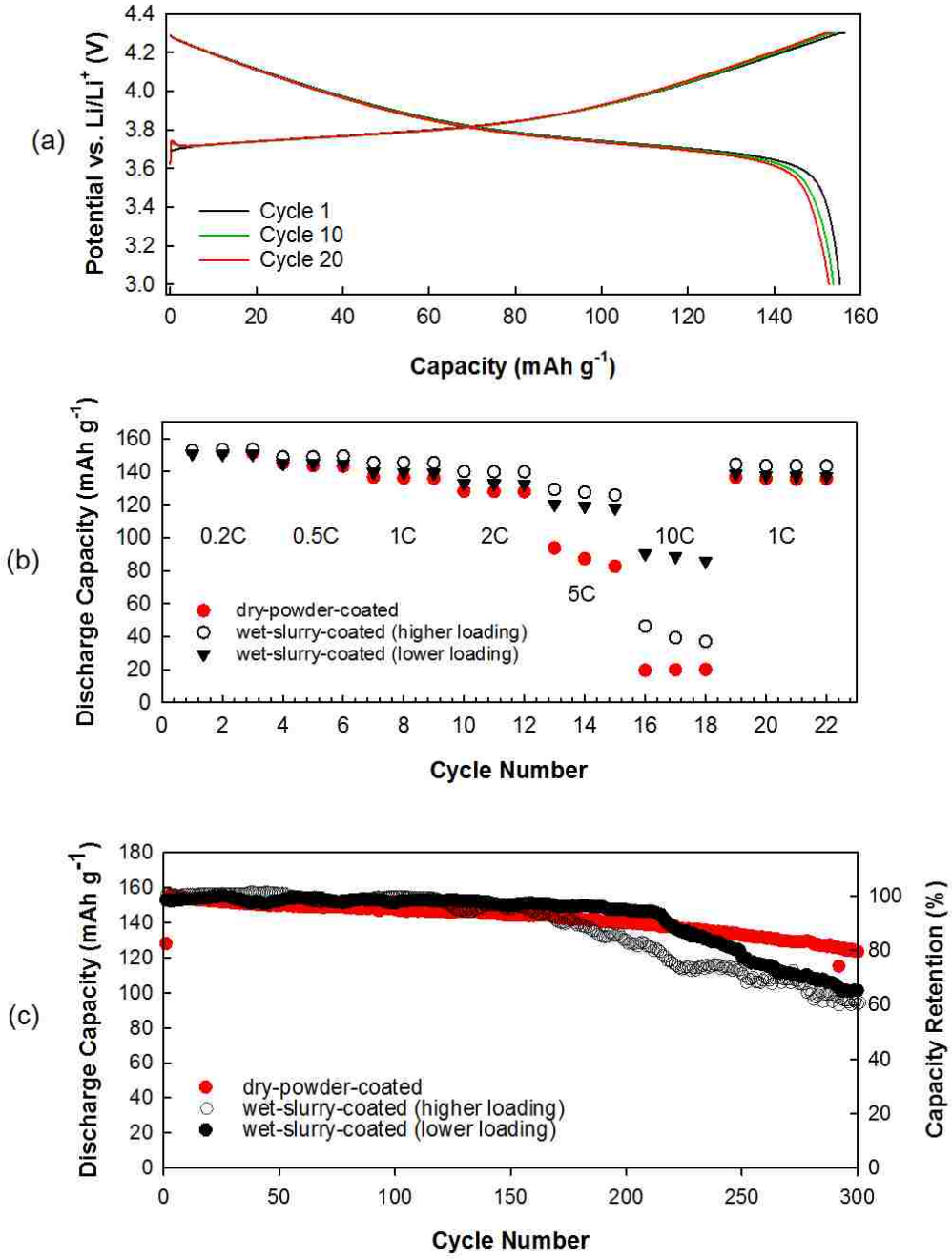

Figure 4.7: (a) Potential vs. capacity profiles of the dry-powder-coated cathode in lithium half cells, for cycle 1, 10 and 20. Cells were cycled in the voltage window from 3.0 V to 4.3 V at 0.5C followed by constant voltage holding with current limitation of 0.05C at the end of each charge. (b) Discharge capacities at various current densities for two types of NMC cathodes. (c) Discharge capacity (left) and capacity retention (right) curves for a wet-slurry coated NMC cathode (0.5C) and a dry-powder coated NMC cathode (0.2C) in lithium half cells cycled between 3.0 V and 4.3 V.

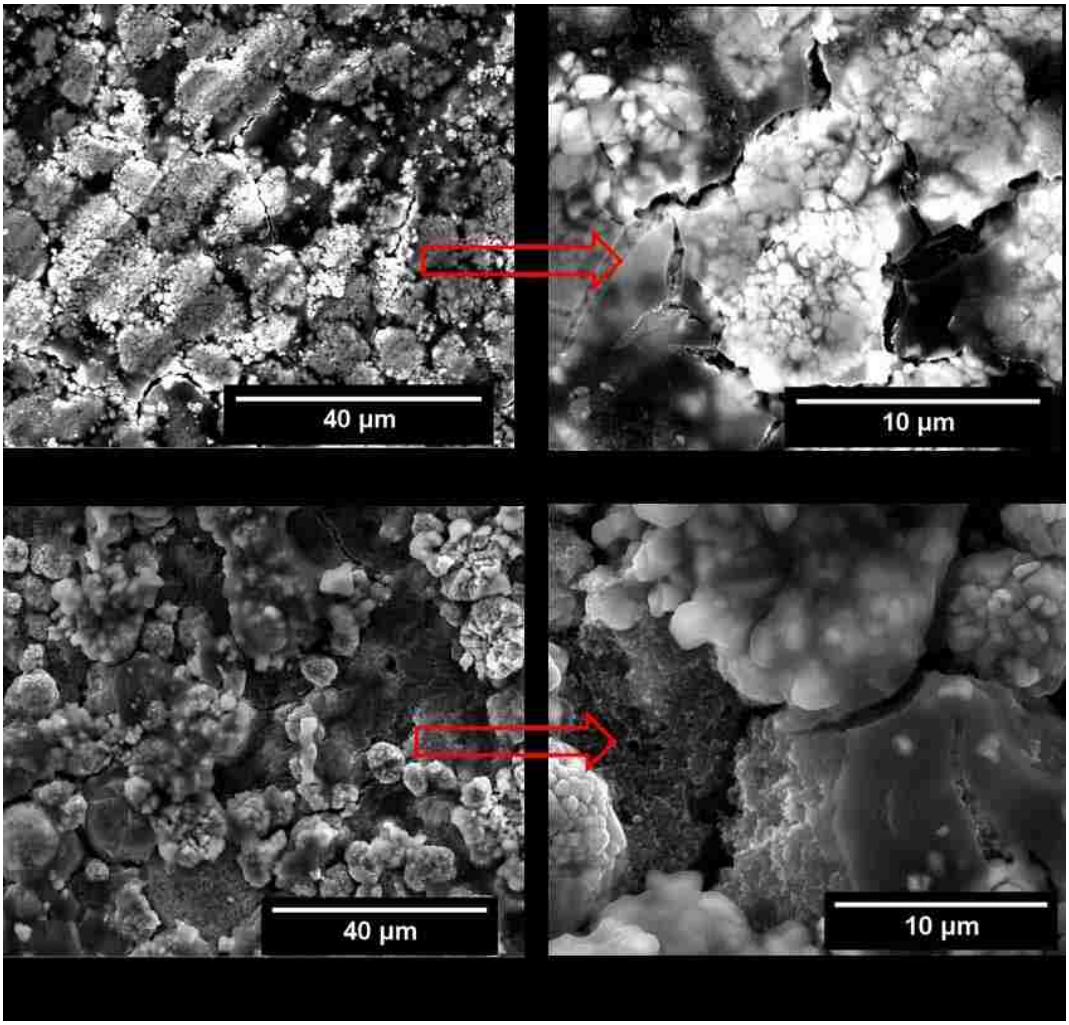

Figure 4.8: SEM images of the top surfaces of electrodes after 300 cycling at 0.2C over a voltage range from 3.0 V to 4.3 V: (a) the dry-powder electrode, (b) magnified dry-powder electrode view, (c) the low mass loading wet-slurry electrode, and (d) magnified wet-slurry electrode view.

4.5 Conclusion

We demonstrated that a solvent-free dry powder coating process, in particular electrostatic spraying, can be used to fabricate NMC-containing cathodes for LIBs. The morphology of the powders and electrodes shows very well distributed particles in the coated layer, and that the binder is well dispersed in dry powder before and after spraying. Constant current charge-discharge test results show that the dry sprayed NMC electrodes with PVDF as binders and CB as a conductive agent exhibit high discharge specific capacity with very good capacity retention, comparable to electrodes made by the conventional, wet-slurry-coating process.

This work is significant because (1) electrodes made by the dry powder coating process can have reversible capacity and cycle life comparable to the electrodes made by the wet slurry method, (2) dry powder coating may lower the cost by reducing the mixing and slurry preparation steps and the reducing drying time, and (3) dry-powder coating eliminates the pollution caused by NMP solvent. Since dry powder coating processes have significantly benefited the paint industry which faced similar issues with the cost and environmental impact associated with solvents, we believe that solvent-free dry coating processes, such as electrostatic spraying, could replace the traditional wet slurry method of making battery electrodes.

Chapter 5 Conclusions and Future Works

5.1 Conclusions

In this dissertation, we have investigated various approaches to understand and improve the manufacturing processes of the Li-ion battery electrodes. The main conclusions are:

Different mixing sequences to improve the performance and durability of Li-ion batteries were studied. The mixing sequences 1, 2, 3, and 4 were optimized. The rheological behavior of the slurries, morphology, conductivity, and mechanical and electrochemical properties of electrodes were investigated. Reproducible results as evaluated by slurry viscosity, electrode morphology, and coin cell performance were achieved. Slurries from sequences 1 and 4 have different rheological properties from 2 and 3. The former is “gel-like” and the latter is ”fluid-like”, according to the relative magnitude of their loss and storage moduli as determined in oscillatory rheology characterization. The amount of NMP required to achieve a comparable final slurry viscosity (evaluated at the shear rate corresponding to coating) differed significantly for the sequences under study and was found to be strongly related to the “gel” or “liquid” characterization. Sequences 2 and 3 (the two “liquid” slurries) required a notably lower amount of solvent than the “gel” like counterparts in order to yield slurries and electrodes of desired attributes. The results suggest better long term cycling behavior from sequences 1 than sequences 1, 2, and 3. The key factor determining fluid or gel-like behavior appears to be whether the NMC and CB are mixed in the presence of or prior to the introduction of the binder solution. The conductivity measurements show that electrodes from Sequence 1 have higher conductivity than the other sequences. The mechanical properties measured using microindantation indicate that the electrodes from sequences 2 and 3 have the highest hardness and elastic modulus,

while electrodes from sequence 1 and 4 have the lowest. These results are consistent with scratch test results, which were used to understand the cohesion between the particles. Interestingly, higher hardness and elastic modulus values do not translate to longer cycle life.

In chapter 3, we develop a new method of making Li-ion battery electrodes with lower-cost, higher-throughput, and more environmentally friendly manufacturing process compared with the conventional wet slurry-based electrode manufacturing method by adapting an immersion precipitation (IP) technology. The exchange of NMP in the slurry with the DI-water can solidify the electrode fast without generating toxic and volatile NMP vapor that occurs during the drying step in conventional electrode manufacturing. The electrodes that prepared by the two methods have similar electrochemical performance and cycling life.

Our results in chapter 4 show that dry powder-coating process can indeed make Li-ion battery electrodes. The long-term cycling performance and durability of dry-powder coated electrodes are similar to those made by the conventional wet slurry-based method. This work is significant because (1) electrodes made by the dry powder coating process can have reversible capacity and cycle life comparable to the electrodes made by the wet slurry method, (2) dry powder coating may lower the cost by reducing the mixing and slurry preparation steps and the reducing drying time, and (3) dry-powder coating eliminates the pollution caused by NMP solvent. Since dry powder coating processes have significantly benefited the paint industry which faced the similar issues with the cost and environmental impact associated with solvents, we believe that solvent-free dry coating processes, such as electrostatic spraying, could replace the traditional wet slurry method of making battery electrodes.

5.2 Future work

This thesis will hopefully pave the way for future researchers to use our methods to prepare Li-ion battery electrodes, leading to commercialization.

In chapter two, we demonstrated that the influence of four mixing sequences on the electrochemical performance, durability, and cost of positive electrodes. Each mixing sequence was shown to have an effect on the rheology behavior of the slurry, which in turn affects the distribution of the electrode materials, conductivity, and the mechanical and electrochemical properties of the electrodes. This study focuses on quantifying the effects of the mixing process on finished battery quality through application of mixing theory, rheology, and morphology. The results establish an important baseline characterization tool set to allow up front slurry optimization, thus accelerating the development process. Further studies of mixing sequences will provide a relationship between mixing sequences, electrode structure, and electrochemical performance of electrodes.

Adapting membrane manufacturing technology to make Lithium-Ion battery electrodes using Immersion precipitation (IP) method is another promising manufacturing approach. Translating a mature technology from the membrane industry to electrode fabrication will enable a robust process for achieving gradients in composition, porosity, and structure which is one of the challenges that limit the performance and cycle life of LIBs. The IP method is expected to provide better control of the structure of the electrode, make thick electrodes, reduce the drying time, lower the manufacturing cost, and prevent volatile organic compound.

In chapter four, we developed a low-cost and environmentally friendly manufacturing method to fabricate lithium ion batteries (LIBs) with high performance and durability. The electrostatic spraying process for dry manufacturing of NMC-

cathodes gave us confidence to further explore the process for making LIBs consisting of a wide range of advanced materials. The future plan will focus on using this process to fabricate the negative electrodes and to make full cells. This method can be used to produce electrode structures that are impossible to make by the conventional wet slurry method, such as graded composition and porosity, multilayer structures, and free-standing electrodes. By exploring experimental parameters for electrostatic spraying to reduce the time and energy consumption of making LIB electrodes, these experiments will provide the basis for a detailed cost comparison between the dry and wet electrode manufacturing methods, an important step towards scale-up the process for production.

The three approaches to electrode manufacturing will hopefully be implemented by battery manufacturers because of the merits of the approaches in terms of performance, durability, environmental impact, and cost.

References

1. Huggins, R., *Advanced Batteries: Materials Science Aspects*, (Springer Science & Business Media, 2008)

2. Al-Shroofy, M., Zhang, Q., Xu, J., Chen, T., Kaur, A.P., and Cheng, Y.-T., 'Solvent-Free Dry Powder Coating Process for Low-Cost Manufacturing of Lini 1/3 Mn 1/3 Co 1/3 O 2 Cathodes in Lithium-Ion Batteries', *Journal of Power Sources*, 2017, 352, pp. 187-193.

3. Li, J., 'Understanding Degradation and Lithium Diffusion in Lithium Ion Battery Electrodes', 2012.

4. Chen, T., Zhang, Q., Pan, J., Xu, J., Liu, Y., Al-Shroofy, M., and Cheng, Y.-T., 'Low-Temperature Treated Lignin as Both Binder and Conductive Additive for Silicon Nanoparticle Composite Electrodes in Lithium-Ion Batteries', *ACS Applied Materials & Interfaces*, 2016, 8, (47), pp. 32341-32348.

5. Kim, K.M., Jeon, W.S., Chung, I.J., and Chang, S.H., 'Effect of Mixing Sequences on the Electrode Characteristics of Lithium-Ion Rechargeable Batteries', *Journal of Power Sources*, 1999, 83, (1), pp. 108-113.

6. Yang, C., Cheng, C., Ho, S., Chen, J., and Hurng, W., 'Performance Study of the Licoo2/Graphite System', *Journal of Power Sources*, 1997, 68, (2), pp. 440-442.

7. Bauer, W., Nötzel, D., Wenzel, V., and Nirschl, H., 'Influence of Dry Mixing and Distribution of Conductive Additives in Cathodes for Lithium Ion Batteries', *Journal of Power Sources*, 2015, 288, pp. 359-367.

8. Liu, F., Hashim, N.A., Liu, Y., Abed, M.M., and Li, K., 'Progress in the Production and Modification of Pvdf Membranes', *Journal of Membrane Science*, 2011, 375, (1), pp. 1-27.

9. Bottino, A., Camera-Roda, G., Capannelli, G., and Munari, S., 'The Formation of Microporous Polyvinylidene Difluoride Membranes by Phase Separation', *Journal of Membrane Science*, 1991, 57, (1), pp. 1-20.

10. Miao, R., Liu, B., Zhu, Z., Liu, Y., Li, J., Wang, X., and Li, Q., 'Pvdf-Hfp-Based Porous Polymer Electrolyte Membranes for Lithium-Ion Batteries', *Journal of Power Sources*, 2008, 184, (2), pp. 420-426.

11. Magistris, A., Mustarelli, P., Parazzoli, F., Quartarone, E., Piaggio, P., and Bottino, A., 'Structure, Porosity and Conductivity of Pvdf Films for Polymer Electrolytes', *Journal of Power Sources*, 2001, 97, pp. 657-660.

12. Cheng, Q., Cui, Z., Li, J., Qin, S., Yan, F., and Li, J., 'Preparation and Performance of Polymer Electrolyte Based on Poly (Vinylidene Fluoride)/Polysulfone Blend Membrane Via Thermally Induced Phase Separation Process for Lithium Ion Battery', *Journal of Power Sources*, 2014, 266, pp. 401-413.

13. Pu, W., He, X., Wang, L., Jiang, C., and Wan, C., 'Preparation of Pvdf–Hfp Microporous Membrane for Li-Ion Batteries by Phase Inversion', *Journal of Membrane Science*, 2006, 272, (1), pp. 11-14.

14. Shiraki, S., Oki, H., Takagi, Y., Suzuki, T., Kumatani, A., Shimizu, R., Haruta, M., Ohsawa, T., Sato, Y., and Ikuhara, Y., 'Fabrication of All-Solid-State Battery Using Epitaxial Licoo 2 Thin Films', *Journal of Power Sources*, 2014, 267, pp. 881-887.

15. Kuwata, N., Kawamura, J., Toribami, K., Hattori, T., and Sata, N., 'Thin-Film Lithium-Ion Battery with Amorphous Solid Electrolyte Fabricated by Pulsed Laser Deposition', *Electrochemistry Communications*, 2004, 6, (4), pp. 417-421.

16. Chiu, K.-F., 'Lithium Cobalt Oxide Thin Films Deposited at Low Temperature by Ionized Magnetron Sputtering', *Thin Solid Films*, 2007, 515, (11), pp. 4614-4618.

17. Bailey, A.G., 'The Science and Technology of Electrostatic Powder Spraying, Transport and Coating', *Journal of electrostatics*, 1998, 45, (2), pp. 85-120.

18. Mazumder, M., Wankum, D., Sims, R., Mountain, J., Chen, H., Pettit, P., and Chaser, T., 'Influence of Powder Properties on the Performance of Electrostatic Coating Process', *Journal of electrostatics*, 1997, 40, pp. 369-374.

19. Zhang, S.S., 'A Review on the Separators of Liquid Electrolyte Li-Ion Batteries', *Journal of Power Sources*, 2007, 164, (1), pp. 351-364.

20. Kim, J.-K., *Advanced Materials for Rechargeable Lithium Batteries*, (Chalmers University of Technology, 2012)

21. Armand, M., Endres, F., MacFarlane, D.R., Ohno, H., and Scrosati, B., 'Ionic-Liquid Materials for the Electrochemical Challenges of the Future', *Nature materials*, 2009, 8, (8), pp. 621-629.

22. Deshpande, R.D., Ridgway, P., Fu, Y., Zhang, W., Cai, J., and Battaglia, V., 'The Limited Effect of Vc in Graphite/Nmc Cells', *Journal of The Electrochemical Society*, 2015, 162, (3), pp. A330-A338.

23. Michan, A.L., Parimalam, B.S., Leskes, M., Kerber, R.N., Yoon, T., Grey, C.P., and Lucht, B.L., 'Fluoroethylene Carbonate and Vinylene Carbonate Reduction: Understanding Lithium-Ion Battery Electrolyte Additives and Solid Electrolyte Interphase Formation', *Chemistry of Materials*, 2016, 28, (22), pp. 8149-8159.

24. Linden, D. and Reddy, T.B., Handbook of Batteries. 3rd', (McGraw-Hill, 2002)

25. Xu, J., 'Lnvestigation of the Critical Role of Polymeric Binders for Silicon Negative Electrodes in Lithium-Lon Batteries', 2016.

26. Pan, J., Cheng, Y.-T., and Qi, Y., 'General Method to Predict Voltage-Dependent Ionic Conduction in a Solid Electrolyte Coating on Electrodes', *Physical Review B*, 2015, 91, (13), p. 134116.

27. Pan, J., 'Understanding Electrical Conduction in Lithium Ion Batteries through Multi-Scale Modeling', 2016.

28. Hausbrand, R., Cherkashinin, G., Ehrenberg, H., Gröting, M., Albe, K., Hess, C., and Jaegermann, W., 'Fundamental Degradation Mechanisms of Layered Oxide Li-Ion Battery Cathode Materials: Methodology, Insights and Novel Approaches', *Materials Science and Engineering: B*, 2015, 192, pp. 3-25.

29. Doeff, M.M., Conry, T., and Wilcox, J., 'Improved Layered Mixed Transition Metal Oxides for Li-Ion Batteries', in, *SPIE Defense, Security, and Sensing*, (International Society for Optics and Photonics, 2010)

30. Loveridge, M.J., Lain, M.J., and Kronfli, E., Binder for Lithium Ion Rechargeable Battery Cells', (Google Patents, 2010)

31. Yao, Y., Huo, K., Hu, L., Liu, N., Cha, J.J., McDowell, M.T., Chu, P.K., and Cui, Y., 'Highly Conductive, Mechanically Robust, and Electrochemically Inactive Tic/C Nanofiber Scaffold for High-Performance Silicon Anode Batteries', *ACS nano*, 2011, 5, (10), pp. 8346-8351.

32. Garcia, A., 'Rheological Behaviour of Na-Cmc and Na-Alginate as Binders for Lithium Ion Batteries', 2015.

33. Https://Www.Cta.Tech/News/I3/Articles/2017/January-February/the-Global-Race-for-Next-Generation-Battery-Power.Aspx.

34. Howell, D., 'Fiscal Year 2011 Annual Progress Report for Energy Storage R&D', *US Department of Energy, Washington, DC*, 2012.

35. Oswal, M., Paul, J., and Zhao, R., 'A Comparative Study of Lithium-Ion Batteries', *USA: University of Southen California*, 2010.

36. Scrosati, B. and Garche, J., 'Lithium Batteries: Status, Prospects and Future', *Journal of Power Sources*, 2010, 195, (9), pp. 2419-2430.

37. IJESD, A., 'Costs of Lithium-Ion Batteries for Vehicles', *Center for Transportation Research, Argonne National Laboratory*, 2000.

38. Mancini, M., Nobili, F., Tossici, R., Wohlfahrt-Mehrens, M., and Marassi, R., 'High Performance, Environmentally Friendly and Low Cost Anodes for Lithium-Ion Battery Based on Tio 2 Anatase and Water Soluble Binder Carboxymethyl Cellulose', *Journal of Power Sources*, 2011, 196, (22), pp. 9665-9671.

39. Xu, J., Zhang, L., Wang, Y., Chen, T., Al-Shroofy, M., and Cheng, Y.-T., 'Unveiling the Critical Role of Polymeric Binders for Silicon Negative Electrodes in Lithium-Ion Full Cells', *ACS Applied Materials & Interfaces*, 2017, 9, (4), pp. 3562-3569.

40. Wood, D.L., Li, J., and Daniel, C., 'Prospects for Reducing the Processing Cost of Lithium Ion Batteries', *Journal of Power Sources*, 2015, 275, pp. 234-242.

41. Li, J., Daniel, C., and Wood, D., 'Materials Processing for Lithium-Ion Batteries', *Journal of Power Sources*, 2011, 196, (5), pp. 2452-2460.

42. Keller, M., Buchholz, D., and Passerini, S., 'Layered Na-Ion Cathodes with Outstanding Performance Resulting from the Synergetic Effect of Mixed P-and O-Type Phases', *Advanced Energy Materials*, 2016, 6, (3).

43. Park, M., Zhang, X., Chung, M., Less, G.B., and Sastry, A.M., 'A Review of Conduction Phenomena in Li-Ion Batteries', *Journal of Power Sources*, 2010, 195, (24), pp. 7904-7929.

44. Sun, C., 'Poly (Vinylidene Fluoride) Membranes: Preparation, Modification, Characterization and Applications', 2009.

45. Huang, X., 'A Lithium-Ion Battery Separator Prepared Using a Phase Inversion Process', *Journal of Power Sources*, 2012, 216, pp. 216-221.

46. Feng, C., Wang, R., Shi, B., Li, G., and Wu, Y., 'Factors Affecting Pore Structure and Performance of Poly (Vinylidene Fluoride-Co-Hexafluoro Propylene) Asymmetric Porous Membrane', *Journal of Membrane Science*, 2006, 277, (1), pp. 55-64.

47. Van de Witte, P., Dijkstra, P., Van den Berg, J., and Feijen, J., 'Phase Separation Processes in Polymer Solutions in Relation to Membrane Formation', *Journal of Membrane Science*, 1996, 117, (1-2), pp. 1-31.

48. Zhang, M., Zhang, A.-Q., Zhu, B.-K., Du, C.-H., and Xu, Y.-Y., 'Polymorphism in Porous Poly (Vinylidene Fluoride) Membranes Formed Via Immersion Precipitation Process', *Journal of Membrane Science*, 2008, 319, (1), pp. 169-175.

49. Ahmad, A., Ideris, N., Ooi, B., Low, S., and Ismail, A., 'Influence of Polymer Concentration on Pvdf Membrane Fabrication for Immunoassay Analysis', *Journal of Applied Sciences*, 2014, 14, (12), p. 1299.

50. Stengaard, F., 'Preparation of Asymmetric Microfiltration Membranes and Modification of Their Properties by Chemical Treatment', *Journal of Membrane Science*, 1988, 36, pp. 257-275.

51. Mazumder, M., Sims, R., Biris, A., Srirama, P., Saini, D., Yurteri, C., Trigwell, S., De, S., and Sharma, R., 'Twenty-First Century Research Needs in Electrostatic Processes Applied to Industry and Medicine', *Chemical Engineering Science*, 2006, 61, (7), pp. 2192-2211.

52. Law, S.E. and Bowen, H.D., Low-Volume Electrostatic Spraying', (Google Patents, 1987)

53. Qiao, M., Zhang, L., Ma, Y., Zhu, J., and Chow, K., 'A Novel Electrostatic Dry Powder Coating Process for Pharmaceutical Dosage Forms: Immediate Release Coatings for Tablets', *European Journal of Pharmaceutics and Biopharmaceutics*, 2010, 76, (2), pp. 304-310.

54. Luo, Y., Zhu, J., Ma, Y., and Zhang, H., 'Dry Coating, a Novel Coating Technology for Solid Pharmaceutical Dosage Forms', *International journal of pharmaceutics*, 2008, 358, (1), pp. 16-22.

55. Sims, R., Mazumder, M., Liu, X., Chok, W., Mountain, J., Wankum, D., Pettit, P., and Chasser, T., 'Electrostatic Effects on First Pass Transfer Efficiency in the Application of Powder Coatings', *IEEE Transactions on Industry Applications*, 2001, 37, (6), pp. 1610-1617.

56. Williams, B.E., Harpur, I., Hearn, G., and Hughes, J.F., Apparatus for Coating Substrates with Inductively Charged Resinous Powder Particles', (Google Patents, 1996)

57. Daniel, C., 'Lithium Ion Batteries and Their Manufacturing Challenges', *FRONTIERS OF*, 2015.

58. Chou, S.-L., Pan, Y., Wang, J.-Z., Liu, H.-K., and Dou, S.-X., 'Small Things Make a Big Difference: Binder Effects on the Performance of Li and Na Batteries', *Physical Chemistry Chemical Physics*, 2014, 16, (38), pp. 20347-20359.

59. Li, X. and Wang, C., 'Engineering Nanostructured Anodes Via Electrostatic Spray Deposition for High Performance Lithium Ion Battery Application', *Journal of Materials Chemistry A*, 2013, 1, (2), pp. 165-182.

60. Chen, C., Agrawal, R., Kim, T.K., Li, X., Chen, W., Yu, Y., Beidaghi, M., Penmatsa, V., and Wang, C., 'Nanostructured Electrodes Via Electrostatic Spray Deposition for Energy Storage System', *ECS Transactions*, 2014, 61, (27), pp. 155-163.

61. Jiang, Y., Yuan, T., Sun, W., and Yan, M., 'Electrostatic Spray Deposition of Porous Sno2/Graphene Anode Films and Their Enhanced Lithium-Storage Properties', *ACS Applied Materials & Interfaces*, 2012, 4, (11), pp. 6216-6220.

62. Dunn, B., Kamath, H., and Tarascon, J.-M., 'Electrical Energy Storage for the Grid: A Battery of Choices', *Science*, 2011, 334, (6058), pp. 928-935.

63. Tarascon, J.-M. and Armand, M., 'Issues and Challenges Facing Rechargeable Lithium Batteries', *Nature*, 2001, 414, (6861), pp. 359-367.

64. Http://Batteryuniversity.Com/Learn/Article/Types_of_Lithium_Ion.

65. Tsumoru O., a.T.D., 'Innovations in Lithium Ion Battery Manufacturing a Continuous Manufacturing Process Applicable to Nano-Scale Materials at a Significant Cost Reduction', *Web: www.primix.jp*, Corp.

66. Lestriez, B., 'Functions of Polymers in Composite Electrodes of Lithium Ion Batteries', *Comptes Rendus Chimie*, 2010, 13, (11), pp. 1341-1350.

67. Zheng, H., Yang, R., Liu, G., Song, X., and Battaglia, V.S., 'Cooperation between Active Material, Polymeric Binder and Conductive Carbon Additive

in Lithium Ion Battery Cathode', *The Journal of Physical Chemistry C*, 2012, 116, (7), pp. 4875-4882.

68. Http://Www.Resodynmixers.Com/Wp-Content/Uploads/2010/06/Ram-Battery-Material-Mixing.Pdf.

69. Liu, D., Chen, L.-C., Liu, T.-J., Fan, T., Tsou, E.-Y., and Tiu, C., 'An Effective Mixing for Lithium Ion Battery Slurries', *Advances in Chemical Engineering and Science*, 2014, 4, (04), p. 515.

70. Marks, T., Trussler, S., Smith, A., Xiong, D., and Dahn, J., 'A Guide to Li-Ion Coin-Cell Electrode Making for Academic Researchers', *Journal of The Electrochemical Society*, 2011, 158, (1), pp. A51-A57.

71. Cho, K.Y., Kwon, Y.I., Youn, J.R., and Song, Y.S., 'Evaluation of Slurry Characteristics for Rechargeable Lithium-Ion Batteries', *Materials research bulletin*, 2013, 48, (8), pp. 2922-2926.

72. Oliver, W.C. and Pharr, G.M., 'Measurement of Hardness and Elastic Modulus by Instrumented Indentation: Advances in Understanding and Refinements to Methodology', *Journal of materials research*, 2004, 19, (1), pp. 3-20.

73. Peterson, S.W. and Wheeler, D.R., 'Direct Measurements of Effective Electronic Transport in Porous Li-Ion Electrodes', *Journal of The Electrochemical Society*, 2014, 161, (14), pp. A2175-A2181.

74. Gebregiorgis, A.W., 'Local Resistivity Measurement on Multicrystalline Silicon', *Institutt for fysikk*, 2012, Master's thesis.

75. Sinha, A. and Farhat, Z., 'A Study of Porosity Effect on Tribological Behavior of Cast Al A380m and Sintered Al 6061 Alloys', *Journal of Surface Engineered Materials and Advanced Technology*, 2014, 5, (01), p. 1.

76. Hill, J., 'How to Uniformly Disperse Nanoparticles', *Advanced Materials & Processes*, 2010, p. 34.

77. Zheng, H.H., Tan, L., Liu, G., Song, X.Y., and Battaglia, V.S., 'Calendering Effects on the Physical and Electrochemical Properties of Li[Ni1/3mn1/3co1/3]O-2 Cathode', *Journal of Power Sources*, 2012, 208, pp. 52-57.

78. Han, Z., Zhan, H., and Zhou, Y., 'Preparation and Performance of Layered Li [Li 0.182 Ni 0.182 Co 0.091 Mn 0.545] O 2 Cathode with Different Binders', *Materials Letters*, 2014, 114, pp. 48-51.

79. Sharma, V. and McKinley, G.H., 'An Intriguing Empirical Rule for Computing the First Normal Stress Difference from Steady Shear Viscosity Data for Concentrated Polymer Solutions and Melts', *Rheologica acta*, 2012, 51, (6), pp. 487-495.

80. Http://Pioneer.Netserv.Chula.Ac.Th/~Sanongn1/Course.Html.

81. Bauer, W. and Nötzel, D., 'Rheological Properties and Stability of Nmp Based Cathode Slurries for Lithium Ion Batteries', *Ceramics International*, 2014, 40, (3), pp. 4591-4598.

82. www.tainstruments.com/pdf/literature/AAN016_V1_U_StructFluids.pdf

83. Wenzel, V., Nirschl, H., and Nötzel, D., 'Challenges in Lithium-Ion-Battery Slurry Preparation and Potential of Modifying Electrode Structures by Different Mixing Processes', *Energy Technology*, 2015, 3, (7), pp. 692-698.

84. Chen, J., Liu, J., Qi, Y., Sun, T., and Li, X., 'Unveiling the Roles of Binder in the Mechanical Integrity of Electrodes for Lithium-Ion Batteries', *Journal of The Electrochemical Society*, 2013, 160, (9), pp. A1502-A1509.

85. Etacheri, V., Marom, R., Elazari, R., Salitra, G., and Aurbach, D., 'Challenges in the Development of Advanced Li-Ion Batteries: A Review', *Energy & Environmental Science*, 2011, 4, (9), pp. 3243-3262.

86. Groot, J., 'State-of-Health Estimation of Li-Ion Batteries: Cycle Life Test Methods', 2012.

87. Nishi, Y., 'Lithium Ion Secondary Batteries; Past 10 Years and the Future', *Journal of Power Sources*, 2001, 100, (1), pp. 101-106.

88. Scrosati, B., 'Recent Advances in Lithium Ion Battery Materials', *Electrochimica Acta*, 2000, 45, (15), pp. 2461-2466.

89. Khaligh, A. and Li, Z., 'Battery, Ultracapacitor, Fuel Cell, and Hybrid Energy Storage Systems for Electric, Hybrid Electric, Fuel Cell, and Plug-in Hybrid Electric Vehicles: State of the Art', *IEEE transactions on Vehicular Technology*, 2010, 59, (6), pp. 2806-2814.

90. Thomas, C., 'Fuel Cell and Battery Electric Vehicles Compared', *international journal of hydrogen energy*, 2009, 34, (15), pp. 6005-6020.

91. Buller, S., Thele, M., De Doncker, R., and Karden, E., 'Impedance-Based Simulation Models of Supercapacitors and Li-Ion Batteries for Power Electronic Applications', *IEEE Trans. Ind. Appl*, 2005, 41, (3), pp. 742-747.

92. Ren, H., Li, X., and Peng, Z., 'Electrochemical Properties of Li [Ni 1/3 Mn 1/3 Al 1/3− X Co X] O 2 as a Cathode Material for Lithium Ion Battery', *Electrochimica Acta*, 2011, 56, (20), pp. 7088-7091.

93. Howell, D., 'Fiscal Year 2014 Annual Progress Report for Energy Storage R&D, U.S. Department of Energy, ' *Office of Energy Efficiency and Renewable Energy, Vehicle Technologies Office,*, 2014, (2014), p. 1.

94. Wu, S.-L., Zhang, W., Song, X., Shukla, A.K., Liu, G., Battaglia, V., and Srinivasan, V., 'High Rate Capability of Li (Ni1/3mn1/3co1/3) O2 Electrode for Li-Ion Batteries', *Journal of The Electrochemical Society*, 2012, 159, (4), pp. A438-A444.

95. Cui, Z.-Y., Xu, Y.-Y., Zhu, L.-P., Wang, J.-Y., and Zhu, B.-K., 'Investigation on Pvdf-Hfp Microporous Membranes Prepared by Tips Process and Their Application as Polymer Electrolytes for Lithium Ion Batteries', *Ionics*, 2009, 15, (4), pp. 469-476.

96. Lin, D.-J., Chang, C.-L., Chen, T.-C., and Cheng, L.-P., 'On the Structure of Porous Poly (Vinylidene Fluoride) Membrane Prepared by Phase Inversion from Water-Nmp-Pvdf System', *Journal of applied science and Engineering*, 2002, 5, (2), pp. 95-98.

97. Sheng, Y., Fell, C.R., Son, Y.K., Metz, B.M., Jiang, J., and Church, B.C., 'Effect of Calendering on Electrode Wettability in Lithium-Ion Batteries', *Frontiers in Energy Research*, 2014, 2, p. 56.

98. Huai, Y., Gao, J., Deng, Z., and Suo, J., 'Preparation and Characterization of a Special Structural Poly (Acrylonitrile)-Based Microporous Membrane for Lithium-Ion Batteries', *Ionics*, 2010, 16, (7), pp. 603-611.

99. Rao, M., Liu, J., Li, W., Liang, Y., Liao, Y., and Zhao, L., 'Performance Improvement of Poly (Acrylonitrile-Vinyl Acetate) by Activation of Poly (Methyl Methacrylate)', *Journal of Power Sources*, 2009, 189, (1), pp. 711-715.

100. Deshpande, R.D., 'Understanding and Improving Lithium Ion Batteries through Mathematical Modeling and Experiments', 2011.

101. Zhang, S., Xu, K., and Jow, T., 'Electrochemical Impedance Study on the Low Temperature of Li-Ion Batteries', *Electrochimica Acta*, 2004, 49, (7), pp. 1057-1061.

102. Wang, L., Zhao, J., He, X., Gao, J., Li, J., Wan, C., and Jiang, C., 'Electrochemical Impedance Spectroscopy (Eis) Study of Lini1/3co1/3mn1/3o2 for Li-Ion Batteries', *Int. J. Electrochem. Sci*, 2012, 7, (1), pp. 345-353.

103. Wang, Z. and Zhou, L., 'Metal Oxide Hollow Nanostructures for Lithium-Ion Batteries', *Advanced materials*, 2012, 24, (14), pp. 1903-1911.

104. Goriparti, S., Miele, E., De Angelis, F., Di Fabrizio, E., Zaccaria, R.P., and Capiglia, C., 'Review on Recent Progress of Nanostructured Anode Materials for Li-Ion Batteries', *Journal of Power Sources*, 2014, 257, pp. 421-443.

105. Nitta, N. and Yushin, G., 'High-Capacity Anode Materials for Lithium-Ion Batteries: Choice of Elements and Structures for Active Particles', *Particle & Particle Systems Characterization*, 2014, 31, (3), pp. 317-336.

106. Obrovac, M. and Chevrier, V., 'Alloy Negative Electrodes for Li-Ion Batteries', *Chemical reviews*, 2014, 114, (23), pp. 11444-11502.

107. Zhang, L., Wu, H.B., and Lou, X.W.D., 'Iron-Oxide-Based Advanced Anode Materials for Lithium-Ion Batteries', *Advanced Energy Materials*, 2014, 4, (4).

108. Zhang, K., Hu, Z., Tao, Z., and Chen, J., 'Inorganic & Organic Materials for Rechargeable Li Batteries with Multi-Electron Reaction', *Science China Materials*, 2014, 57, (1), pp. 42-58.

109. Huang, B., Lithium Ion Battery Electrode and Its Fabrication Method', (Google Patents, 2013)

110. Doberdò, I., Löffler, N., Laszczynski, N., Cericola, D., Penazzi, N., Bodoardo, S., Kim, G.-T., and Passerini, S., 'Enabling Aqueous Binders for Lithium Battery Cathodes–Carbon Coating of Aluminum Current Collector', *Journal of Power Sources*, 2014, 248, pp. 1000-1006.

111. Loeffler, N., von Zamory, J., Laszczynski, N., Doberdo, I., Kim, G.-T., and Passerini, S., 'Performance of Lini 1/3 Mn 1/3 Co 1/3 O 2/Graphite Batteries Based on Aqueous Binder', *Journal of Power Sources*, 2014, 248, pp. 915-922.

112. Xu, J., Chou, S.-L., Gu, Q.-f., Liu, H.-K., and Dou, S.-X., 'The Effect of Different Binders on Electrochemical Properties of Lini 1/3 Mn 1/3 Co 1/3 O 2 Cathode Material in Lithium Ion Batteries', *Journal of Power Sources*, 2013, 225, pp. 172-178.

113. Wu, Q., Ha, S., Prakash, J., Dees, D.W., and Lu, W., 'Investigations on High Energy Lithium-Ion Batteries with Aqueous Binder', *Electrochimica Acta*, 2013, 114, pp. 1-6.

114. ABE, H., KONDO, A., NAITO, M., and YAMAGUCHI, M., 'Electrostatic Spray Deposition for Fabrication of Li-Ion Batteries'.

115. Ludwig, B., Zheng, Z., Shou, W., Wang, Y., and Pan, H., 'Solvent-Free Manufacturing of Electrodes for Lithium-Ion Batteries', *Scientific reports*, 2016, 6.

116. Mohanty, D., Dahlberg, K., King, D.M., David, L.A., Sefat, A.S., Wood, D.L., Daniel, C., Dhar, S., Mahajan, V., and Lee, M., 'Modification of Ni-Rich Fcg Nmc and Nca Cathodes by Atomic Layer Deposition: Preventing Surface Phase Transitions for High-Voltage Lithium-Ion Batteries', *Scientific reports*, 2016, 6.

117. Patel, P., 'Improving the Lithium-Ion Battery', *ACS central science*, 2015, 1, (4), p. 161.

118. *The library of manufacturing*, 2015, http://www.thelibraryofmanufacturing.com, (Accessed 15 Sept 2015).

119. Malmonge, L.F., Langiano, S.d.C., Cordeiro, J.M.M., Mattoso, L.H.C., and Malmonge, J.A., 'Thermal and Mechanical Properties of Pvdf/Pani Blends', *Materials Research*, 2010, 13, (4), pp. 465-470.

120. Campos, J.S.d.C., Ribeiro, A.A., and Cardoso, C.X., 'Preparation and Characterization of Pvdf/Caco 3 Composites', *Materials Science and Engineering: B*, 2007, 136, (2), pp. 123-128.

121. Geder, J., Song, J.H., Kang, S.H., and Denis, Y., 'Thermal Stability of Lithium-Rich Manganese-Based Cathode', *Solid State Ionics*, 2014, 268, pp. 242-246.

122. Kang, H., Lim, C., Fu, Y., and Zhu, L., 'Geometric and Electrochemical Characteristics of Nmc Electrodes with Different Calendering Conditions', 2016.

Vita

Education

- M.Sc. in Materials Engineering /Extractive Engineering, Department of Materials Engineering, University of Technology, Iraq.
  2006
- B.Sc. in Materials Engineering, Department of Materials Engineering, University of Technology, Iraq.
  2003

Publications

1. Mohanad Al-Shroofy, Qinglin Zhang, Jiagang Xu, Tao Chen, Aman Preet Kaur, and Yang-Tse Cheng. "Solvent-free dry powder coating process for low-cost manufacturing of $LiNi_{1/3}Mn_{1/3}Co_{1/3}O_2$ cathodes in lithium-ion batteries." *Journal of Power Sources* 352 (2017): 187-193.
2. Chen, Tao, Qinglin Zhang, Jie Pan, Jiagang Xu, Yiyang Liu, Mohanad Al-Shroofy, and Yang-Tse Cheng. "Low-Temperature Treated Lignin as Both Binder and Conductive Additive for Silicon Nanoparticle Composite Electrodes in Lithium-Ion Batteries." *ACS Applied Materials & Interfaces* 8, no. 47 (2016): 32341-32348.
3. Xu, Jiagang, Long Zhang, Yikai Wang, Tao Chen, Mohanad Al-Shroofy, and Yang-Tse Cheng. "Unveiling the Critical Role of Polymeric Binders for Silicon Negative Electrodes in Lithium-Ion Full Cells." *ACS Applied Materials & Interfaces* (2017).